

# Evolution of Movement Smoothness and Submovement Patterns in Persons with Stroke

by

Brandon Robinson Rohrer

S.M., Mechanical Engineering, 1999  
Massachusetts Institute of Technology

B.S., Mechanical Engineering, 1997  
Brigham Young University

Submitted to the Department of Mechanical Engineering  
in partial fulfillment of the requirements for the degree of

Doctor of Philosophy

at the

MASSACHUSETTS INSTITUTE OF TECHNOLOGY

June 2002

© Massachusetts Institute of Technology 2002. All rights reserved.

Author .....

Department of Mechanical Engineering

April 29, 2002

Certified by .....

Neville Hogan

Professor, Mechanical Engineering, Brain and Cognitive Sciences

Thesis Supervisor

Accepted by .....

Ain A. Sonin

Chairman, Department Committee on Graduate Students



# Evolution of Movement Smoothness and Submovement Patterns in Persons with Stroke

by

Brandon Robinson Rohrer

Submitted to the Department of Mechanical Engineering  
on April 29, 2002, in partial fulfillment of the  
requirements for the degree of  
Doctor of Philosophy

## Abstract

Smoothness is characteristic of coordinated human movements, and stroke patients' movements seem to grow more smooth with recovery. A robotic therapy device was used to analyze five different measures of movement smoothness in the hemiparetic arm of thirty-one patients recovering from stroke. Four of the five metrics showed general increases in smoothness for the entire patient population. However according to the fifth metric, the movements of patients with recent stroke grew less smooth over the course of therapy. This pattern was reproduced in a computer simulation of recovery based on submovement blending, suggesting that progressive blending of submovements underlies stroke recovery.

Submovements are hypothesized fundamental building blocks of human movement. All available evidence is consistent with their existence and no other theory has been proposed that can fully account for observed phenomena in human movement. However, there is no obvious way to *prove* their existence. Nevertheless, repeatedly successful decomposition of movement data into submovements may produce sufficient evidence to make the question moot.

The component submovements of stroke patients' point-to-point movements were estimated using a novel submovement extraction algorithm. Over the course of therapy, patients' submovements tended to increase in peak speed and duration. The number of submovements employed to produce a given movement decreased. The time between the peaks of adjacent submovements decreased for inpatients (those less than 1 month post-stroke), but not for outpatients (those greater than 12 months post-stroke) as a group. Submovements became more overlapped for all patients, but more markedly for inpatients. This pattern of changes in the extracted submovement parameters 1) provides an objective basis for evaluating patients' state of motor recovery and 2) provides some degree of additional support for the existence of submovements.

Thesis Supervisor: Neville Hogan

Title: Professor, Mechanical Engineering, Brain and Cognitive Sciences



# Acknowledgments

This thesis and the work behind it are the product of the effort, support, and ideas of many.

First, I would like to thank Professor Neville Hogan. He has served as an insightful doctoral committee chair, a patient yet exacting research advisor, and a source of invaluable professional and intellectual guidance. I have been consistently amazed and appreciative of his ability to read, critique, and return any written material within a matter of hours. He has also been very generous with his time and always makes a window in his week to meet with his students, whenever asked. Professor Hogan's passion for playing with hardware and respect for clean, raw data are infectious and have been ingrained in me as a desire to always return to the hard truths of the physical world after indulging in my flights of theoretical fancy.

I would also like to thank the other members of my doctoral committee, Dr. Hermano Igo Krebs, Professor Seth Lloyd, and Dr. Bruce Volpe, for their direct and indirect contributions to this work. Not only did they make time in their extremely busy schedules to meet (sometimes from great distances) but they also listened carefully, were very encouraging, and gave thoughtful feedback.

Members of the Newman Lab, past and present, have had a great impact on this work as well. In my early years, Joe Doeringer and Justin Won suffered through teaching me the rudiments of hands-on research. The current members of the lab not only give me good feedback on my work and support during crazy times, they make the Newman Lab a place that I am proud of and glad to be able to spend time in each day. Steve Buerger has been a patient sounding board and a great analyst in issues of electromagnetic interaction, real time control, and friction. James Celestino has taught me that everything in life is a little brighter when taken with Beethoven and an Entemann's chocolate chip cookie. (Mmmmm, chocolate chip cookie...) Jerry Palazzolo has motivated me to keep my shoulder to the wheel—you have to get up pretty early to get into the lab before he does. Phil Tang nearly has me convinced that everything in life actually does relate to sports, with any sport involving a ball

and bat being inherently superior to all others. Belle Kuo has shown me that all of engineering—from mechanical design to lettering to PowerPoint presentations—is really an art form. Sue Fasoli has shown that, yes, it really is possible to do seven things at one time and do them all well. And Laura DiPietra has driven home a fact that we have all suspected for years now—the lab desperately needs to have a resident electrical engineer.

I have been fortunate to be able to work with exceptional staff. Tatiana Koleva and Lori Humphrey have helped me out and bailed me out many times: Tatiana with her incredible efficiency (always with a smile) and Lori with the protective way she watches out for students. Leslie Regan and Joan Kravit in the graduate office have also been wonderful, acting more as my well-connected friends than as administrators.

I am very grateful for the support I have received from my mother, father, and mother-in-law. It has given me confidence to know that they thought I could do it and that they didn't think I was crazy to spend five more years in school. (At least they never said so in my hearing.)

My daughter Megan's encouragement has been particularly motivational: "Daddy, when are you going to graduate and get a job so we can have a house and get a kitty?" Even more helpful has been the affection and distraction provided by Megan, my other daughter Andrea, and, more recently, my son Samuel, continually reminding me what the important things in life really are.

Unquestionably the greatest contribution to this work has come from my wife, Melissa. She has been extremely unselfish in her willingness to be uprooted and move far from home, and in her patience during the five years of my slow academic progress. Her strength and cheerfulness have been for me a buoy and a lifeline. Her prayers have carried me through the rougher times, and her encouragement has kept me moving during the smooth times. Melissa has given color and relief to so many days that would otherwise be flat and gray. Thank you, Melissa. I could not have done this without you.

# Contents

<b>1</b>	<b>Introduction</b>	<b>17</b>
1.1	Motivation . . . . .	18
1.1.1	Why quantify stroke patients' motor impairment? . . . . .	18
1.1.2	Why pursue a characterization of segmentation? . . . . .	19
1.2	Stroke . . . . .	19
1.3	Outline of remaining chapters . . . . .	21
<b>2</b>	<b>Movement smoothness changes during stroke recovery</b>	<b>23</b>
2.1	Summary . . . . .	23
2.2	Introduction . . . . .	24
2.3	Methods . . . . .	25
2.3.1	Subjects . . . . .	25
2.3.2	Apparatus . . . . .	25
2.3.3	Procedure . . . . .	26
2.3.4	Analysis . . . . .	26
2.3.5	Statistical tests . . . . .	31
2.3.6	Simulation . . . . .	31
2.4	Results . . . . .	32
2.4.1	Simulation results . . . . .	33
2.5	Discussion . . . . .	35
2.5.1	Movement smoothness increases during recovery . . . . .	35
2.5.2	Evidence for discrete submovements . . . . .	36
2.5.3	Jerk as a smoothness metric . . . . .	37

<b>3</b>	<b>Is the existence of submovements provable?</b>	<b>39</b>
3.1	Summary . . . . .	39
3.2	Introduction . . . . .	39
3.3	The existence of submovements is plausible . . . . .	40
3.3.1	Summary of experimental observations of segmentation . . . .	41
3.3.2	Other theories of movement production are not consistent with all experimental observations of segmentation . . . . .	44
3.3.3	Submovements are consistent with experimental observations of segmentation . . . . .	46
3.4	The provability of the existence of submovements . . . . .	49
3.4.1	A theory of submovements . . . . .	49
3.4.2	Difficulties in testing . . . . .	49
3.4.3	Toward a <i>testable</i> theory of submovements . . . . .	50
3.4.4	A first pass . . . . .	52
<b>4</b>	<b>The curvature–velocity relation of human movements</b>	<b>53</b>
4.1	Summary . . . . .	53
4.2	Introduction . . . . .	53
4.3	Curvature maxima and velocity minima in human movements are in fact <i>not</i> strictly synchronous . . . . .	54
4.4	There is no mechanical requirement that curvature and velocity ex- trema be synchronous in general . . . . .	56
4.5	A kinematic velocity-curvature relation . . . . .	58
4.6	A condition for synchrony between velocity extrema and curvature extrema . . . . .	58
4.7	A dynamics-based condition for synchrony . . . . .	59
4.7.1	A special case . . . . .	60
4.8	A note on near-synchrony in human movements . . . . .	61
4.9	The Two-thirds Power Law . . . . .	61
4.9.1	Shortcomings of the Power Law . . . . .	63



4.10	A relationship between synchrony and the two-thirds Power Law . . .	64
4.10.1	Is synchrony an epiphenomenon? . . . . .	65
<b>5</b>	<b>Avoiding spurious submovement decompositions: A globally optimal algorithm</b>	<b>67</b>
5.1	Summary . . . . .	67
5.2	Introduction . . . . .	68
5.2.1	The difficulty of making a good initial guess . . . . .	70
5.2.2	Initial guess methods . . . . .	70
5.3	Method . . . . .	72
5.3.1	Algorithm outline . . . . .	73
5.3.2	Bounding $\mathcal{E}(\mathbf{p})$ (step 5) . . . . .	75
5.3.3	Breaking down of solution subspaces (step 7) . . . . .	75
5.3.4	Terminating the search (step 8) . . . . .	76
5.3.5	Minimizing the number of submovements . . . . .	76
5.4	Results . . . . .	77
5.4.1	Solution-finding performance . . . . .	77
5.4.2	Required computing power . . . . .	78
5.4.3	Convergence . . . . .	79
5.4.4	Fixed submovement parameterization does not imply a fixed submovement shape . . . . .	79
5.5	Conclusion . . . . .	80
5.5.1	Limitations of the branch-and-bound decomposition algorithm	81
<b>6</b>	<b>The scattershot decomposition algorithm</b>	<b>83</b>
6.1	Summary . . . . .	83
6.2	Scattershot Algorithm . . . . .	83
6.2.1	Statistical tests . . . . .	85
6.2.2	Sensitivity Analysis . . . . .	86
6.3	Results of Sensitivity Analysis and Discussion . . . . .	88

6.3.1	Parameter <i>values</i> vary between decomposition conditions but follow repeatable patterns . . . . .	89
6.3.2	Parameter <i>changes</i> are consistent between decomposition conditions . . . . .	91
6.4	Conclusion . . . . .	92
<b>7</b>	<b>Submovements grow larger, fewer, and more blended during stroke recovery</b>	<b>93</b>
7.1	Summary . . . . .	93
7.2	Methods . . . . .	94
7.2.1	Neuromotor noise test . . . . .	94
7.3	Results . . . . .	95
7.3.1	Submovement Characteristics . . . . .	95
7.3.2	Neuromotor noise test . . . . .	97
7.4	Discussion . . . . .	98
7.4.1	Recovery as system identification . . . . .	101
<b>8</b>	<b>Conclusion and future work</b>	<b>103</b>
8.1	Conclusion . . . . .	103
8.1.1	Motor behavior during stroke recovery . . . . .	103
8.1.2	Submovements . . . . .	104
8.1.3	Applications of submovements . . . . .	104
8.2	Future Work . . . . .	106
8.2.1	Brain-computer interfaces (BCI's) . . . . .	106
8.2.2	Biologically-motivated discrete control systems . . . . .	107
8.2.3	Manually-operated systems . . . . .	108
<b>A</b>	<b>Mathematical definitions of curvature</b>	<b>111</b>
A.1	Summary . . . . .	111
A.2	Introduction . . . . .	111
A.3	Comparison . . . . .	112

A.3.1	The “rate of change of the unit tangent vector” formula . . . .	112
A.3.2	Frenet Formula . . . . .	115
A.3.3	The “cross product” formula . . . . .	115
A.4	Conclusion . . . . .	117
<b>B</b>	<b>Derivations related to the Branch-and-Bound algorithm of Chapter 5</b>	<b>119</b>
B.1	Calculating $U'$ . . . . .	119
B.1.1	Minimum-jerk submovements . . . . .	120
B.1.2	Gaussian submovements . . . . .	121
<b>C</b>	<b>Empirical submovement descriptions</b>	<b>125</b>
C.1	Submovements in tangential velocity data . . . . .	125
C.1.1	Symmetric vs. asymmetric submovement velocity profiles . . .	125
C.1.2	Straightness of submovements . . . . .	126
C.1.3	Inter- and intra-subject consistency . . . . .	126
C.1.4	Frequency of submovements . . . . .	127
C.1.5	Duration of submovements . . . . .	127
C.1.6	Shape of submovements . . . . .	127
C.2	Submovements in force data . . . . .	128
C.3	Submovements in EMG data . . . . .	128
<b>D</b>	<b>Raster plots of submovement characteristics</b>	<b>131</b>
	<b>Bibliography</b>	<b>163</b>



# List of Figures

2-1	Reaching task, top view . . . . .	27
2-2	Simulated vs. actual speed profiles . . . . .	29
2-3	A constructed “tent” profile . . . . .	30
2-4	Changes in each smoothness metric over the course of therapy for each patient . . . . .	33
2-5	Comparison of smoothness metrics during the simulated blending of two minimum-jerk curves . . . . .	34
3-1	Vallbo and Wessberg’s observations of intermittent EMG in finger flexion	44
3-2	An example of decomposition of the tangential velocity of an accurate movement into prototype submovements, taken from [60]. . . . .	48
3-3	An example of non-unique, zero-error decompositions of a function. .	50
4-1	Abend et al.’s data in which was observed synchrony between velocity dips and curvature peaks. . . . .	55
4-2	Magnification of the previous figure . . . . .	55
4-3	Asynchrony in speed-curvature data, reproduced from [88] . . . . .	56
4-4	Instances of asynchrony in data taken from a stroke patient’s movements while holding a manipulandum . . . . .	57
4-5	An elliptical path, such as is produced by out-of-phase sinusoidal oscillations. . . . .	62
5-1	Problematic decompositions for current algorithms . . . . .	69

5-2	A step-by-step example of the branch-and-bound algorithm in one dimension . . . . .	74
5-3	Minimization of the number of submovements . . . . .	77
5-4	Decomposition of simulated speed profiles composed of minimum-jerk and Gaussian submovements . . . . .	78
5-5	An example of shape variations in a single submovement parameterization	80
6-1	Definitions of inter-peak interval and submovement overlap. . . . .	84
6-2	Creation of a “change bar” used in the results summary plots. . . . .	85
6-3	The three submovement shapes used in decompositions . . . . .	89
6-4	Sensitivity analysis of submovement extraction to algorithm conditions: maximum duration, accuracy requirement, and submovement shape. . . . .	90
7-1	Typical simulated movements at various times during the progression of the simulation . . . . .	95
7-2	Changes in submovement characteristics by patient. . . . .	96
7-3	The number of patients who showed increases and decreases in each of five submovement characteristics. . . . .	97
A-1	Instantaneous velocity, acceleration, and radius of curvature in a movement trajectory. . . . .	116

# List of Tables

2.1	Fugl-Meyer scores and time post-stroke. . . . .	26
7.1	Summarized changes in the submovement parameters of simulated data containing Gaussian noise . . . . .	98





# Chapter 1

## Introduction

Identifying fundamental building blocks that underlie human movement is a major goal of motor control studies. If such a structure could be identified and accurately characterized, it would provide the ability to scrutinize human movement at a deeper level than has been previously possible. The phenomenon of segmentation, i.e. the observation that human movements appear to consist of blended, discrete submovements, hints at the existence of such building blocks.

As segmentation has been observed to be more pronounced in recovering stroke patients [42, 50], studying their movements is likely to lead to a clearer understanding of it. Furthermore, the increase of smoothness (i.e. the more complete blending of submovements) of stroke patients' movements during recovery may provide a useful means to quantify patients' motor performance and of charting and projecting their recovery. The goal of this work is to address the following question:

**Does the evolution of the nature of segmentation in stroke patients' upper-limb movements follow a stereotypical pattern during recovery?**

If this question can be answered with a 'yes', it will provide a tool for characterizing stroke patients' motor behavior and projecting their recovery. In addition, it will provide a meaningful quantitative measure of patients' motor performance, complementing the sometimes coarsely-scaled clinical measures, such as the Fugl-Meyer

exam.

If similarities are not found in the evolution of segmentation patterns of recovering stroke patients, this would suggest that segmentation and its manifestation are highly individualized and that it may not be directly related to the processes underlying patients' motor recovery.

## 1.1 Motivation

### 1.1.1 Why quantify stroke patients' motor impairment?

The motivation for this work comes from several sources. Most significantly, pursuing this work is worthwhile because it has the potential to improve the quality of life for individuals suffering the after-effects of stroke.

Physical therapy is used as a means of helping stroke patients regain lost motor function. While there is general agreement in the medical and therapy fields that this benefits patients, the therapy program adopted is usually chosen based on clinical tradition and the therapist's bias. Therapy programs are not closely tailored to individual subjects, to their age, lesion location and size, etc. In order to do this, highly sensitive measures of motor impairment are necessary, so that small differences in patient response to different courses of therapy can be detected and used to learn how to individualized treatment.

Existing clinical measures of motor impairment are coarsely quantified and subjective. An objective, finely quantified measure may reduce the "noise" in these measures and may allow better understanding of how different factors affect response to therapy. In addition, many clinical evaluation tools are insensitive to hemiplegia, and thus to any changes in the level of motor impairment in the stroke patient's affected arm. The Fugl-Meyer test, for instance, widely considered to be the "Gold Standard" of post-stroke impairment measurement in the clinic, can be largely completed with only one arm. A better measure of impairment would improve the accuracy and strengthen the predictive ability of models of recovery. This in turn would lead

to more effective therapy and, presumably, faster and more complete recovery from stroke.

### **1.1.2 Why pursue a characterization of segmentation?**

Aside from improvements in the rehabilitation process, studying the movements of recovering stroke patients may provide new insights into the nature of motor control. In order to study the structure of the atom, atomic physicists use high-powered accelerators to smash them and then watch the pieces fly. Similarly, by observing the changes in movement patterns that occur when nature “breaks” a human brain, much can be learned about how movement is controlled. In addition, when observing stroke there is the added advantage of observing the slow process of movement returning (somewhat) to normal over time.

This unique experimental opportunity gives researchers a chance to see “pieces” of movement and to watch how they grow together and blend. Establishing the existence of a set of fundamental “pieces” or “building blocks” for human movement is one of the major goals of motor control research. Segmentation is a theory which describes one such set of building blocks. Any step toward proving or disproving the theory of segmentation would be a significant contribution to the field of motor control, and analysis of stroke patients’ data provides potentially fertile ground for yielding insights about segmentation. The phenomenon of segmentation appears to be more pronounced in stroke patients. This improves the chances of supporting or refuting its existence. In addition, segmentation appears to decrease during the course of recovery [50, 42]. Thus, a characterization of segmentation may also provide a meaningful way to quantify the recovery process.

## **1.2 Stroke**

If therapy can be made more effective, there is a large population that may benefit from it. Stroke is the leading cause of disability in the United States [3] afflicting about 750,000 annually [4]. This number is likely to increase, given US Census Bureau

projections that the 65+ age group (now accounting for two-thirds of all strokes [4]) will increase by more than 80% in the next 25 years [10]. The fraction of victims that survive their strokes is increasing as well: in 1950, 88.8 percent of stroke victims died within a year, but by 1996 that number had decreased to 29 percent [84]. There are about 4.5 million stroke survivors in the United States today [3]. While it is good news that fewer people are dying from strokes, it also means that a larger group is living with the after-effects. According to the estimates of the National Stroke Association, about one-third of stroke survivors are mildly impaired, one-third moderately impaired, and one-third severely impaired [4].

People who have suffered a stroke commonly suffer from the following movement deficits [15].

- weakness of specific muscles on the side contralateral to the lesion
- abnormal muscle tone
- abnormal postural adjustment
- abnormal movement synergies
- lack of mobility between structures at the shoulder girdle and pelvic girdle
- incorrect timing of components within a movement pattern
- loss of interjoint coordination
- slowness, spatial and temporal discontinuity, and abnormal patterns of muscle activation in goal-directed movements
- lower movement amplitudes, prolonged movement times, and higher dispersion and segmentation in trajectories of pointing movements

Specifically, Levin [50] describes features of hemiplegic patients' point-to-point reaching patterns relative to those of healthy subjects. They include:

- Longer duration

- Lower movement amplitudes
- Increased dispersion (deviation from a straight-line path)
- Increased segmentation (many-peaked velocity profile and a squiggly path, described by Levin as “jerky and saccadic”)

In many cases, motor impairment is severe enough to render the effected limb useless in the stroke patient’s daily activities. It is the goal of therapy to restore ability as completely as possible.

### 1.3 Outline of remaining chapters

The remaining chapters will describe the process of quantifying stroke patients’ movement smoothness and submovement characteristics and discuss their evolution during the course of stroke recovery.

- Chapter 2. Five smoothness measures are used to quantify movement smoothness in 31 stroke patients. Smoothness is shown to increase with therapy. A counter-intuitive behavior of a jerk-based smoothness metric is shown to be consistent with a theory of recovery as the progressive blending of submovements.
- Chapter 3. Background on previous experimental observations of submovements is presented together with a treatment of the feasibility of establishing the existence of submovements by proof.
- Chapter 4. This chapter provides a deeper look into the question of whether the speed-curvature relations observed in human movement (e.g. synchrony and the 2/3 power law) are likely to be due to neuromuscular mechanics or segmented control.
- Chapter 5. Although many attempts to extract submovements from human movement data produce visually convincing results, all of the methodologies

that have been employed are prone to produce spurious decompositions. Examples of potential failures are given. A branch-and-bound algorithm for submovement extraction, capable of global nonlinear minimization (and hence, capable of avoiding spurious decompositions) is developed and demonstrated.

- Chapter 6. A scattershot decomposition algorithm is presented. It is less rigorous than the branch-and-bound algorithm of Chapter 5, but still tends to seek the globally optimal decomposition. A sensitivity analysis is performed to determine the effect of algorithm conditions on the results.
- Chapter 7. The results of the scattershot algorithm of Chapter 6 applied to the same 31 patients as in Chapter 2 are presented. During recovery submovements tend to increase peak speed, increase movement duration, grow fewer in number, and become more completely blended. Differences in inpatients' and outpatients' submovement evolution patterns are consistent with a "system identification" theory of movement: a forward model is trained first (i.e. the "sensors" are calibrated) and then an inverse model is trained (i.e. the "actuators" are calibrated).
- Chapter 8. A summary of results is given together with suggestions for future work.

# Chapter 2

## Movement smoothness changes during stroke recovery

From a manuscript submitted to The Journal of Neuroscience.

Authors: B Rohrer, S Fasoli, HI Krebs, R Hughes, B Volpe, J Stein, WR Frontera, N Hogan

### 2.1 Summary

Smoothness is characteristic of coordinated human movements, and stroke patients' movements seem to grow more smooth with recovery. We used a robotic therapy device to analyze five different measures of movement smoothness in the hemiparetic arm of 31 patients recovering from stroke. Four of the five metrics showed general increases in smoothness for the entire patient population. However according to the fifth metric, the movements of patients with recent stroke grew less smooth over the course of therapy. This pattern was reproduced in a computer simulation of recovery based on submovement blending, suggesting that progressive blending of submovements underlies stroke recovery.

## 2.2 Introduction

Recent epidemiological data that has suggested increasing prevalence of stroke has prompted vigorous novel treatment trials and the use of unique brain imaging tools to begin to understand the pathophysiology of stroke [14, 18]. Most survivors of stroke will have impaired brain function and permanent levels of disability. As survival from stroke improves with modern medical care, the increasing number of these patients has also prompted the drive to understand the functional motor recovery process. Recently, investigators, armed with new tools [43, 42, 53, 38], have begun the detailed kinematic analysis of motor recovery. Based on observations of changes in movement smoothness in recovering stroke patients [43], we measured the development of movement smoothness as patients with stroke recovered motor function in formerly paralyzed arms.

Movement smoothness has been used as a measure of motor performance of both healthy subjects [73] and persons with stroke [83, 38]. Smoothness measures have most often been based on minimizing jerk, the third time derivative of position [23], though many other measures are possible, including snap, the fourth time derivative of position [21] and counting peaks in speed [8, 22, 15, 38]. Smoothness in the minimum-jerk sense has been used to identify pre-symptomatic individuals with Huntington’s disease [79] and has also been shown to account for the two-thirds power law, widely considered an invariant in human movement [88, 32, 82, 76].

Though smoothness is a characteristic of unimpaired movements, perhaps the most striking feature of the earliest movements made by patients recovering from stroke is their lack of smoothness: they appear to be composed of a series of discrete submovements [42]. Evidence of discrete submovements has also been found in the movements of healthy subjects [60, 85]. Complex movements have been decomposed into submovements as an analysis tool [63, 24, 6, 9] with apparent success. Although the existence of submovements has not been demonstrated unequivocally, they account for many patterns in human movement [20, 36].

Krebs et al., [42] report that movements made by patients recovering from stroke



become smoother as recovery proceeds. This was attributed to a progressive overlapping and blending of submovements, though only isolated examples of submovement blending were reported. In this paper we present further evidence that recovery proceeds by progressive blending of submovements. We quantify the smoothness of movements made by stroke patients with their affected limb and how it changed over the course of recovery. We present an analysis of how progressive blending of submovements would affect measures of smoothness and show that it is consistent with our experimental observations.

## **2.3 Methods**

### **2.3.1 Subjects**

Thirty-one subjects, 10 women and 21 men, participated in this study performed at the Spaulding Rehabilitation Hospital in Boston, Massachusetts. Twelve subjects were acute-stage inpatients who had suffered their first unilateral infarct less than one month before beginning the study, and 19 were chronic-stage outpatients from 12 to 53 months post-stroke. Subjects were between 19 and 78 years of age (mean age 55.6 years for inpatients, 56.2 years for outpatients), hemiparetic, and able to understand and carry out verbal instructions. See Table 2.1 for a summary of clinical evaluation scores and times post-stroke for inpatient and outpatient groups. Only subjects who participated in more than five therapy sessions and had completed more than 100 point-to-point movements were included in this analysis. The protocol was approved by the Human Studies Committee at Spaulding Rehabilitation Hospital and by the Committee on the Use of Human Experimental Subjects of the Massachusetts Institute of Technology. All subjects gave informed consent.

### **2.3.2 Apparatus**

MIT-MANUS, a planar robot, was designed as a therapy aid in the Newman Laboratory at the Massachusetts Institute of Technology [34, 42, 45]. A key characteristic of

Fugl-Meyer scores and time post-stroke: mean (min, max)			
group	initial FM	final FM	months post-stroke
inpatients (N=12)	13.0 (3, 35)	16.4 (6, 31)	1 (1, 1)
outpatients (N=19)	27.3 (11, 50)	31.1 (15, 54)	30.5 (12, 53)

Table 2.1: Fugl-Meyer scores and time post-stroke. Inpatient and outpatient group means, minima, and maxima for Fugl-Meyer scores and time between stroke and the beginning of their participation in the study. A Fugl-Meyer score of 66 represents no impairment.

MIT-MANUS is its “backdrivability”, that is, its ability to “get out of the way” when pushed by a subject. Thus, subjects’ movements were minimally obscured by the dynamics of the robot. During all movements analyzed and presented in this paper, the robot was unpowered and acted as a passive measurement device that restricted patients’ hand motion to a horizontal plane.

### 2.3.3 Procedure

Over the course of a therapy session, subjects were directed to make a number of point-to-point movements, ending as near to the directed point as possible. With a computer display of a center target, eight targets equally spaced around a circle, and the current position of the robot endpoint, subjects moved from the center to each target, and back, starting at “North” and proceeding clockwise (see Figure 2-1). Each target was 14 cm from the center. Inpatient subjects typically received robot therapy five times per week, for four weeks; outpatients three times per week, for six weeks. Each session lasted approximately one hour. A computer recorded the position, velocity, and force exerted at the robot handle. In addition, each subject was clinically assessed by a “blinded” clinician at the beginning, middle, and end of therapy using a collection of several clinical scales. In this paper, only the results of the Fugl-Meyer Test of Upper Extremity Function [26] are reported.

### 2.3.4 Analysis

Five measures of smoothness were applied to the kinematic data collected during point-to-point movements. All metrics have been defined such that higher values of

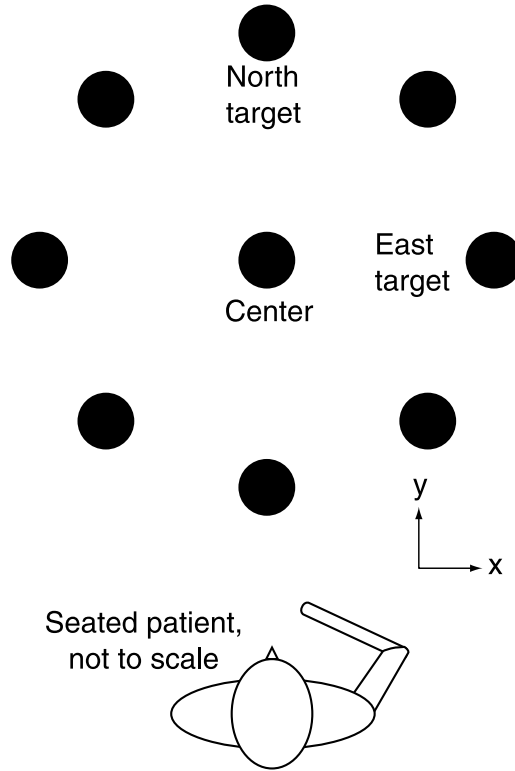


Figure 2-1: Reaching task, top view. The task required each subject to attempt to move from the center position to a target and then return to the center, beginning at the North target and repeating for each target in a clockwise pattern around the circle. Subjects were presented with a visual display of the task similar to that in the figure, which also included a display of the subject's hand position. The robot remained unpowered for the duration of all the trials incorporated into this analysis. Each target is 14 cm from the center.

the metric correspond to smoother movements. A movement was considered to begin when the speed first became greater than 2% of the peak speed and was considered to end after the speed dropped and remained below the 2% threshold again.

### **Jerk metric**

The jerk metric characterizes the average rate of change of acceleration in a movement. It is calculated by dividing the negative mean jerk magnitude by the peak speed. Taking the negative of the mean jerk causes increases in the jerk metric to correspond with increases in smoothness, that is, it transforms the jerk metric from a measure of “non-smoothness” into a measure of smoothness. Dividing the jerk magnitude by

peak speed is identical to first normalizing x- and y- velocities by the peak speed, and then calculating jerk. Normalizing mean jerk in this way made the metric a measure of smoothness only, and did not confound it with changes in overall movement speed. While the other four measures have no units associated with them, the jerk metric has units of  $1/s^2$ . The other four metrics each quantify some shape characteristic of the speed curve thought to be related to smoothness, and hence can remain dimensionless. The jerk metric, however, is based directly on a mathematical definition of smoothness and by definition must carry units.

### **Speed metric**

The speed metric is the normalized mean speed, that is, the mean of the speed divided by the peak speed. Early in recovery, subjects' movements appear to be composed of a series of short, episodic submovements. The resulting speed profile has a series of peaks with deep valleys in between, representing complete or near-complete stops between each apparent submovement (see Figure 2-2). The mean speed of such a movement is much less than its peak. In this case, the normalized mean speed is relatively low, particularly when the interval between submovements is significant. However, as subjects recover, submovements tend to have shorter and less complete breaks between them, resulting in speed profiles with shallower valleys between peaks. The normalized mean speed for these movements is significantly higher.

### **Mean Arrest Period Ratio**

Early in recovery it is common for subjects to move in an episodic fashion, stopping multiple times before reaching their objective. A speed profile resulting from this type of movement will have many intervals of zero velocity. On the other hand, as subjects reach their goal more directly, without unnecessary stops, the speed profiles will tend to spend less time near zero speed. "Movement Arrest Period Ratio" (MAPR) as described by Beppu et al. [5] quantifies this change; it is the proportion of time that movement speed exceeds a given percentage of peak speed. By nature, the MAPR with a low threshold is less likely to be informative when studying movements that

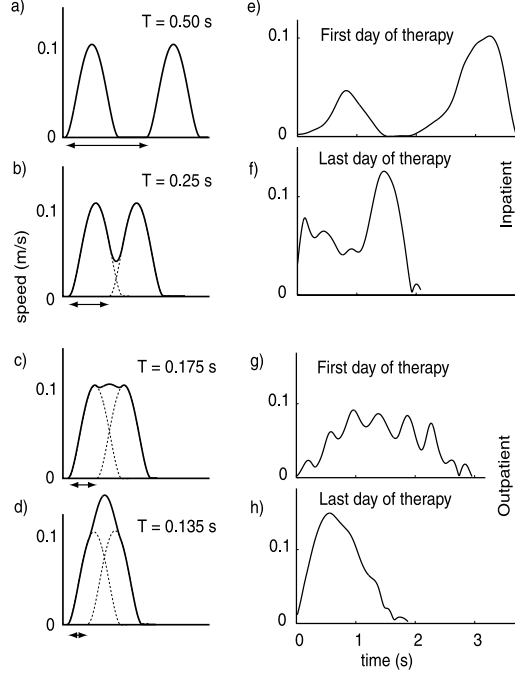


Figure 2-2: Simulated vs. actual speed profiles. a)-d) Progressive blending of two minimum-jerk curves at various states of blending ( $T$ ). See the Method section for a detailed description of the simulation. e)-h) Actual patient speed profiles. e) and f) are taken from the first and last therapy sessions of an inpatient and g) and h) are taken from the first and last therapy sessions of an outpatient. Simulated speed profiles qualitatively resemble the actual patient data. a) contains two distinct speed peaks, just as the patient speed profile e). Continuing down the columns, b) and f) are qualitatively similar, as c) somewhat resembles g), and d) is similar to h). Progression from the first to the last therapy sessions qualitatively suggests an increase in submovement blending. Also, the movements of the subject that is longer post-stroke (the outpatient) have characteristics of more highly blended submovements, compared to those of the inpatient.

are close to normal. However, outpatients' movements in this study, although better than those of inpatients, are still far from normal. They move at about half the speed of healthy subjects and show significantly non-straight paths. 10% was selected as the MAPR threshold in this analysis.

### Peaks metric

The number of peaks in a speed profile have been used to quantify smoothness in healthy subjects [22, 8] and in stroke patients [38]. Fewer peaks in speed represents fewer periods of acceleration and deceleration, making a smoother movement. In this

study the peaks metric is taken to be the negative of the number of peaks in order to relate increases in the peaks metric to increases in smoothness.

### “Tent” metric

The “tent” metric is the ratio of the area under the speed curve to the area under a curve “stretched” over the top of it. It is based on a graphical analysis of the difference between a speed profile and a similarly scaled, single-peaked speed profile, i.e. a speed profile with a single acceleration and a single deceleration phase. An example of a tent curve is shown in Figure 2-3.

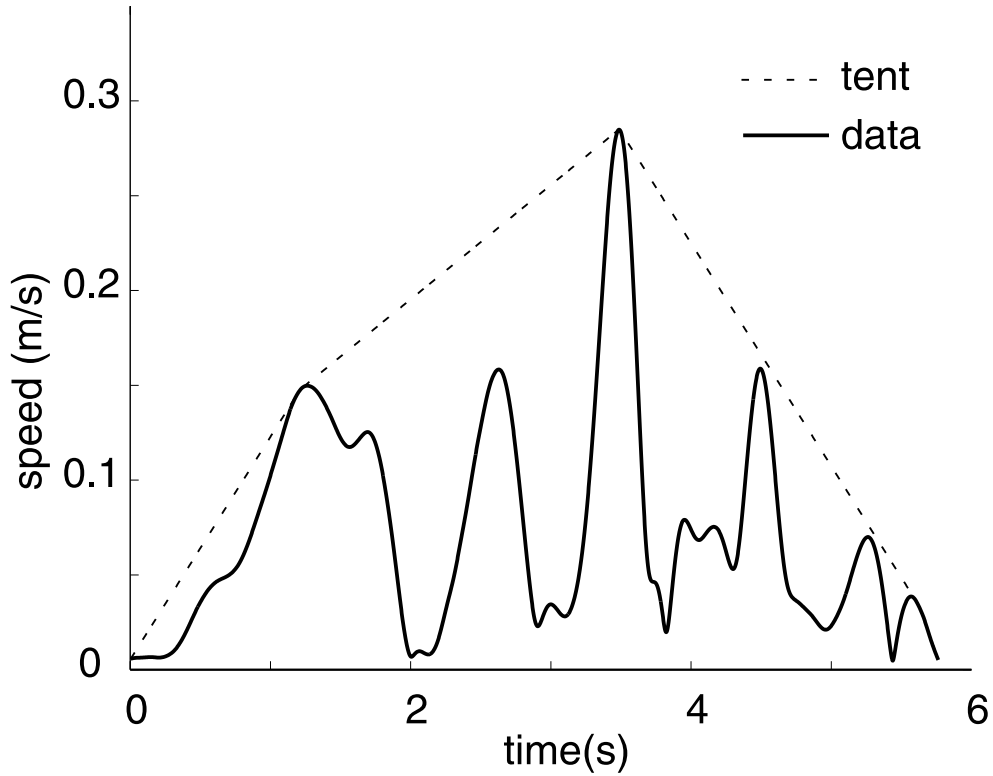


Figure 2-3: A subject’s speed profile is superimposed with the corresponding tent profile constructed during the calculation of the tent metric. It should be noted that, unlike the other metrics, the tent metric is sensitive to “permutations”. Consider two movements, each of which have four peaks, two large and one small. In one movement, the peaks are ordered [Large1, Small1, Small2, Large2] with periods of no movement in between, and in the second movement, peaks are ordered [Small1, Large1, Large2, Small2]. The tent metric will show higher smoothness in the second movement.

### 2.3.5 Statistical tests

Using linear regression, a line was fit to each of the smoothness metrics over the course of therapy for each subject, and the confidence interval for the slope was determined. See Press et al. [74] for a detailed mathematical description. Student's t-tests were also performed to compare changes in each of the smoothness metrics in acute and chronic populations.

### 2.3.6 Simulation

To test whether changes in the smoothness of movements made by recovering stroke patients were due to progressive blending of submovements, a simulation of submovement blending was performed. A simulated movement was composed of two minimum-jerk speed profiles of the same amplitude and width, initiated an interval  $T$  apart, as shown in Figure 2-2, panels a-d. Blending was simulated by performing scalar summation of the overlapping portion of the speed profiles [63] as opposed to vector summation [24]. Note that in the case of straight line movement, the two summing modalities are equivalent.

As  $T$  is varied, the extent of overlap of the two submovement speed curves varies as well, although the net displacement of the simulated movement remains constant, consistent with the fixed-distance point-to-point movements required by the experimental task. Sample speed profiles from subjects shown in Figure 2-2, panels e-h lend support to this description of movement. The sample movement taken from the inpatient's first day of therapy is clearly divided into two stages, with the subject coming to a complete stop in between them. The movement taken from the inpatient's last day of therapy shows a speed profile with shallower valleys between the peaks. As interpreted by the simulation, the submovements are more completely blended together than those of the earlier movement. In comparison, on the outpatient's final day of therapy, the speed profile is nearly unimodal. This effect occurs in the simulation as well when there is such a high degree of blending that individual peaks are no longer distinguishable.

In the simulation, the five smoothness metrics are calculated for many values of  $T$ . In order to remain consistent with the data processing methods used on actual subject data, a “movement” was considered to begin when the speed first became greater than 2% of the peak speed and to end after the speed dropped and remained below the 2% threshold again.

## 2.4 Results

The differences between first-day and last-day values of the fits for each smoothness measure are plotted in Figure 2-4. An increase in any metric indicates an increase in smoothness, as defined by that metric. Filled circles represent statistical significance ( $p < 0.05$ ).

All subjects but one showed a significant increase in one or more of the smoothness metrics, 22 of them showing an improvement in 4 or more metrics. The movements of both inpatients and outpatients tended to get smoother over the course of therapy. The amount of change in smoothness metrics varied between inpatient and outpatient populations. For all smoothness metrics except the tent metric the amount of change between the two groups differed significantly ( $p < 0.05$ ). In the speed metric, MAPR, and the peaks metric, inpatients showed greater increases in smoothness than outpatients. However, inpatients tended to show decreases in smoothness as measured by the jerk metric, where outpatients tended to show increases.

Although the patients’ age range was quite large, there was no statistically significant difference in age between inpatients and outpatients as groups. Therefore, the observed differences in inpatient and outpatient performance in 4 out of the 5 smoothness metrics cannot be attributed to variations in patients’ ages. Correlation analysis shows that patients’ age correlates weakly with their performance; the highest level of correlation is 0.33, which occurs with changes in the peaks metric.

As shown in Table 2.1, inpatients and outpatients had a wide range of Fugl-Meyer scores both at the beginning and end of therapy. On average, however, inpatients began therapy lower on the Fugl-Meyer scale.



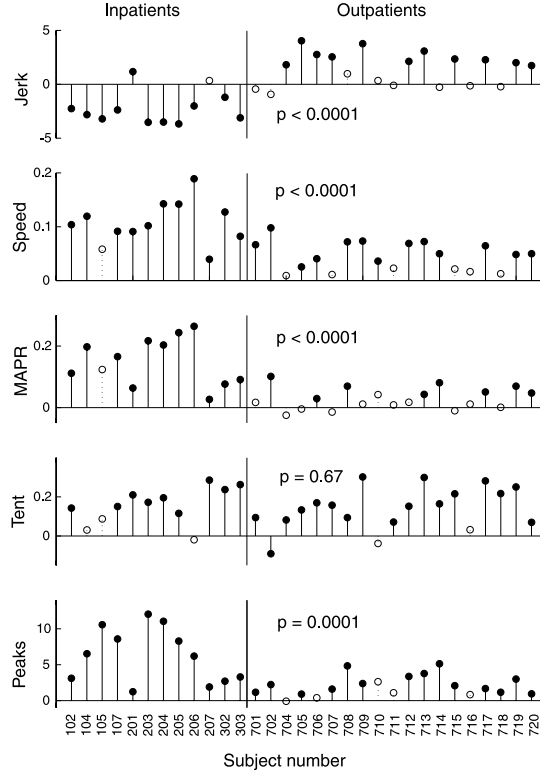


Figure 2-4: Changes in each smoothness metric over the course of therapy for each patient. Increases in smoothness are represented by positive changes in a smoothness metric in every case. Solid circles denote changes that are statistically significant ( $p < 0.05$ ). Statistical significance (p-value) of the difference between the changes in smoothness of inpatient (acute) and outpatient (chronic) populations is shown for each metric. Note that, with one exception, every incidence of a significant decrease in smoothness occurred in the jerk metric with the inpatient group.

In the interest of a clear presentation, the clinical data included here has intentionally been limited to that which was directly relevant to the specific topic of the paper. Other aspects of the data will be discussed in future work.

### 2.4.1 Simulation results

Figure 2-5 displays all five smoothness metrics as a function of simulated submovement blending. Note that increasing blending corresponds to decreasing T, that is, moving from right to left in the figure, rather than left to right. See the Methods section for a detailed description of the simulation.

As T decreases, the metrics generally tend to show an increase in smoothness.

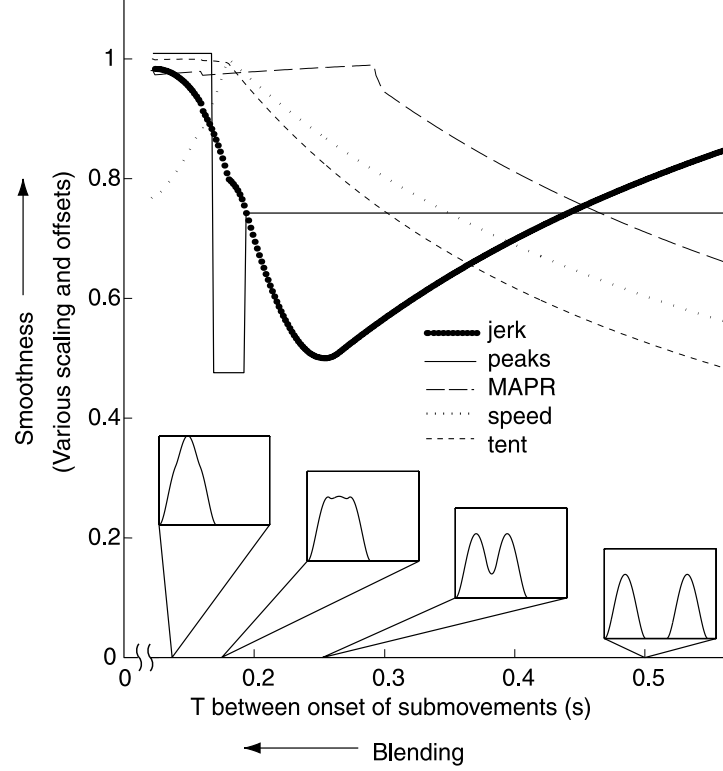


Figure 2-5: Comparison of smoothness metrics during the simulated blending of two minimum-jerk curves. The values of the 5 smoothness metrics are shown for a range of values of  $T$ . Translation to the left along the x-axis represents an increase in sub-movement blending. Translation up the y-axis represents an increase in smoothness. Speed profiles for selected values of  $T$  are shown along the horizontal axis, depicting the state of the simulation at various degrees of blending.

There are a few exceptions to this pattern. The speed metric, MAPR, the peaks metric, and the tent metric increase all saturate or peak at low  $T$  (high blending). Nevertheless, the general trend is that these four metrics increase as blending becomes more complete.

In contrast to the other four metrics, the jerk metric does not generally increase with blending. Although the jerk metric increases with increasing blending over the interval  $0.12s < T < 0.26s$ , it decreases with increasing blending for  $T > 0.26s$ . For most of the range considered, the jerk metric shows that the simulated movements become less smooth as submovements blend. This behavior is not an artifact of the minimum-jerk curves used in the simulation; similar behavior was observed using support-bounded lognormal [70] and Gaussian curves.

As an aside, it is interesting to note that near  $T = 0.19s$ , the peaks metric drops briefly. This occurs because there is a small range of  $T$  for which the composite curve, a blend of two submovements, has three peaks. See Figure 2-2c for an illustration of this phenomenon. This counter-intuitive result, that the sum of two single-peaked curves produces a triple-peaked composite, emphasizes the difficulty of reliably identifying submovements underlying continuous motions. Although this phenomenon is dependent on the nature submovement shape (It does not occur when using Gaussian-shaped submovements, for instance.) it is worthy of consideration. It raises questions about the validity of common methods for submovement identification that rely on counting speed peaks, or on using speed peak locations to initialize local minimization algorithms.

## 2.5 Discussion

### 2.5.1 Movement smoothness increases during recovery

Subjects' increased movement smoothness raises the question: Is the tendency to make movements with smooth, symmetric, bell-shaped speed profiles an epiphenomenon of musculo-skeletal dynamics or is it the result of learned motor behavior? To a limited extent, movement smoothness is a natural consequence of the low-pass filtering properties of the neural, muscular, and skeletal systems. Krylow and Rymer [46] demonstrated this phenomenon, showing that a simple train of electrical pulses produced a movement with a smooth acceleration phase. However, it is notable that the complete movement had a highly asymmetric speed profile, quite unlike normal human movement, indicating that some form of neural coordination (e.g., appropriately timed recruitment of agonist and antagonist muscle groups) would be necessary to produce the approximately symmetric speed profiles typically observed.

Studies of development and recovery from neural injury strongly suggest that smoothness is a result of learned coordination. Infants' movements have been shown to become more smooth (in the sense of having fewer speed peaks) as motor control

improves [87]. This indicates that movement smoothness is a result of a learned, coordinative process, rather than a natural consequence of the structure of the neuromuscular system. Additionally, there is evidence that the segmented nature of stroke patients' arm movements can be attributed to a deficit in interjoint coordination [50]. Taken with our observation that smoothness increases with recovery, the conclusion that smooth movement is a result of well-developed coordination seems inescapable.

### 2.5.2 Evidence for discrete submovements

The 'V'-shape of the jerk metric curve in Figure 2-5 predicts that subjects with poorer blending (on the right half of the 'V') will show decreases in jerk-based smoothness as they recover, whereas subjects with more complete blending (on the left half of the 'V') will show increases in jerk-based smoothness as they continue to recover. This is reflected clearly in the fact that exclusively inpatient subjects showed significant decreases in the jerk metric whereas outpatients, who are presumably closer to their asymptote of recovery, showed only increases.

A second prediction of the curves in Figure 2-5 is that subjects with poorer blending will show marked increases in the other four smoothness metrics as they recover, whereas subjects with more complete blending will show only modest increases as the metrics saturate or peak. This is shown by the fact that increases in smoothness are significantly lower for outpatients than inpatients as measured by MAPR, the peaks metric, and the speed metric. The fact that submovement blending can explain the observed behaviors of the several smoothness metrics we considered lends support to the theory that movement is composed of discrete submovements.

Could the improvement in motion smoothness reflect peripheral factors such as restoring the capability of the system to recruit a sufficiently large number of motor units? If impaired patients were only limited by the magnitude of their neural activation signals, and this quantity increased over the course of recovery, then this theory would predict an increase in peak speed of the movements as well. The data does not support this hypothesis, however. More subjects show peak speed decreases than show increases.

### 2.5.3 Jerk as a smoothness metric

Low jerk is not the only way to quantify smoothness; there are many other possible smoothness measures. For example, minimum-snap (the fourth time derivative of position) described the kinematics of point-to-point drawing movements more accurately than minimum-jerk [72]. However, the measure of the rate of change of movement acceleration provides a compelling real world description of smoothness, and offers several advantages: analytical tractability, computational manageability, and theoretical simplicity.

The fact that many subjects showed an increase in the jerk metric during recovery highlights a distinction between jerk-based notions of smoothness and submovement blending. Care should be taken when assuming that less smooth movements (as measured with jerk) are more impaired or less skilled. The counter-intuitive behavior of the jerk metric in the data and in simulation suggests that, at least during post-stroke recovery, jerk-minimization may not be the primary criterion governing refinements in movement patterns.

The fact that the jerk metric reports a higher degree of smoothness with very low blending than with a moderate amount of blending follows from the definition of the metric. High smoothness corresponds to low average jerk; when a simulated movement consists of two submovements separated by a large period of rest, average jerk will be relatively low, and smoothness therefore is high. And as the two submovements become more blended, they begin to approach each other and the period of rest is shortened. This increases average jerk, decreasing smoothness.

Before embarking on an attempt to extract submovements directly from continuous movement data, the following two chapters present previous published experimental evidence for the existence of submovements, consider and refute alternative explanations for those observations, and address the question of whether it is possible to prove the existence of submovements through experimental observation.



## Chapter 3

# Is the existence of submovements provable?

### 3.1 Summary

All available evidence points toward submovements' existence and no other theory of movement has been proposed that can account for observations of segmentation. However, there is no obvious way to *prove* their existence. Nevertheless, although repeatedly successful decomposition of movement data into submovements may not provide proof of submovements, the quantity of evidence may become so great as to make the question of proof moot.

### 3.2 Introduction

The analysis of stroke patients' movement smoothness tells a story that is consistent with the progressive blending of submovements. However, the existence of submovements is still debated; it would be desirable to establish their existence conclusively. The purpose of this chapter is to explore the provability of the existence of submovements.

The term "segmentation" was originally used to describe the approximately straight

path segments that are produced when humans attempt to make constant curvature movements [1]. Since then, it has been used to describe any scheme of dividing a movement path up into discrete pieces or segments, particularly in handwriting. More generally, it has been used to identify the characteristics of motion that are usually employed to break movements up: non-smoothness of the motion, including velocity maxima or minima and curvature peaks. In this document, segmentation is intended to denote the general episodic, intermittent, and saccadic quality of human movement. For example, segmentation is reflected in the existence of eye saccades and the difficulty humans have moving in constant curvature paths or at constant velocity.

The term “submovements” will be taken to mean specifically the hypothesized, discrete units of movement, which when combined, produce human movement and account for segmentation. The evidence for submovements is a primary topic of this chapter and is presented in the following section.

Section 3.3 examines the compatibility of submovements with reported experimental observations of segmentation. This does not serve to prove or disprove the existence of submovements, but does establish the plausibility of submovements’ existence. Section 3.4 deals strictly with the provability of the existence of submovements.

### **3.3 The existence of submovements is plausible**

Section 3.3.1 contains a summary of the major observations of segmentation in human movement. In section 3.3.2 will present several theories explaining some of these observations, but it will be shown that none of the theories discussed are consistent with *all* the observations. In section 3.3.3, it will be argued that a theory of submovements is consistent with each of these.



### **3.3.1 Summary of experimental observations of segmentation**

#### **Intermittency in human movement**

Woodworth made perhaps the first observation of the intermittent nature of human movement [94] in repetitive reaching tasks. Crossman and Goodeve [17] presented another one of the early descriptions of movement intermittency. They wrote about “systematic fluctuations” in movement velocity which they describe mathematically using Gaussian curves. Theirs is the first of a series of theories presented to describe this phenomenon. Meyer et al. [56] provide a thorough review of these theories.

Intermittency has been observed repeatedly in manual tracking tasks as well [89, 59, 58].

Doeringer [19] observed in a crank turning task that even when subjects are presented with visual feedback of their velocity, they are unable to maintain a constant velocity when asked to do so. Instead, subjects’ velocities fluctuated around the target velocity in an irregular oscillatory fashion. In addition, removal of visual feedback altogether did not remove the intermittent nature of the movements.

#### **Invariant velocity profile**

Many have commented on the invariance of the velocity profile of moderate-speed, low-accuracy, point-to-point movements through space. A number of mathematical descriptions have been presented. Plamondon et al. [72] presents a list of 23 of these descriptions and fits them to movement data. Although more than half of the models fit the data to within two percent, Plamondon et al. are able to show with statistical significance that the support-bounded lognormal curve provides the best fit of all proposed models. Plamondon et al.’s ability to statistically distinguish between so many profiles of such similar shape emphasizes the highly invariant nature of humans’ tangential velocity profiles.

Todorov and Jordan [82] note in their observations of subjects’ unconstrained tracing of various geometric figures that, “the relationship between path and speed

is stronger for movements of shorter duration and is not affected by spatial scale or average speed (it is also rather uniform across tasks and movement paths)” (pg 713). This statement supports the existence of a discrete, highly invariant unit of movement. The fact that, when they are sufficiently short, movements are highly repeatable is consistent with a notion of a movement containing only a single, repeatable discrete unit. That this close correlation breaks down in longer movements suggests that longer movements are composed of multiple units.

### **Asymmetry in accurate movements**

Woodworth [94], a pioneer in psychophysics of movement, made observations over 100 years ago noting asymmetry in the velocity profiles of accurate point-to-point movements<sup>1</sup>. He described a typical movement as consisting of an *initial adjustment* phase and a *current control* phase. In the initial adjustment phase, the limb is transported to the neighborhood of the target, and in the current control phase, small corrections are made to compensate for the inaccuracies of the previous movement(s). The two phases are now more commonly referred to as the transport phase and the correction phase.

This two-phase pattern has been repeatedly noted by researchers. The higher velocity of the transport phase gives the velocity profile a lop-sided or asymmetric appearance. Milner and Ijaz [61] observed that as the size of the target decreased, the shape of the velocity profile during the correction phase became increasingly irregular while that of the transport phase remained relatively constant. Other researchers have also observed that the initial phase of accurate movements is highly invariant [92, 61].

In studying infants’ reaching movements, Von Hofsten [87] observed that the structuring of the movement into two distinct phases was not present in extremely young children, but began at around 4 months. This suggests that the structure of segmentation is a behavior that is learned rather than a product of the neuromuscular system.

---

<sup>1</sup>i.e. point-to-point movements that require the hand to be accurately positioned at movement termination

### **Peaks in curvature occur when tracing circular paths**

Abend et al. [1] demonstrated that peaks in path curvature occur when subjects attempt to trace a constant curvature guide. Rather than following the guide smoothly, subjects' paths deviated from the guide in characteristic patterns. Actual subject paths appeared to be composed of several approximately straight segments, somewhat blended together at their endpoints.

### **Peaks of curvature occur near tangential velocity minima**

Abend et al. [1] noted also that peaks in curvature tend to be coincident with velocity valleys. At the same moment that one nearly straight movement segment was transitioning into the next, the tangential velocity was at or near a minimum. The same relation has been observed in infants' movements [22] and has been referred to as the defining characteristic of human movement [63].

This relationship has been further defined and extended in the  $2/3$  power law. The  $2/3$  power law is an observation that the speed of a movement is approximately inversely proportional to the cube root of the curvature of the movement<sup>2</sup>.

### **Intermittent nature of EMG (in finger movements)**

Vallbo and Wessberg [85] observed movement saccades in subjects attempting to move make very slow finger movements. These saccades were accompanied by pulse-like EMG activity. Agonist and antagonist EMG activity was temporally correlated with the acceleration/deceleration patterns observed, and directly accounted for the intermittent movement. This observation is significant in showing that intermittency (at least in this case) is not simply of mechanical origin (e.g. an oscillating spring-mass system), but is actuated by the muscle.

---

<sup>2</sup>This formulation might be more accurately called the  $1/3$  power law, since the curvature is raised to the  $1/3$  power. Two-thirds came from the original formulation of this law, which was in terms of angular velocity, rather than cartesian velocity, and contained a power of  $2/3$ .

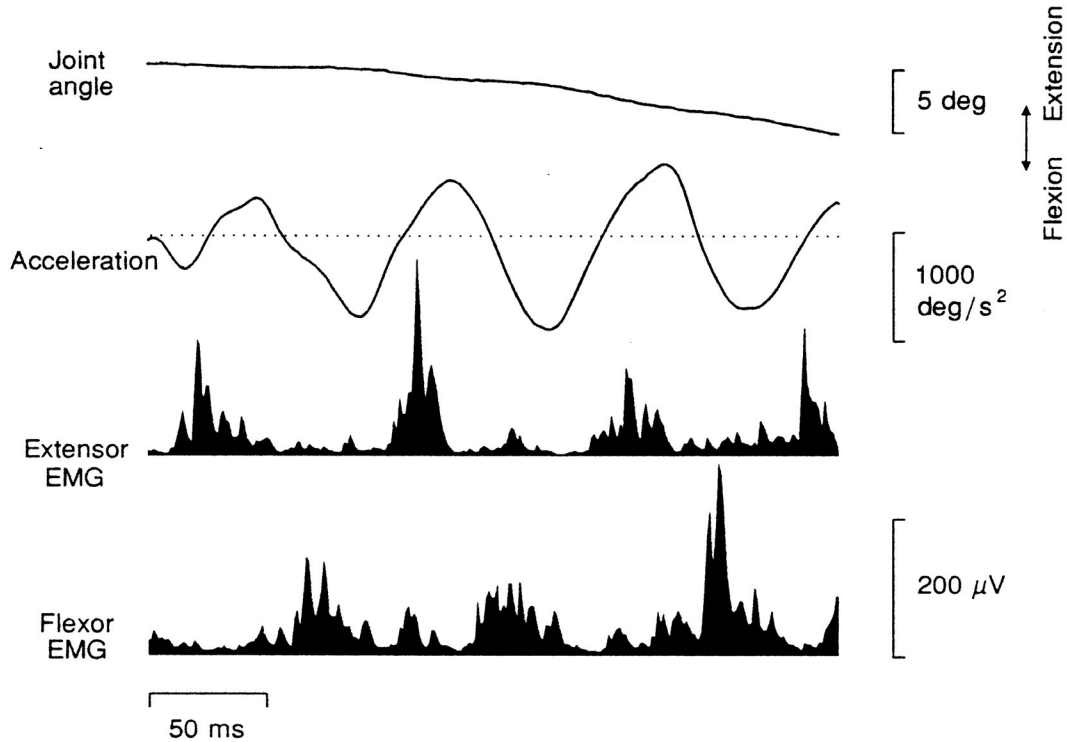


Figure 3-1: Vallbo and Wessberg’s observations of intermittent EMG in finger flexion, reproduced from [85]. Regular, repeatable intermittent movements are observable in position plateaus and acceleration dip/peak pairs. Agonist and antagonist EMG show good temporal correlation with accelerations and decelerations, respectively, showing that the oscillations are not simply mechanical, but are actuated by the muscle.

### 3.3.2 Other theories of movement production are not consistent with all experimental observations of segmentation

#### Neuromuscular mechanics

One explanation for some of the observations of intermittency is that they are in fact due to the mechanics of the neuromuscular system, rather than to any intermittent or episodic activation [41, 78]— for instance, the speed valleys and peaks in curvature that occur in curved movements may only be a manifestation of joint reversals [1].<sup>3</sup>

However, in the case of the preceding examples at least, observations contra-

<sup>3</sup>Instants at which the sign of the angular velocity of a given joint changes sign

dict this theory. In experiments that required subjects to make straight and curved movements in a plane, Abend et al. [1] demonstrated that, during all of the straight movements and some of the curved movements, velocity valleys did not occur, even when joint reversals were required.

On a stronger note, Massey et al. [55] observed a temporal correlation of velocity valleys and curvature peaks in *isometric* “drawing” tasks, effectively eliminating arm mechanics as a possible cause. The velocity and curvature even obeyed the  $2/3$  power law typical of movements in space.

Setting aside the observations of Massey et al [55], that suggest that arm mechanics plays no major role in the temporal correlation between tangential velocity minima and curvature maxima, it is interesting to consider the potential for arm mechanics to explain the phenomenon. See chapter 4 for a more detailed discussion of the significance of temporal curvature-velocity relationships.

## Neural noise

A skeptic may propose that the multi-peaked velocity profiles observed during accurate movements are simply due to neural noise, generating unwanted velocity fluctuations, while a continuous controller homes in on the target.

Doeringer in his Ph.D. Dissertation [19] showed that of three possible locations of an “intermittency generator”, or intermittency source, two were incompatible with his observations. Assuming the intermittency generator could be located in the feedback path, in the direct feedforward path, or in a bypassable feedforward path, Doeringer was able to rule out the visual feedback path and a bypassable feedforward path. He found that the source of the intermittency was in either the direct feedforward path or else in the haptic feedback path.

Although Doeringer was able to narrow down the source of the intermittency, his experiments were not able to establish whether the intermittency was due to random fluctuations or structured variations. However, there are two points in the work of others that undermine the hypothesis that segmentation phenomena are a result of neural noise.

The first is the extraordinarily high invariance of the velocity profile of moderate-speed low-accuracy movements. They contain no evidence of this hypothesized neural noise.

The second is the structure of the fluctuations. They occur at (roughly) regular intervals, rather than at random. The EMG measurements of Vallbo and Wessberg [85] in both the agonist and antagonist muscles showed very periodic and well-coordinated bursts of activity—two attributes very uncharacteristic of random noise.

However the preceding arguments do not imply that the existence of submovements are incompatible with neural noise. Indeed submovements have been shown to be an effective strategy for minimizing movement execution time in the presence of neural noise. Simulations show that both the shape of submovements [93] and their relative timing and amplitude [56] tend to optimize performance in the presence of random noise.

## **Visual feedback**

In pursuit tracking tasks with visual feedback, subjects' movements have been shown to have significant frequency content in the 1-2 Hz range [69, 59]. This is consistent with the visuomotor time delay. Could it not be that all the observations of segmentation are simply due to the effects of visual feedback?

If that were so, then removing visual feedback altogether ought to remove velocity fluctuations, which it does not [19].

In addition, Doeringer and Hogan [20] present an analysis of the effect of feedback delay on linear and non-linear systems. They show that it is unlikely that movement intermittency is the result of a feedback delay. See also [57].

### **3.3.3 Submovements are consistent with experimental observations of segmentation**

A theory of submovements is consistent with each of the observations in the previous section.

**Intermittency** Intermittency would be expected from a process that sums discrete units in time to create a whole. It is not unreasonable to expect that the characteristics of the individual units would be at least partly apparent in the finished product.

**Invariance of the velocity profile** The velocity profile invariance that has been so often reported is consistent with movement that is produced using movement units that are not only discrete, but very similar in nature.

**Asymmetry in accurate movements** Several researchers have theorized that asymmetry in accurate movements is a result of discrete corrective movements being appended to an initial, larger movement. The theory describes the initial movement as a first approximation to the goal and the following movements as corrective refinements.

These asymmetric tangential velocity profiles have been described as a linear superposition of the velocity profiles discussed in section 3.3.1 [9, 63] (see figure 3-2, taken from [60].).

**Peaks in curvature when tracing circular paths** These peaks are not only consistent with discrete movement units, but suggest that those movement units are approximately straight.

**Peaks in curvature near tangential velocity minima** This also is consistent with straight submovements being spliced together, each having the bell-shape of the invariant tangential velocity profiles mentioned earlier. Providing additional support for this idea is the work of Flash and Henis [24] in which they showed a convincing picture of the summation of discrete bell-shaped speed profiles during movements in which patients were presented with a second target mid-movement.

**Intermittent EMG** This is certainly consistent with submovements as well. An episodic muscle activation signal is to be expected if episodic movement is the

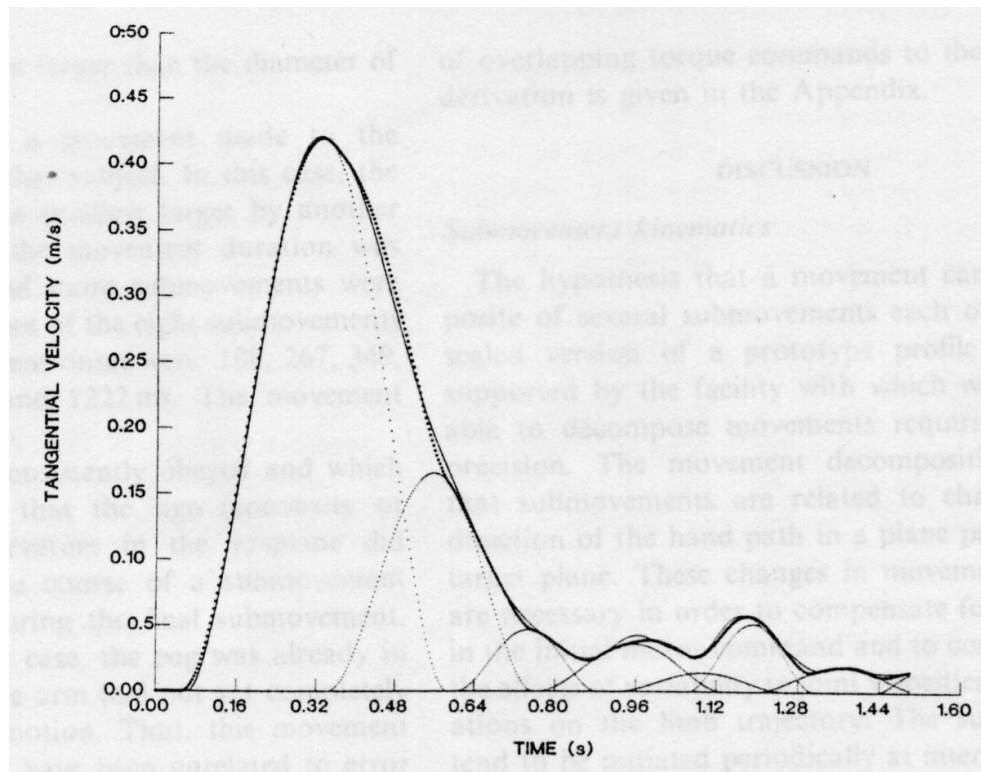


Figure 3-2: An example of decomposition of the tangential velocity of an accurate movement into prototype submovements, taken from [60].



result of discrete movement commands, and not an artifact of some other process.

The ability of a theory of submovements to explain observations of segmentation does not prove its validity. There certainly may be other theories that are also consistent with existing observations of segmentation. However, the plausibility of submovements does indicate that the endeavor to prove or disprove their existence is a worthwhile one.

## **3.4 The provability of the existence of submovements**

### **3.4.1 A theory of submovements**

The provability of the existence of submovements is a strong function of the way in which a theory of submovements is formulated. For the purposes of this work, the essential feature of a theory of submovements is its discrete nature. The theory can be formulated as follows:

**Movement is composed of discrete units.**

### **3.4.2 Difficulties in testing**

It is not immediately obvious how to test this theory. If a movement is composed of discrete units, that implies that it can be decomposed into those units, given that there is sufficient information about the nature of the units and how they combine. On the other hand, even if a movement can be decomposed into discrete units, that does not necessarily imply that it was created by summing discrete units. No amount of success in decomposing a movement into submovements can constitute proof that the original movement was constructed through a combination of those submovements, however strongly suggestive it might be. A graphical example is given in figure 3-3, illustrating that even decomposition with zero error does not show uniqueness of

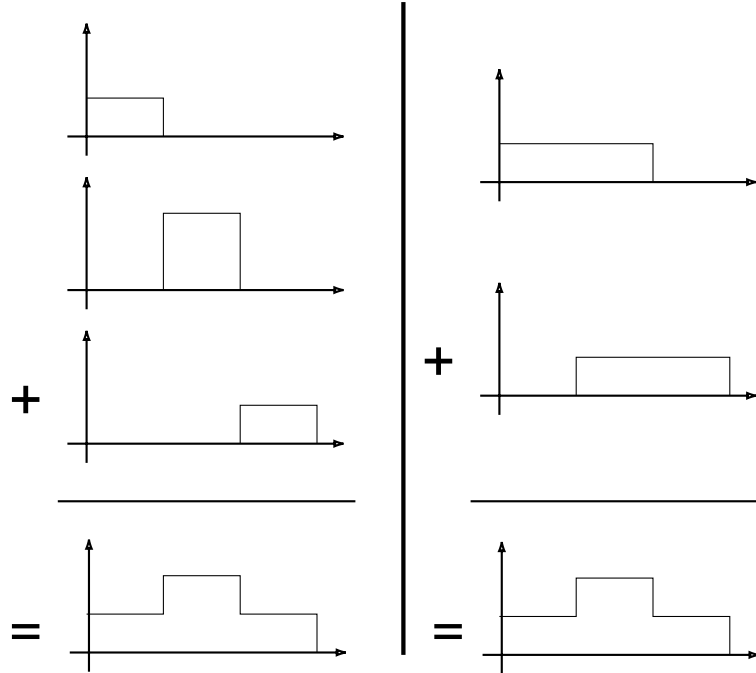


Figure 3-3: An example of non-unique, zero-error decompositions of a velocity profile. In each case, the function consists of linearly summed “sub-functions”: translated, dilated, and scaled versions of a unit box. The decomposition of the composite function (shown at bottom) is non-unique, despite the fact the sum of the sub-functions recreates the original function with zero error.

decomposition. It may be that the only way to prove such a theory would be to perform measurements on the higher levels of the neuromotor system until a discrete representation of the descending commands is isolated.

### 3.4.3 Toward a *testable* theory of submovements

Despite the bleak prognosis of the previous paragraph, it may be possible to provide a preponderance of evidence for submovements, such as would make the question of proof moot. For instance, if it is possible, given many subjects at a variety of ages and with a variety of neuropathologies, to show similar patterns in the decompositions of all their movements, that would provide strong evidence in favor of discrete submovements. In addition, if it was discovered that a certain population (e.g. patients with a certain neurological disease) had movements that decomposed very differently or did not decompose cleanly at all, this would help pinpoint the physiological location

where submovements are generated (if such an area exists).

Given this, it becomes necessary to aim a little lower and reformulate a testable, but lesser theory of submovements.

A number of possible statements of a lesser theory of submovements is listed here in order to illustrate the differences in what may be included in such a theory.

1. Tangential velocity profiles of the hand during unconstrained movements can be accurately described by summing translated, scaled, and dilated versions of a prototype tangential velocity profile.
2. Spatial velocity profiles of the hand during unconstrained movements can be accurately described by vector summing translated, scaled, dilated, and rotated versions of a prototype velocity profile directed along a straight line.
3. Joint torque profiles of the elbow and shoulder can be accurately described by summing translated, scaled, and dilated versions of a prototype joint torque profile.
4. Neural excitation of a given muscle (as measured by EMG activity) occurs at intervals in discrete “packets” of activity, which may combine to produce complex EMG profiles.
5. Descending motor commands from the CNS are discrete, resulting in the observations of segmentation reported previously in section 3.3.
6. Thought itself is fundamentally discrete and this is manifest not only in the discrete nature of discrete movement, but also in the discrete nature of speech (put forth in [11]).

It is clear from examination of the list above that, depending on how one chooses to define a theory of submovements, proof of that theory may either be trivial or essentially impossible. In theories 1, 2, and 3, if the number of prototypes used is permitted to grow very large, any function can be described as a composite of the scaled prototype functions with arbitrary accuracy. If no lower bounds are placed

on submovement duration or the number of submovements employed, verification of these three theories is trivial. On the other hand, there is no obvious way to prove theory 6 as no (engineering) tools currently exist that are capable of recording thought or measuring its characteristics.

The majority of the work done that discusses submovements, follows along the lines of theory 1. Investigation of theory 1 has likely been motivated by the fact that it requires only kinematic data from movements and is limited to a single dimension. Although theory 2 uses only kinematic data as well, it makes the problem multi-dimensional. Theory 3 requires estimation of arm mechanics, making it still more complex. Theory 4 requires measurement of EMG, which is characteristically difficult to do reliably, and once done, difficult to process. Validation of theory 5 requires access to signals and information that are difficult to obtain. And it is not clear how to approach the validation of theory 6.

#### **3.4.4 A first pass**

Theory 1 provides a good starting point for validating the existence of submovements. This approach has the advantage of being familiar to the motor control community, and thus simpler to communicate to others. When candidate speed profile descriptions of submovements are limited to a single base shape, this method is straightforward to implement. It is also logical to choose a kinematic description of submovements, as many of the observations of movement invariance have been kinematic in nature.

In testing theory 1, a reliable method for extracting submovements from continuous human movement data is required. Chapter 5 outlines shortcomings in existing methods and develops a novel extraction algorithm. See Appendix C for a literature review of experimental observations of some submovement properties.

The following chapter explores more fully the potential for the commonly observed curvature-velocity relation in human movement to be explained by neuro-muscular mechanics, as opposed to a segmented control scheme.

## Chapter 4

# The curvature–velocity relation of human movements

### 4.1 Summary

The reported synchrony between curvature maxima and velocity minima is approximate. A condition that ensures synchrony in a mechanical system is given. Synchrony follows from the two-thirds power law. The two-thirds power law is argued to be an epiphenomenon, an artifact of the inherent smoothness of movement, and not of segmented control. It is possible that synchrony is an epiphenomenon as well. Any arguments or analysis based on an a priori assumption of the validity of the two-thirds power law or synchrony should be viewed with skepticism.

### 4.2 Introduction

In the course of investigating the potential for neuro-muscular mechanics to explain movement phenomena attributed to submovements, the following analysis was performed. Some debate in the motor control community has centered around the strikingly close temporal relationship between curvature and velocity in unconstrained human movements.

Why is an investigation into the temporal relation of curvature peaks and velocity minima worthwhile? It has been used as a support for the existence of submovements as a feature of motor control. Showing that the relation is explainable by mechanics would undermine this argument.

### 4.3 Curvature maxima and velocity minima in human movements are in fact *not* strictly synchronous

The synchrony reported between velocity minima and curvature maxima is only approximate. This is apparent in the data reported by Abend et al. [1], one of the first groups to report the synchrony. The figure 4-1 is an excerpt from [1] that Abend et al. use to demonstrate the synchrony phenomenon. As can be seen from the curve on the left, synchrony is shown where there is not even a minimum, only a 'dip' in velocity. Also, a magnification of the center curve, shown in figure 4-2 shows that the synchrony is not exact. The velocity minimum distinctly lags the curvature peak.

In addition, Wann et al.'s plot of simulated ellipse drawing (figure 3A in [88], reproduced in Figure 4-3, shows slight, but distinct asynchrony. The simulation performed by the authors employed summations of *asymmetric* velocity profiles; simulations of symmetric velocity profiles do not produce this effect. Human submovements tend to be symmetric, but often deviate from symmetry on a given movement [67].

These observations are consistent with the preliminary analyses of the movements of stroke patients, which also show some small asynchrony between velocity minima and curvature maxima.

Despite the fact that the synchrony is approximate, the question still remains: Is the approximate synchrony simply an epiphenomenon due to mechanics?

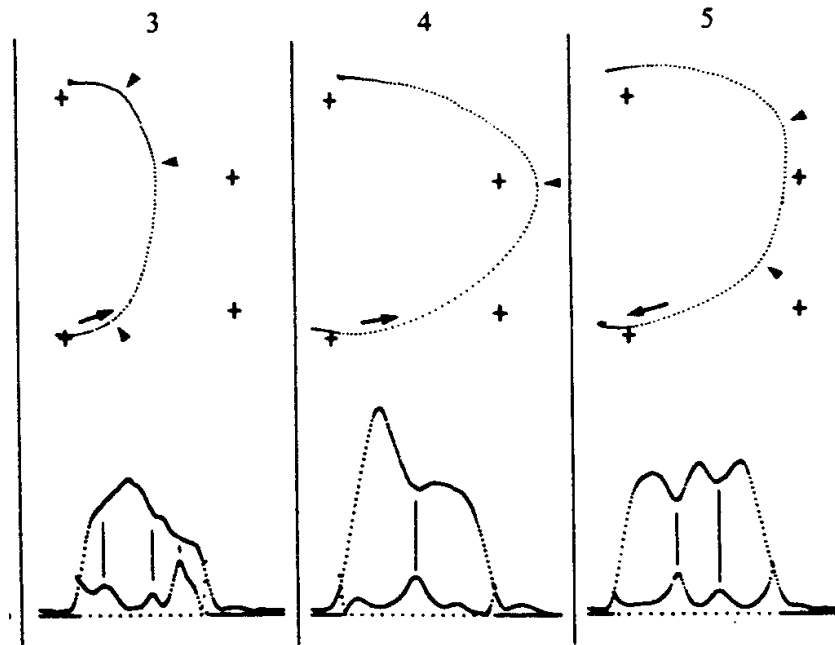


Figure 4-1: Abend et al.'s data in which was observed synchrony between velocity dips and curvature peaks. Note that the 'dips' in velocity in the plot on the left are not minima at all.

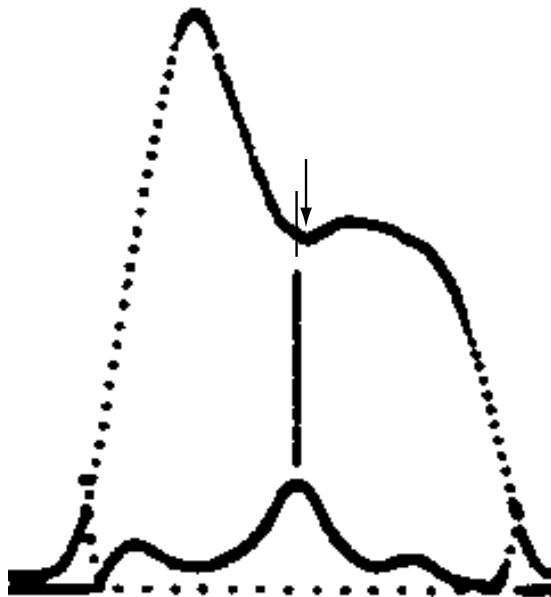


Figure 4-2: Magnification of the previous figure Note the asynchrony between the curvature maximum and the velocity minimum.

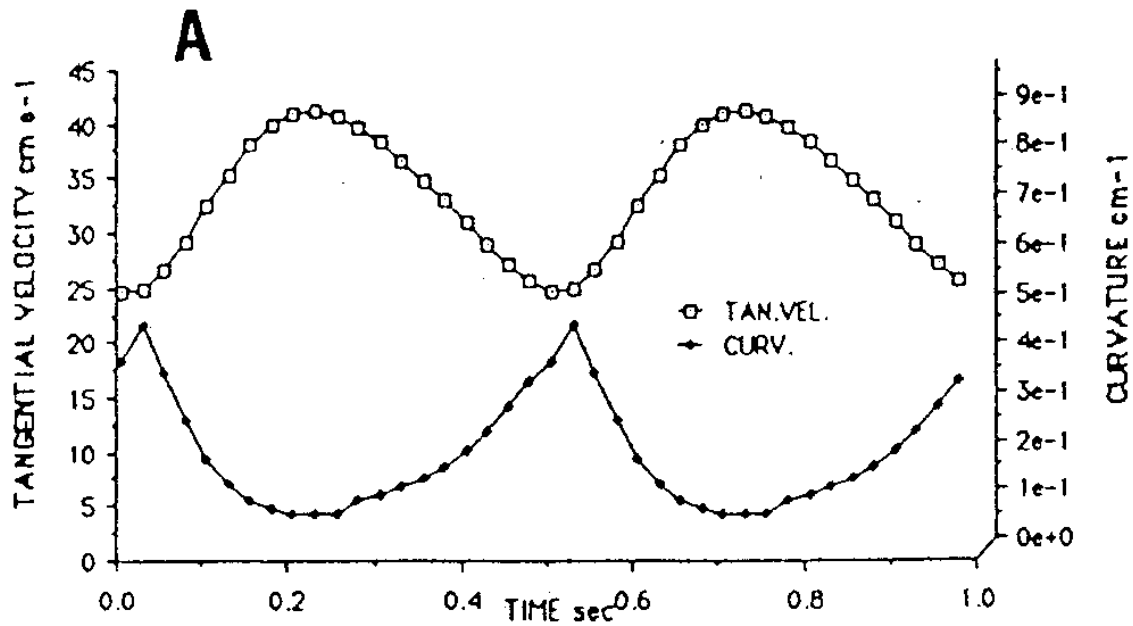


Figure 4-3: Asynchrony in simulated speed-curvature data, reproduced from [88]. Note that the peak in curvature lags the dip in speed by a full sample, 25 ms.

#### 4.4 There is no mechanical requirement that curvature and velocity extrema be synchronous in general

A thought experiment shows that there need not necessarily be any temporal relation between curvature and velocity extrema in a mechanical system. Given any smooth path (any finite curvature as a function of path length) and any continuous, piecewise differentiable velocity profile as a function of path length, the forces required to move a mass according to the specified path and velocity will be finite, and thus the trajectory will be theoretically feasible.

This example can be pictured as an idealized car traveling on a winding road. If the tires are sticky enough, the brakes good enough, and the engine powerful enough, the car will be capable of following any desired velocity profile, regardless of the curvature of the road.



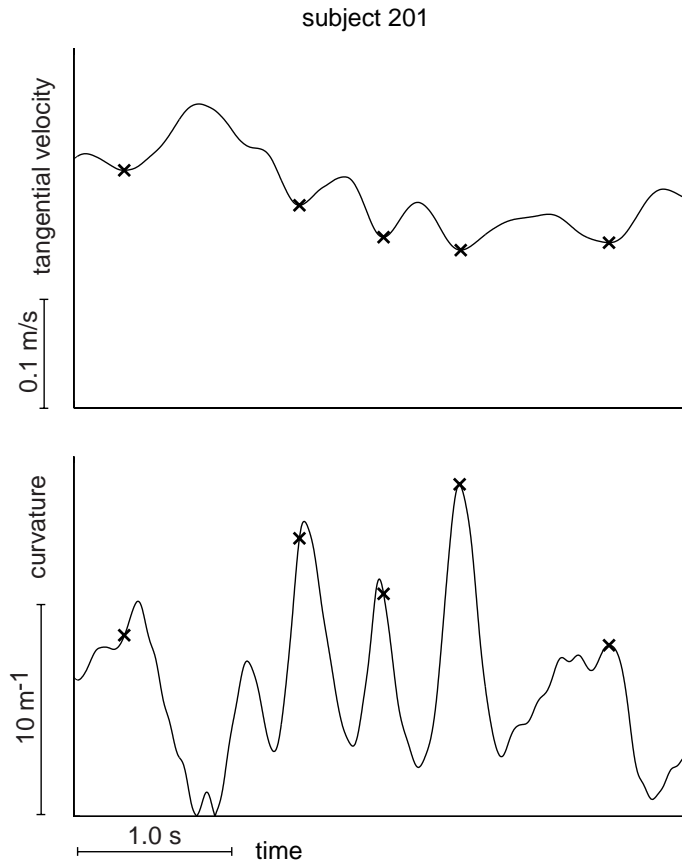


Figure 4-4: Instances of asynchrony in data taken from a stroke patient's movements while holding a manipulandum. Each "x" marks the time at which a minimum in tangential velocity is reached. Curvature tends to be a maximum at these points, but can peak before or after velocity does. The largest of the time discrepancies between speed and curvature in the data shown here is approximately 90 ms.

## 4.5 A kinematic velocity-curvature relation

An appropriate follow-on question remains: Which minimal set of characteristics of a mechanical system must exist in order to produce temporal correlation of velocity minima and curvature maxima? The kinematic velocity-curvature relation given in this section represents a first step toward an answer for this question.

For a general trajectory, where  $r$  is the instantaneous radius of curvature,  $v$  is the magnitude of the velocity at a given instant and  $a_r$  is the magnitude of the component of acceleration that is perpendicular to the tangential velocity, a simple kinematic relation between velocity and curvature can be derived.

$$a_r = \frac{v^2}{r} \quad (4.1)$$

$$\frac{a_r}{v^2} = \frac{1}{r} \quad (4.2)$$

$$\equiv \kappa \quad (4.3)$$

It should be noted that equation 4.3 is valid, regardless of the trajectory or the system that generated it.

## 4.6 A condition for synchrony between velocity extrema and curvature extrema

In order for velocity extrema to coincide with curvature extrema, their time derivatives must both be zero at the same instant.<sup>1</sup> Taking the derivative of equation 4.3 gives the following:

$$\dot{\kappa} = \frac{v\dot{a}_r - 2a_r\dot{v}}{v^3} \quad (4.4)$$

Inspection of equation 4.4 shows that, for  $\dot{\kappa} = 0$ ,  $\dot{v} = 0$  necessarily only when

---

<sup>1</sup>This analysis, for the time being, does not consider inflection points.

$v\dot{a}_r = 0$  and  $a_r \neq 0$ . For the purposes of this analysis, it will be assumed that  $a_r \neq 0$ , since  $a_r = 0$  implies zero curvature, a degenerate case. Likewise, as curvature is undefined when  $v = 0$ , it will be assumed that  $v \neq 0$ .

This leaves  $\dot{a}_r$  as the quantity of interest. Only if  $\dot{a}_r = 0$  when  $\dot{v} = 0$  can velocity extrema and curvature extrema said to be coincident (points of zero curvature excluded).

Since  $v$  is the magnitude of the velocity,  $\dot{v}$  is the magnitude of the tangential acceleration,  $a_t$ , or acceleration along the path of the trajectory. The condition for synchrony then becomes:  $\dot{a}_r = 0$  when  $a_t = 0$ .

## 4.7 A dynamics-based condition for synchrony

A condition for synchrony can be found through a dynamics-based analysis.

Consider a planar system with a fixed (inertial) coordinate system.  $\mathbf{h}$  is the momentum vector,  $\mathbf{I}$  is the inertia tensor,  $\mathbf{v}$  is the velocity vector,  $\mathbf{a}$  is the acceleration vector, and  $\mathbf{F}$  is the force vector.

$$\mathbf{h} = \mathbf{I}\mathbf{v} \quad (4.5)$$

$$\dot{\mathbf{h}} = \dot{\mathbf{I}}\mathbf{v} + \mathbf{I}\mathbf{a} \quad (4.6)$$

$$= \mathbf{F} \quad (4.7)$$

$$\dot{\mathbf{F}} = \ddot{\mathbf{I}}\mathbf{v} + 2\dot{\mathbf{I}}\mathbf{a} + \mathbf{I}\dot{\mathbf{a}} \quad (4.8)$$

$$\mathbf{I}\dot{\mathbf{a}} = \dot{\mathbf{F}} - \ddot{\mathbf{I}}\mathbf{v} - 2\dot{\mathbf{I}}\mathbf{a} \quad (4.9)$$

Assuming that the inertia is non-zero, it is clear that

$$\dot{\mathbf{F}} = \dot{\mathbf{I}} = \ddot{\mathbf{I}} = \mathbf{0} \Rightarrow \dot{\mathbf{a}} = \mathbf{0} \quad (4.10)$$

and since

$$\dot{\mathbf{a}} = \mathbf{0} \Rightarrow \dot{a}_r = 0 \quad (4.11)$$

equation 4.10 gives three conditions which, when met, guarantee synchrony: a) external forces are constant and b) first and c) second derivatives of the inertia with respect to time are zero.

### 4.7.1 A special case

It can be shown that a mass ( $m$ ) connected by a linear spring (of stiffness  $k$ ) to a fixed point satisfies these conditions and thus exhibits perfect synchrony between velocity minima and curvature maxima.  $F$  is the force in the spring,  $s$  is the spring displacement,  $v$  is the tangential velocity of the mass, and  $E$  is the total energy in the system.

$$E = \frac{1}{2}ks^2 + \frac{1}{2}mv^2 \quad (4.12)$$

$$\dot{E} = ks\dot{s} + mv\dot{v} \quad (4.13)$$

$$\dot{E} = 0 \text{ (conservative mechanical system)} \quad (4.14)$$

$$\dot{v} = 0 \text{ (velocity is at a minimum)} \quad (4.15)$$

$$\Rightarrow \dot{s} = 0 \quad (4.16)$$

$$\text{Also, } F = ks \quad (4.17)$$

$$\dot{F} = k\dot{s} + \dot{k}s \quad (4.18)$$

$$\dot{k} = 0 \text{ (} k \text{ is constant wrt time and position)} \quad (4.19)$$

$$\Rightarrow \dot{F} = 0 \quad (4.20)$$

This result, together with the fact that  $\dot{m} = 0$  and  $\ddot{m} = 0$ , shows that synchrony must hold for the mass-spring system.

## 4.8 A note on near-synchrony in human movements

Despite the fact that condition 4.10 is not met in general during human movements, they exhibit near-synchrony. The special case of the simple mass and spring system given above may provide an explanation for why this is so. The fact that the human neuromuscular system can be modeled to a first approximation as an inertia being pulled on by a spring indicates that neuromuscular mechanics may well be responsible for the near-synchrony.

However, it should be noted that this is mere speculation and is not rigorously supportable by the analysis presented here. In order to strengthen this argument, two key questions would need to be answered:

1. How big an affect do departures from the conditions in equation 4.10 have on synchrony?
2. How significant are the departures from the conditions in equation 4.10 in human movement?

Based on the analysis in this chapter alone, it is impossible to rule out that synchrony is due to arm mechanics.

## 4.9 The Two-thirds Power Law

The two-thirds power law can be formulated as follows:

$$v = \frac{C}{\kappa^{(\beta-1)}} \quad (4.21)$$

where  $v$  is tangential velocity,  $C$  is a constant of proportionality,  $\kappa$  is curvature, and  $\beta$  is a constant. In observations of human movements,  $\beta$  varies somewhat, but generally  $\beta \approx 2/3$  [55]. This law has been cited by a number of researchers and described as a defining characteristic of human movement. Viviani and Cenzato

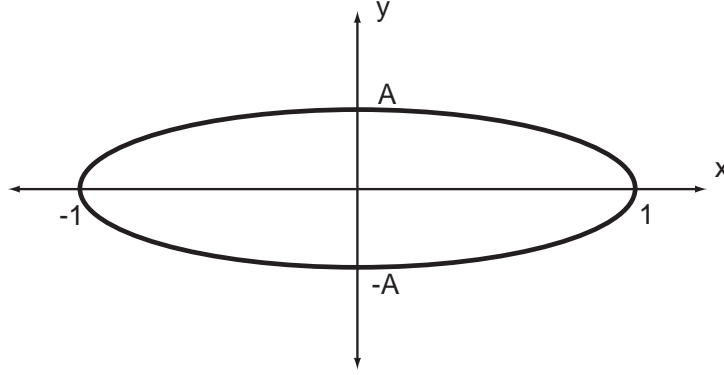


Figure 4-5: An elliptical path, such as is produced by out-of-phase sinusoidal oscillations. The major axis is of length 1 and the minor axis is of length  $A$ .

assume its validity in their analysis of segmentation of complex movements [86]. Does this law provide insights into control strategy? or is it explainable in some other way?

Just as with synchrony in the preceding sections, it can be shown that some simple mechanical systems obey the two-thirds law. For instance, any ellipsoidal oscillations resulting from coupled orthogonal sinusoidal oscillations (such as are found in linear-spring-point-mass systems) obey the two-thirds power law [88].

A simple example, consisting of an elliptical path (see Figure 4-5) is shown here:

$$x = \cos(t) \quad (4.22)$$

$$y = A \sin(t) \quad (4.23)$$

$$v_x = -\sin(t) \quad (4.24)$$

$$v_y = A \cos(t) \quad (4.25)$$

$$a_x = -\cos(t) \quad (4.26)$$

$$a_y = -A \sin(t) \quad (4.27)$$

$$v = (v_x^2 + v_y^2)^{1/2} \quad (4.28)$$

$$\kappa = \frac{v_x a_y - a_x v_y}{(v_x^2 + v_y^2)^{3/2}} \quad (4.29)$$

$$= \frac{(-\sin(t))(-A \sin(t)) - (-\cos(t))(A \cos(t))}{v^3} \quad (4.30)$$

$$= \frac{A(\sin^2(t) + \cos^2(t))}{v^3} \quad (4.31)$$

$$= \frac{A}{v^3} \tag{4.32}$$

$$v\kappa^{1/3} = A \tag{4.33}$$

In this example, which is typical of motion created in a point-mass-central-spring system, the tangential velocity is shown to be inversely proportional the the cube root of the curvature, as is necessary for compliance with the two-thirds power law.

Similarly, a simple inertia–stiffness model of the neuromuscular system provides a plausible mechanical explanation for observations of the two-thirds power law.

### 4.9.1 Shortcomings of the Power Law

Wann et al [88] show that the two-thirds power law breaks down when significantly asymmetric velocity profiles are employed to generate movement. They demonstrate that, in a repetitive ellipse–drawing task, subjects do indeed generate significantly asymmetric velocity profiles when temporal and path constraints are relaxed and subjects are allowed to choose a comfortable movement speed. They warn that any movement analysis that is based on an a priori assumption of compliance with the two-thirds power law should be viewed with a healthy amount of suspicion.

Along similar lines, Todorov and Jordan [82] show that the two-thirds power law is a special case of a jerk-minimization optimization criteria and conclude that observations of the power law are simply an artifact of the inherent smoothness of movements<sup>2</sup>. They demonstrate that the two-thirds power law fails to account for significant features in experimental data, and that those features are accounted for by a minimum-jerk model.

In a pair of papers Sternad and Schaal [80, 76] took this a step further They showed that two criteria that have been used previously for segmenting continuous movements—sudden changes in parameters the two-thirds power law and observations of piecewise planar movement paths—can be reproduced very well in a *continuously*

---

<sup>2</sup>The origin of the smoothness in human movement, whether in the neural control system or in the low-pass filtering characteristics of the neuromuscular system, is a separate topic and will not be addressed here. But it is surely one worthy of attention.

controlled anthropomorphic seven degree of freedom robot. They argue that the observation of the two-thirds power law is limited to movements in which the mapping from joint-space to workspace is nearly linear, and that non-negligible departures from the power law occur when the non-linearities of arm kinematics become significant. Unlike Todorov and Jordan, Sternad and Schaal do not assume a minimum jerk model. Instead, they assert more generally that smoothness of the movement in *joint coordinates* explains both the observations of the power law and departure from the power law. It should be noted that Sternad and Schaal investigated cyclical, unconstrained movement, and they caution the application of their theory to discrete movements.

## 4.10 A relationship between synchrony and the two-thirds Power Law

Synchrony is implied by the two-thirds power law. Differentiating the power law yields a relation which guarantees synchrony.

$$v = \frac{C}{\kappa^{\frac{1}{3}}} \quad (4.34)$$

$$\dot{v} = (-1/3) \frac{C}{\kappa^{\frac{4}{3}}} \dot{\kappa} \quad (4.35)$$

$$\dot{v} = 0 \Rightarrow \dot{\kappa} = 0 \text{ (given } C \neq 0, \kappa \neq 0) \quad (4.36)$$

Since  $v$  and  $\kappa$  are inversely related, a minimum in tangential velocity corresponds to a maximum in curvature. If the two-thirds power law holds, then synchrony must be present as well. The contrapositive, that a departure from synchrony is necessarily accompanied by a departure from the power law, is also true. It is noteworthy that the conditions under which large departures from the power law were observed, in particular large movements, are also conditions under which deviations from synchrony would be expected to fail. Recall the sufficient condition given for synchrony



in equation 4.10:

$$\dot{\mathbf{F}} = \dot{\mathbf{I}} = \ddot{\mathbf{I}} = \mathbf{0} \quad (4.37)$$

The inertia tensor of the arm can be modeled to a first approximation as constant within a moderately small workspace. However, expanding the workspace increases the variability of  $\mathbf{I}$  over the course of the movement, and makes contributions to  $\dot{\mathbf{I}}$  and  $\ddot{\mathbf{I}}$  more significant. In the phraseology of Sternad and Schaal, in larger movements the kinematic nonlinearities of the arm play a more significant role in determining the characteristics of the movement. This *may* effect a departure from synchrony. However, since the condition given in equation 4.10 is only a sufficient and not a necessary one, it is not clear whether non-zero values of  $\dot{\mathbf{I}}$  and  $\ddot{\mathbf{I}}$  necessitate a departure from synchrony.

#### 4.10.1 Is synchrony an epiphenomenon?

Although several of the authors cited above have concluded that the two-thirds power law is an epiphenomenon, the validity of synchrony as a phenomenon remains in question. Even though synchrony can be derived from the power law, synchrony is a more general condition. And even though the previous paragraph postulates departures from synchrony with larger movements, this remains speculative and is an open research question. Either with further data processing on the experiments conducted in [80, 76, 82] or with a new experiment, the evidence necessary to support or refute synchrony as a phenomenon still needs to be gathered. For the time being, the validity of any analysis that is based on an a priori assumption of either synchrony or the two-thirds power law should be called into question.

Taking the evidence and discussion of chapter 3 as sufficient to form a working hypothesis of submovements, the following chapter outlines an algorithm for directly extracting them from continuous movement data, rather than relying on markers such as velocity minima or curvature maxima. A reliable method capable of global

nonlinear optimization is outlined.

# Chapter 5

## Avoiding spurious submovement decompositions: A globally optimal algorithm

From a manuscript in review.

Authors: B Rohrer, N Hogan

### 5.1 Summary

Evidence for the existence of discrete submovements underlying continuous human movement has motivated many attempts to “extract” them. Although they produce visually convincing results, all of the methodologies that have been employed are prone to produce spurious decompositions. Examples of potential failures are given. A branch-and-bound algorithm for submovement extraction, capable of global nonlinear minimization (and hence, capable of avoiding spurious decompositions) is developed and demonstrated.

## 5.2 Introduction

Observations of the submovement-like phenomena, such as those listed in section 3.3, have motivated several attempts to produce a general methodology for isolating submovements. See [63, 24, 60, 6, 49, 9]. If successful, such decompositions of movement into their constituent discrete building blocks would provide a new window through which to observe the operation of the human motor control system. In this paper, we show that previous decomposition attempts can produce spurious results, and we present an algorithm that is guaranteed not to do so.

Submovements are theoretically attractive, because they provide a compact language for concisely coding movement. Under the working hypothesis that these discrete units of movement exist, the ability to accurately isolate and characterize them would provide a description of human movement on a fundamental level that has not previously been available. As such, submovement analysis could provide new insights into studies of motor performance, rehabilitation, and the human motor control system.

However, since the posited underlying discrete commands are not directly available, there is no way to verify that a given decomposition is accurate. Accuracy can be inferred only by examination of the residual error. It is important to note that, although inaccurate decompositions may only have slightly higher residual error, the characteristics of the submovements that they employ may be completely spurious. Figure 5-1c and d shows an example of this phenomenon, and will be discussed in more detail in the following section. Of course, even zero decomposition error does not prove that submovements actually exist. Nevertheless, in testing an empirically-motivated theory of submovements, highly successful decompositions would certainly lend some degree of support to the theory.

Submovement decomposition is a non-linear optimization problem: simultaneously maximizing goodness of fit and minimizing the number of submovements used, given a submovement shape (e.g. minimum-jerk [35] or Gaussian [17]; see Appendix B) and a summing modality (e.g. scalar summation [63]) or vector summa-

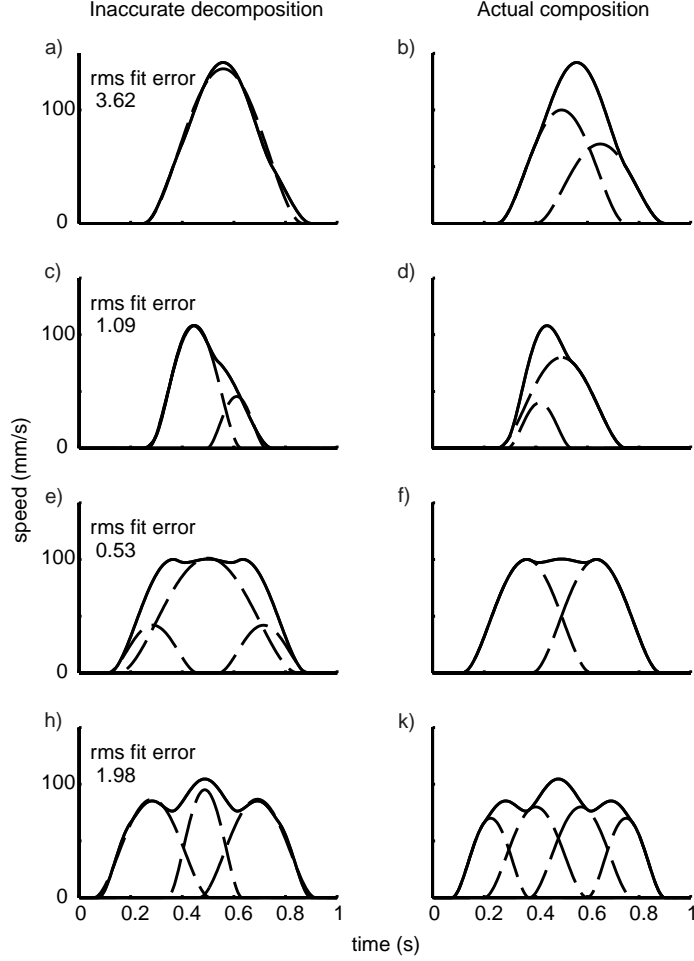


Figure 5-1: Problematic decompositions for current algorithms. The panels on the right show the construction of the curves. The panels on the left show local minima in decomposition. In each case the decomposition error is low, but the submovement characteristics do not resemble those used to construct the curve.

tion [24]). As a non-linear optimization problem, it may have multiple local minima. However, all the optimization methods that have been applied to it previously are sensitive to getting caught in local minima and cannot guarantee a globally optimal solution. Gradient descent [6] and Powell’s Direction Set Method [49] have been used in this context, as well as manually adjusting (“eyeballing”) submovement parameters [63, 60]. The optimality of the solution for these methods depends heavily on the quality of the initial guess; unless the initial guess is in the neighborhood of the global minimum, they will not find the best solution.

### 5.2.1 The difficulty of making a good initial guess

Making an initial guess that is in the neighborhood of the solution is not trivial. The right column of Figure 5-1 shows several examples of speed profiles that pose problems for existing decomposition methods. Each speed profile is composed of minimum-jerk submovements which sum in a scalar fashion. Despite the fact that only a few, simply-parameterized submovements are used, the false decompositions are accurate to within as little as 0.5%. This illustrates the challenge that decomposition algorithms face in attempting to find the optimal solution.

Each speed profile shown has a different number of peaks than it has submovements. Any method that uses the number of peaks to estimate the number of submovements would fail to make an initial guess in the neighborhood of the global optimum. Examples of such failed decompositions are shown in Figure 5-1, panels **a**, **e**, and **f**.

The second movement (panels **c** and **d**) of Figure 5-1 is of particular interest. It resembles the observed speed profiles of target-directed movements made by human subjects under moderate accuracy constraints [61]. Although decompositions similar to those shown in panel **c** have been assumed in previous analyses of such movements [60], this example shows that other combinations of submovements can yield very similar shapes (see also Figure 3-3). Figure 5-1 panels **h** and **k** provide a similar example (compare to Figure 2-2, panel **g** to see biological plausibility). These cases illustrate the difficulty in making objective initial guesses and shows the high level of caution required when employing any technique that relies on subjective judgments.

Listed below are several methods for making initial guesses that have been previously applied to submovement decomposition. As originally implemented, some of the initial guessing methods below have not been used to initialize local minimization routines (such as gradient descent), but could be used to do so in theory.

### 5.2.2 Initial guess methods

*Subjective selection.* Lee et al. [49] have made initial guesses based on subjective

estimation of submovement characteristics. This method is subject to the limitations illustrated in Figure 5-1; submovement characteristics are difficult to intuit based on the speed profile, and therefore the initial guess is not guaranteed to be near the global optimum.

*Matching Pursuit* [54]. Matching Pursuit is a “greedy” algorithm; it finds the best fit for a single element at a time, rather than for a set of elements. Matching Pursuit iteratively finds the submovement which, when subtracted from the function, minimizes the residual error. This repeats until some minimum error threshold is reached. The limitations of the Matching Pursuit algorithm are described in detail by Chen et al. [13]. The fact that Matching Pursuit fits a single submovement at a time does not allow it to optimize the fit for all submovements. Simple functions composed of as few as two submovements are incorrectly decomposed, because of the greedy nature of the algorithm, as shown by Doeringer [19]).

*Local fitting of the highest peak.* The Irregular Sampling Radial Basis Function algorithm [44] and the method of Berthier [6] are also greedy algorithms. At each iteration, both of these algorithms fit a submovement to the highest speed peak and its local neighborhood, and the fit function is subtracted from the original speed profile. As in Matching Pursuit, the process is repeated until either an error threshold is reached or a maximum number of submovements are fit. As illustrated in Figure 5-1, aligning submovements with the highest speed peak provides no guarantee that the sub-functions chosen actually coincide with those used to construct the original function.

*Milner’s method.* Milner used zero velocity and maximum curvature points along individual axes to mark the onset of submovements in 3D movements [60]. As implemented, Milner’s method is dependent on the choice of coordinate system and leads to a somewhat arbitrary division of the movement into submovements. Using maximum curvature points as submovement delimiters suffers additionally from the fact that, although curvature tends to be maximum between submovements, it still does not need to be significant. Consecutive submovements in the same direction may have no clear peak in curvature by which to distinguish them.

*High Resolution Pursuit.* Another greedy algorithm, High Resolution Pursuit (HRP) [37] is similar to Matching Pursuit in that it minimizes the residual error, but differs in that it emphasizes local fidelity of the fit and does not necessarily seek out the highest peak. Unfortunately, local fidelity of fit is not generally the best way to estimate submovements’ characteristics. Consider for example the movement depicted in Figure 5-1k; HRP would likely fail to make an accurate initial guess for a speed profile, since the chief characteristics of the speed profile do not resemble any of its component submovements.

The second movement of Figure 5-1 (panels **c** and **d** ) provides an informative benchmark for gauging an algorithm’s decomposition ability; it is both simple and resembles laboratory data. However, even assuming a priori knowledge of the correct number of submovements, the initial guesses of Milner’s method and each of the greedy algorithms (Matching Pursuit, ISRBF, Berthier’s method, and High Resolution Pursuit) yield solutions that resemble Figure 5-1c. Both the amplitude and the peak location of the decompositions would be spurious.

None of the initial guess methods listed above guarantee a guess that is in the neighborhood of the global optimum, and as shown in Figure 5-1c and **d**, given plausible biological data they may yield inaccurate and misleading decompositions. Minimization based on these methods find, at best, locally optimal solutions to the submovement extraction problem. In order to reliably find the global minimum and solve the decomposition problem accurately, an algorithm capable of global nonlinear optimization is necessary.

## 5.3 Method

Branch-and-bound algorithms have been successfully applied to classical problems, such as the traveling salesman problem, as well as to economics problems, [51, 52, 64] and are commonly used whenever it is necessary to find a *globally optimal* solution to a nonlinear problem, rather than an approximate or a locally optimal solution.

“Branch-and-bound” actually describes a class of algorithms, rather than a specific



implementation. The idea underlying branch-and-bound algorithms is simple: to find the global minimum of a function over a bounded parameter space, repeatedly divide (branch) the parameter space into subspaces and bound the value of the function over each subspace. If the lower bound of the function over a subspace is higher than a known value of the function elsewhere, that subspace need not be searched further. This continues until the location of the solution is known sufficiently well. This algorithm requires that each parameter be bounded.

The application of the branch-and-bound algorithm to submovement extraction is straightforward. Consider a speed profile,  $g$ , and the current estimate of the speed profile  $f(\mathbf{p})$ , given by

$$f(\mathbf{p}) = \sum_{j=1}^N \lambda_j \quad (5.1)$$

where each  $\lambda_j$  is a submovement, completely described by  $m$  parameters.  $\mathbf{p}$  is a vector containing the parameters of all the submovements. If  $N$  is the total number of submovements, then the total number of parameters in  $\mathbf{p}$ , is given by  $M = N * m$ . The formulation in equation 5.1 assumes scalar summation of submovements, but could be generalized to other modes of combination.

The objective function to be minimized is the absolute error,  $\mathcal{E}$ , given by

$$\mathcal{E}(\mathbf{p}) = \int |g - f(\mathbf{p})| \quad (5.2)$$

The absolute error is chosen, rather than the rms error, because it simplifies the process of bounding error over solution subspaces. (See Appendix B.)

### 5.3.1 Algorithm outline

The outline of the branch-and-bound algorithm as implemented in this work is as follows (Refer to Figure 5-2 for a step-by-step example in one dimension):

1. Bound the solution space. This requires finding upper and lower bounds for each element of  $\mathbf{p}$ . These parameter bounds can be thought of as describing an

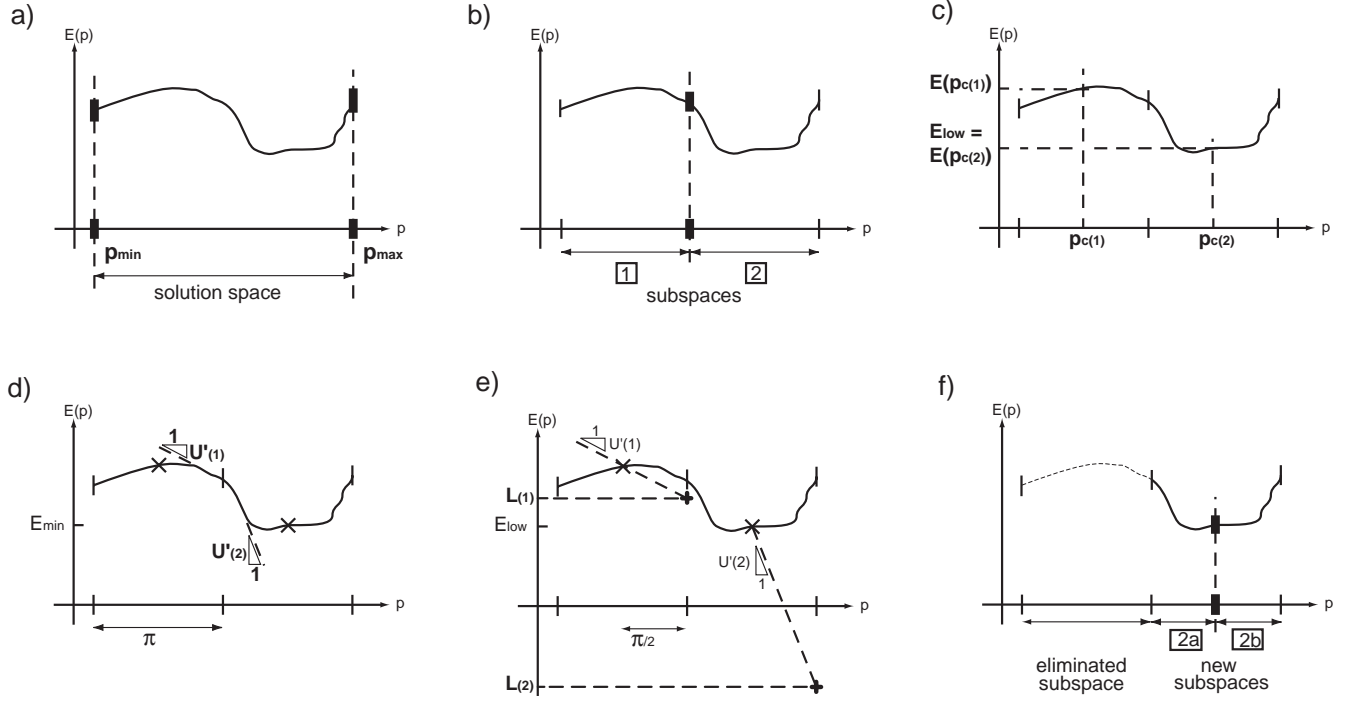


Figure 5-2: A step-by-step example of the branch-and-bound algorithm in one dimension: minimizing  $\mathcal{E}(p)$  over a range of  $p$ . **a)** Bound the solution space between  $p_{\min}$  and  $p_{\max}$ . **b)** Break the solution space into subspaces 1 and 2. **c)** Calculate the value of the objective function at the center of each subspace,  $p_c(1)$  and  $p_c(2)$ . Retain the lowest value,  $\mathcal{E}_{\text{low}}$  in memory. **d)** Calculate an upper bound for the slope of the objective function over each subspace,  $U'(1)$  and  $U'(2)$ . **e)** Calculate a lower bound for the objective function over each subspace,  $L(i) = \mathcal{E}(p_c(i)) - \frac{\pi_i}{2}U'(i)$ , where  $\pi_i$  is the span (width) of each subspace. **f)** Eliminate subspaces that cannot contain the solution. Break down remaining subspaces. Return to **c)** and repeat until the error falls below a predetermined threshold, i.e. subspaces for which  $L_i > (\mathcal{E})_{\text{low}}$ .

$M$ -dimensional hyperbox which contains all permissible values of  $\mathbf{p}$ . Any given set of parameter values describes a point within the box, and has a single value of  $\mathcal{E}(\mathbf{p})$  associated with it. The goal of the algorithm is to find the point in the hyperbox for which  $\mathcal{E}(\mathbf{p})$  is at a minimum.

2. Break the solution space into a number of subspaces.
3. Evaluate  $\mathcal{E}(\mathbf{p}_c)$  (the value of  $\mathcal{E}$  at the center of a subspace) for all subspaces.
4. Set  $\mathcal{E}_{\text{low}} = \min(\mathcal{E}(\mathbf{p}_c))$  over all subspaces.  $\mathcal{E}_{\text{low}}$  is the lowest known error in the solution space.

5. Calculate a lower bound  $L$  for  $\mathcal{E}(\mathbf{p})$  over each subspace.
6. Subspaces for which  $L > \mathcal{E}_{low}$  cannot contain the solution and therefore are eliminated.
7. Break remaining subspaces down into yet smaller subspaces.
8. Return to step 3 and repeat until a termination criterion is met.

There are a few points in the algorithm that bear further explanation.

### 5.3.2 Bounding $\mathcal{E}(\mathbf{p})$ (step 5)

One method for calculating a lower bound on  $\mathcal{E}(\mathbf{p})$  over a solution subspace is as follows:

1. Calculate an upper bound for  $\left| \frac{\partial \mathcal{E}(\mathbf{p})}{\partial p_i} \right|$  (call it  $U'_i$ ) over the subspace. See Appendix B for methods of calculating  $U'_i$  for minimum-jerk and Gaussian speed curves.
2. Define  $\pi_i$ , the span of parameter  $i$ , as  $\pi_i \equiv \max(p_i) - \min(p_i)$  over the subspace.
3. A lower bound,  $L$ , for  $\mathcal{E}(\mathbf{p})$  over the subspace is given by:

$$L = \mathcal{E}(\mathbf{p}_c) - \sum_i \frac{\pi_i}{2} U'_i \quad (5.3)$$

This guarantees that

$$\mathcal{E}(\mathbf{p}) \geq L \quad (5.4)$$

for all  $\mathbf{p}$  in the current subspace.

### 5.3.3 Breaking down of solution subspaces (step 7)

There are many ways that the solution subspaces could be broken down into smaller subspaces. As implemented, the subspace was simply bisected along the parameter

axis that had the greatest average value of  $\frac{\pi_i}{2}U'_i$  on the previous iteration. This was done to shrink the error bounds of each subspace in as few iterations as possible.

Trisecting, rather than bisecting, may increase performance. When trisecting, values of  $p_c$  from previous iterations are also valid  $p_c$ 's for future iterations. Because previously calculated values of  $\mathcal{E}(\mathbf{p}_c)$  can be retained, subspaces can be divided more quickly with a very small increase in computational cost. Bisection does not have this advantage.

### 5.3.4 Terminating the search (step 8)

Iterations continue until every portion of the solution space has either 1) been eliminated or 2) has had its error range bounded sufficiently narrowly. The error range of a subspace is calculated by taking the difference between the error at the center of the subspace,  $\mathcal{E}(\mathbf{p}_c)$ , and the lower bound of the error over the subspace,  $L$ . Once the error range falls below a certain threshold ( $\mathcal{E}(\mathbf{p}_c) - L < \epsilon$ ) the subspace is not searched further.

This termination criteria does not ensure uniqueness of the solution. Uniqueness checks can be performed by checking whether the parameters for all the remaining solution spaces fall within a sufficiently small radius.

### 5.3.5 Minimizing the number of submovements

It should be noted that, to this point, the branch and bound algorithm has assumed that the number of submovements is given. Minimizing the number of submovements used can be performed by starting with one submovement and iteratively incrementing the number of submovements fit to the objective curve until the error falls below a given threshold (see Figure 5-3).

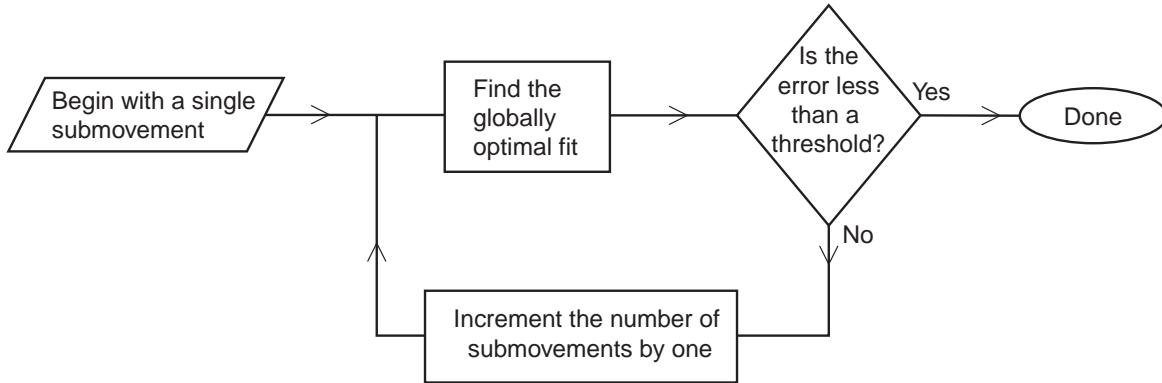


Figure 5-3: Minimization of the number of submovements. An iterative error-checking algorithm provides a framework for minimizing the number of submovements while optimizing the fit of the submovements employed.

## 5.4 Results

### 5.4.1 Solution-finding performance

In order to test the solution-finding performance of the branch-and-bound algorithm, two simulated speed profiles were created, one consisting of two minimum-jerk curves, and one consisting of two Gaussian curves. Each was decomposed twice, using two min-jerk curves in one attempt and two Gaussian curves in a second attempt. The results are summarized in Figure 5-4.

A litmus test for any decomposition algorithm is how well it decomposes a synthetic speed profile where the submovement characteristics are known beforehand. Due to its likelihood of producing spurious solutions and to its similarity to patient data, the speed profile shown in Figure 5-1c serves as a good initial benchmark. The simulated speed profiles in Figure 5-4 were selected specifically to have the characteristics of speed profile in Figure 5-1c—a single peak with and a clearly discernible “lobe” following, created by summing two submovements: a small one followed by a larger one. As can be seen in Figure 5-4, both of these were successfully decomposed. Not only did the range of decomposition error include zero, but the submovement characteristics (peak location, peak height, submovement width) of the original function were captured, as well.

Another test of a decomposition algorithm might be to reliably differentiate be-

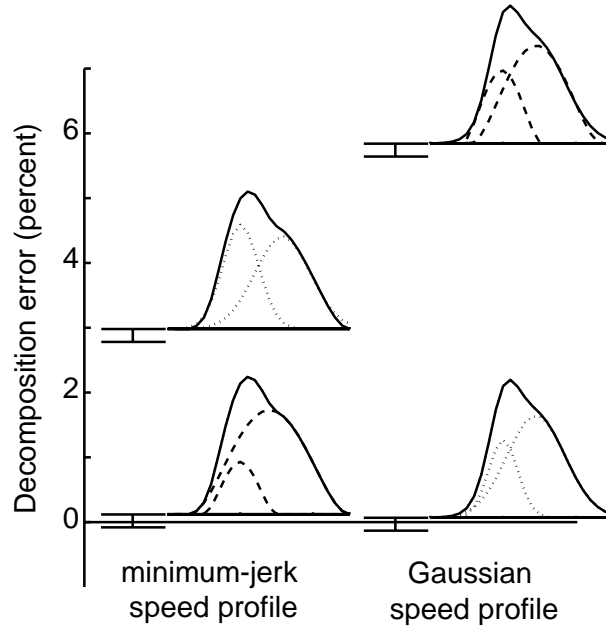


Figure 5-4: Decomposition of simulated speed profiles composed of minimum-jerk and Gaussian submovements. Solid lines represent the original function in each case; dashed lines show the decompositions into minimum-jerk submovements, and dotted lines show the decompositions into Gaussian submovements. The plots show bounds on the decomposition error in each case.

tween speed profiles composed of different types of submovements. Figure 5-4 shows that the bounds on the decomposition error for each submovement function do not intersect. Non-intersection of the error bars shows the algorithm's ability to discriminate between the functions used to create each curve. It is also interesting to note that, because decomposition error cannot be negative, the fact that the error bounds extend below the x-axis in some cases illustrates the conservative nature of error bound estimation.

The Gaussian function's infinite tails did not distort this analysis; only the portion of the function that fell within the time window under consideration was used in error calculations.

#### 5.4.2 Required computing power

The calculations required to do the decompositions in Figure 5-4 took approximately 30 hours on a 1.2 GHz Athlon processor. This is a very modest decomposition com-

pared to, say, decomposing the velocity profile produced while slowly tracing a circle, which may have 10 or more submovements. As the number of submovements increases, the dimensionality of the solution space,  $M$ , increases. The number of subspaces to be evaluated at any given iteration is on the order of  $C^M$ , where  $C$  is a function of the specific problem parameters and the iteration number. As the solution space dimensionality increases, the computational requirements increase dramatically. Computational cost is the primary weakness of the branch-and-bound algorithm.

The “branching” that occurs during the execution of the branch-and-bound algorithm lends itself to efficient parallel computing. The optimization problem can be efficiently divided up into a number of nearly independent subproblems. Each separate process only needs to have access to, and the ability to modify, the lowest known value of the error across the solution space.

### 5.4.3 Convergence

Convergence (i.e. reaching the termination criteria) can be guaranteed because of the nature of the error bounds on each solution subspace.  $U'_i$  for each parameter is a scalar that is a function of the maximum parameter values in each subspace. Because each parameter is bounded individually,  $U'_i$  is bounded as well. Therefore, as the span,  $\pi$  of each parameter decreases, that is, as the subspaces are divided and re-divided, the difference between the known error at the center of the subspace,  $\mathcal{E}(\mathbf{p}_c)$  and the lower bound of the error over the subspace  $L$  will necessarily decrease as well, eventually becoming arbitrarily small. It is guaranteed to fall below the chosen threshold  $\epsilon$  at some point.

### 5.4.4 Fixed submovement parameterization does not imply a fixed submovement shape

The branch-and-bound algorithm requires that all submovements have a fixed parameterization, i.e. be describable through the same set of parameters throughout the decomposition process. In the case of minimum jerk submovements, this implies

that all submovements have the same shape; that is, that they can all be represented by scaled, dilated, and translated versions of a single “mother shape”. This is not necessarily true for other types of submovements, however.

Support-bounded lognormal submovements, for instance, are completely described by five parameters and can take on a variety of shapes as can be seen in Figure 5-5. Keeping fixed the amplitude and start and stop points, the shape can be varied considerably by varying the other two parameters. One modifies the symmetry and the other modifies the kurtosis or “fatness” of the curve.

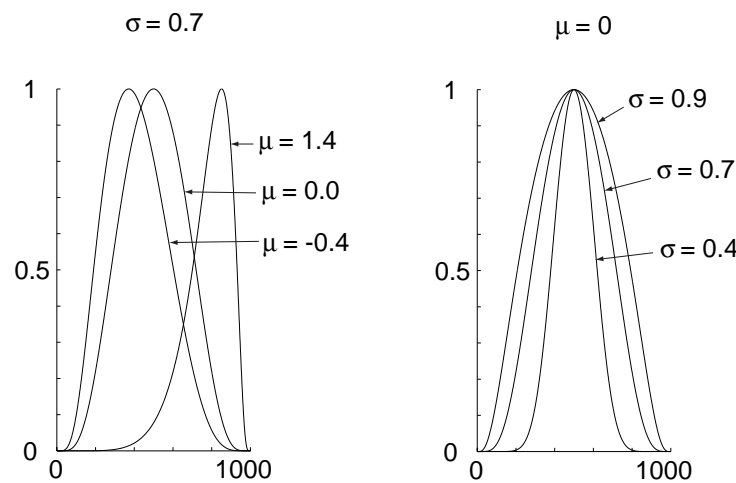


Figure 5-5: An example of shape variations in a single submovement parameterization. The support-bounded lognormal function can take on a variety of shapes. Varying  $\mu$  changes the symmetry, and changes  $\sigma$  affect the kurtosis.

## 5.5 Conclusion

The branch-and-bound algorithm described above is capable of finding the globally optimal decomposition for simulated speed data, making it unique among decomposition algorithms. This advance, if successfully applied to submovement decomposition in actual data, has the potential to clarify submovement structure in human movements. The insights gained from this process would provide a new window for observing the operation of the human motor control system and may allow for advances in measurement of motor performance, diagnostic procedures for motor disorders, and



identification of motor control strategies.

### 5.5.1 Limitations of the branch-and-bound decomposition algorithm

One approach to more accurately describing the kinematic signatures of submovements is to use submovements that employ an ever-larger number of parameters, as Plamondon and Alimi have done with their seven-parameter  $\Delta\Lambda$  movement model [71]. This may reduce the description error to near zero and provide a plausible biological account of the phenomenon, but it introduces a new problem for decomposition. The larger the number of parameters, the more highly dimensional the solution space and, potentially, the more closely locally optimal solutions will approximate the global optimum. The decomposition errors obtained in the false decompositions of Figure 5-1 were small, 0.5% in one case, despite large differences in the number, position, and shape of submovements. The submovement candidates used in creating the profiles in Figure 5-1 required only 3 parameters; submovement candidates with more parameters could assume a greater range of shapes and might be capable of erroneous decompositions that fit even more closely. The presence of even a small amount of measurement noise or discretization error may be enough to corrupt the decomposition and make it impossible to distinguish which of several local minima is actually optimal. If the abundance of local minima makes it infeasible to ensure the accuracy of the global optimum, then the analysis is no longer submovement extraction, but merely high-dimensional non-linear curve-fitting. The decomposition will have lost its value in plausibly describing a process underlying production and control of movement.

The following chapter describes another decomposition algorithm that does not focus on guaranteeing a global optimum, but is satisfied with finding a good local minimum. It utilizes a scattershot algorithm, which, although less rigorous than the branch-and-bound algorithm, has far fewer computational demands and can reliably characterize changes in submovement parameters over time. Decompositions made

in this way could not be used to directly support a theory of submovements by showing high-fidelity fits. No claims could be made about the exact characteristics of a single submovement. But such a method has proven useful in making compelling, biologically motivated descriptions of the smoothness with which a subject executes a task.

# Chapter 6

## The scattershot decomposition algorithm

### 6.1 Summary

A scattershot decomposition algorithm is applied to the nonlinear optimization problem of submovement extraction. As it is not guaranteed to find the optimal fit, it was necessary to test whether the patterns in the submovements that it produces are robust to changes in submovement shape, required accuracy of fit, and parameter bounds of the extraction algorithm. A sensitivity analysis reveals that although the values of the submovement parameters are sensitive to the conditions of decomposition, the direction and statistical significance of the *changes* in parameters was robust to every condition tested.

### 6.2 Scattershot Algorithm

Submovements were extracted using a local optimization algorithm (a line-search algorithm, as implemented in MATLAB's 'fmincon' function) initialized at 10 different, randomly selected points in the solution space. Submovements were allowed to take on a duration between 200 ms and 833 ms. Additional submovements were fit to each

movement until the error fell below 1%. Five characteristics of the submovements are summarized in the results plots. Each submovement is characterized individually by its duration and peak speed. The relative and collective characteristics of the submovements are represented by number of submovements in the entire movement, inter-peak interval (interval between peaks of consecutive submovements), and overlap (interval between initiation of a submovement and termination of the previous one. See Figure 6-1).

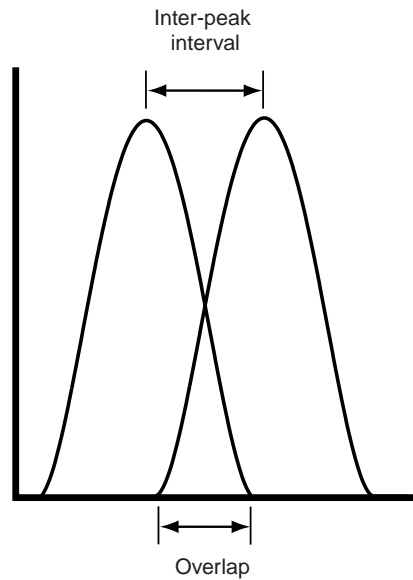


Figure 6-1: Definitions of inter-peak interval and submovement overlap. Note that, due to the nature of the overlap measure, it can be negative, indicating a period of no activity between submovements.

The submovement parameters chosen are not entirely independent; the number of submovements and inter-peak interval are related. Employing fewer submovements in decomposing a given movement increases the typical distance between submovement peaks.

Inter-peak interval and submovement duration are related as well, through overlap, as can be seen in Figure 6-1. Given fixed submovement peak locations, as the duration increases so will the overlap. Similarly, given a fixed duration for two submovements, as the distance between their peak locations decreases (i.e. they move closer together), the extent to which they overlap will increase.

### 6.2.1 Statistical tests

Using linear regression, a line was fit to each of the submovement characteristics over the course of therapy for each subject, and the confidence interval for the slope was determined. See Press et al. (1992) for a detailed mathematical description. The change bars in the results summary plots were generated by fitting a line to the data using least-squares regression, and taking the value of that fit at the first and last days of therapy. See Figure 6-2, for an illustration of the process.

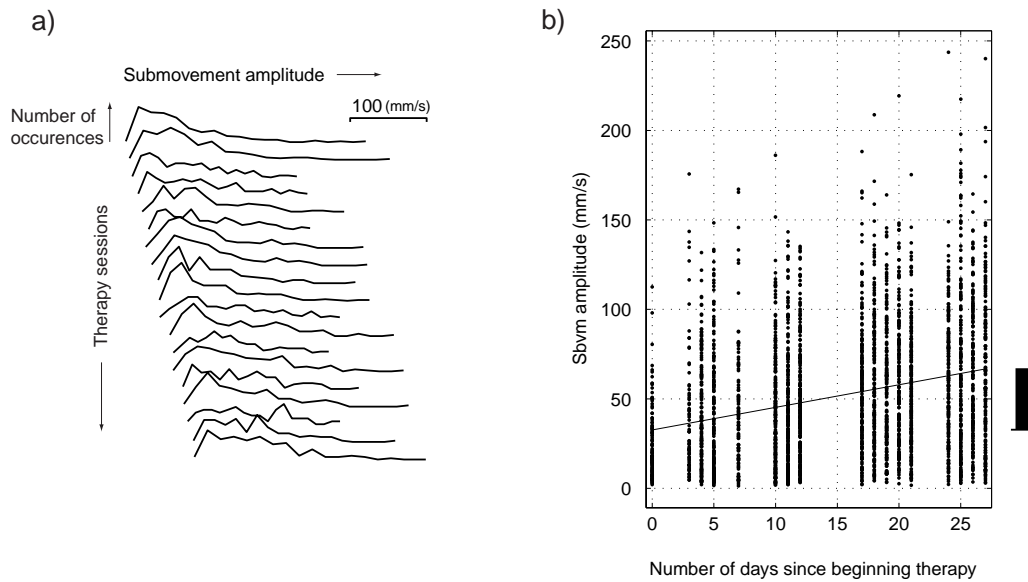


Figure 6-2: Two different displays of the same type of data (from two different patients) is shown: a raster plot in panel a) and a dot plot in panel b). **a)** Raster plot of a single subject's submovement peak speed over the course of therapy. Each line represents the submovements generated during a single therapy session. The height of the line represents the total number of submovements with approximately that peak speed. Note the slight broadening of the peak representing low-speed movements toward the end of therapy. Tail lengths vary according to the maximum value of the parameter found on a given therapy day. **b)** Each point represents a single submovement. A line was fit to the data using least-squares regression. The bar to the right of the plot represents the change in the parameter value over the course of therapy, with the line on the bottom end indicating the beginning of therapy and the height box indicating the extent of the change during therapy. In subsequent plots, a solid bar represents a statistically significant change ( $p < 0.05$ ), while an unfilled bar represents a change that did not reach statistical significance.

### 6.2.2 Sensitivity Analysis

The scattershot extraction algorithm is not guaranteed to produce an optimal result. In fact, given the number of guesses attempted (10) and the dimensionality of the solution space (as high as 60) the probability that algorithm found the optimal solution in more than a few cases is negligible. Additionally decreasing the chances that an accurate representation of the underlying submovements was achieved is the fact that the submovement shape was not known; minimum-jerk was assumed because it has been shown to fit human ballistic speed profiles to within a few percent [35] and the computational requirements are minimal, but other work has shown that submovement shapes vary considerably, even within a given subject [67] and that other mathematical functions describe submovements with less error [72].

To test whether the submovement parameters were influenced by changes in algorithm conditions, including the submovement shape used, the accuracy constraints, and bounds on submovement duration, we performed a sensitivity analysis. This was done by decomposing data for which the underlying submovement shape and parameters were known a priori, while varying conditions of the extraction algorithm.

The sensitivity analysis was performed on data derived from the movements of actual patients: subjects 203 and 708, an inpatient and an outpatient representative of qualitatively different regimes of recovery. The data set was generated by taking the original patient data for a given movement, extracting its submovements, and then summing the extracted submovements to create new movement data, similar to the original data (within a 1% error bound), but different in that it could be perfectly fit by a small, known set of submovements. The resulting data was both biologically plausible and had a known submovement composition. Using this data, we addressed the question: If a set of movements is composed of submovements, the characteristics of which change over time, can those changes be reliably detected despite poorly selected conditions in the extraction algorithm?

Submovements were extracted from the data set under 6 conditions:

**Minimum-jerk submovements** Submovement extraction was repeated under the

same conditions as the original: 1% fit error was tolerated, and submovement duration was limited to 0.833 s. This decomposition is a check that the extraction algorithm is well behaved. One would expect it to produce results that are similar to the original, although not identical, as it has a 1% margin of error in which to differ.

#### **Minimum-jerk submovements with low accuracy constraints (10%)**

Accuracy constraints were reduced by an order of magnitude to allow for 10% error in the decomposition. There is a trade-off in selecting a good accuracy requirement. If the required accuracy is too high, submovements are fit to measurement noise or, perhaps, to the effects of neuro-muscular dynamics on an underlying submovement shape; if the required accuracy is too low, large portions of movement may be adequately fit by a single submovement, and features may be lost. This decomposition quantifies the extent of distortion caused by low accuracy.

#### **Minimum-jerk submovements with high maximum duration (1.5 s)**

The extraction algorithm requires that all submovement parameters be bounded at the outset. The submovements generated during decomposition of patient data show that a significant fraction of submovements have the maximum permissible duration, 0.833 s (see Chapter 7). This suggests that an upper bound on submovement duration of 0.833 s may be too low. Decomposing the data with a maximum duration of 1.5 s will help quantify the effect of selecting a maximum submovement duration that is not well matched to the duration of the submovements underlying the data.

**Submovement shape** Instead of minimum-jerk, several other submovement shapes were tested in decomposition. In each case the accuracy required was 10%. These decompositions quantify the effect of submovement shape on the parameters of the extracted submovements. See Figure 6-3 for an illustration of each of the submovement shapes used.

**Gaussian submovements** Gaussian submovements were among the first used

in mathematical descriptions of submovements [17]. Gaussian submovements are described with three parameters: mean, standard deviation, and height. Maximum duration (defined as six- standard deviations) was 2.0 s. The value of the function is less than 1.2% outside of this nominal duration, and the area under the function within the six- $\sigma$  duration is greater than 99% of the total area under the curve.

**Symmetric support-bounded lognormal submovements** Support-bounded lognormal (LGNB) submovements were proposed by Plamondon [70] and found to fit point-to-point drawing movements better than 22 other candidate functions [72]. Although the LGNB distribution can be asymmetric, in this decomposition the curves were constrained to be symmetric. In its full form, the LGNB has five parameters, but two of them were fixed here in order to constrain the symmetry and shape. Maximum duration was 1.5 s.

**Asymmetric support-bounded lognormal submovements** In this extraction, LGNB submovements were used, and were allowed to be asymmetric. All five parameters were used. Maximum duration was 1.5 s.

Although multiple submovement summing modalities have been applied in previous work (e.g. scalar summation [63] and vector summation [24]), scalar summation was used in this analysis in every case.

## 6.3 Results of Sensitivity Analysis and Discussion

The results of the sensitivity analysis produced submovement parameter distributions, many of which varied over time. See Figure 6-2 for two different sample displays of the data. The complete results are summarized in Figure 6-4.



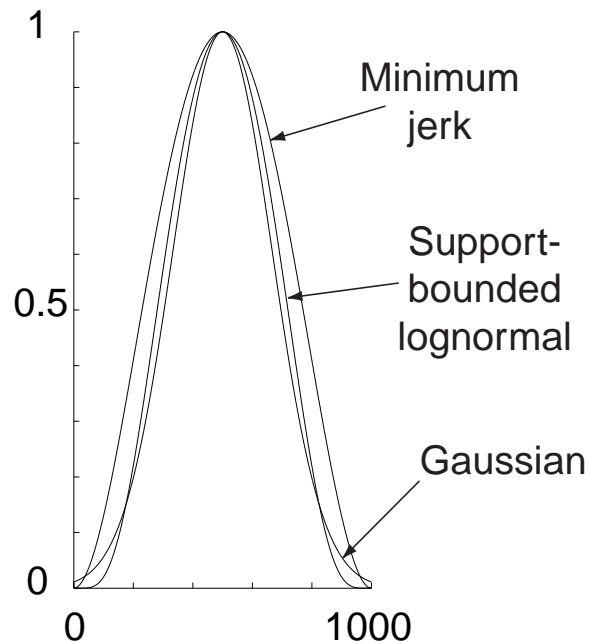


Figure 6-3: The three submovement shapes used in decompositions. In each case, the peak height is 1, the peak is centered at 500, and the nominal duration is 1000. The LGNB curve has  $\mu = 0$  and  $\sigma = 0.7$ . Using six- $\sigma$  duration for the Gaussian curve makes it comparable to the others.

### 6.3.1 Parameter *values* vary between decomposition conditions but follow repeatable patterns

Each of the submovement parameters shows a wide range of variation (as great as a factor of two in the case of duration), depending on the conditions under which they were extracted. The dependence is structured, following similar patterns for both data sets. For example, in submovement duration (see Figure 6-4 b and bb), both data sets show that the repeat decomposition yields approximately the same values as the original data, but that low accuracy, increased duration, symmetric LGNB, Gaussian, and asymmetric LGNB each in turn yield progressively higher values.

Several aspects of the dependence of submovement parameters on extraction conditions are predictable without any reference to biology. For instance, the number of submovements decreases slightly between the original data and the repeat decompo-

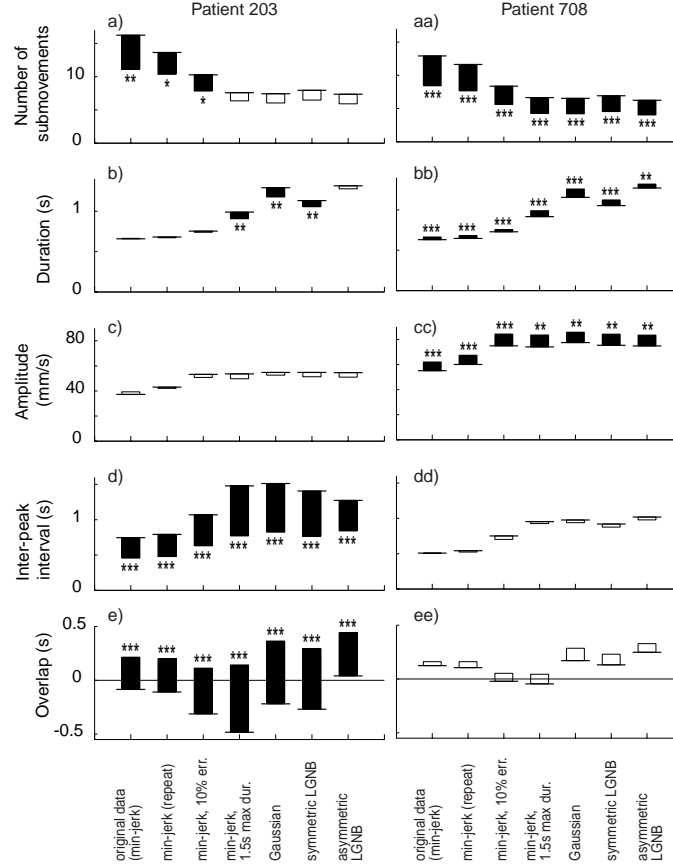


Figure 6-4: Sensitivity analysis of submovement extraction to algorithm conditions: maximum duration, accuracy requirement, and submovement shape. Here are shown the changes in submovement characteristics of data based on the movements of patients 203 and 708, as reported by a variety of decompositions. The initial value is represented by the end of the bar with a horizontal bar. For statistically significant changes ( $p < 0.05$ ) the box is filled, otherwise it is left hollow. The level of significance is further indicated by asterisks:  $0.01 < p < 0.05$ :\*,  $0.001 < p < 0.01$ \*\*,  $p < 0.001$ :\*\*\*.

sition, due to the 1% fitting error(see Figure 6-4 a and aa); the repeat decomposition avoids fitting some of the fine features of the movement (which would require more submovements), and still falls within acceptable error. Similarly, a significant decrease in the number of submovements occurs when the allowable error is increased to 10%. When increasing maximum duration to 1.5, one would also expect a decrease in submovement count; longer segments of the movement are fit by a single submovement.

Predictions of differences in number of submovements for different submovement

shape are not straightforward to make, except for one: asymmetric LGNB decompositions result in fewer submovements than symmetric LGNB decompositions. This is due to the fact that an asymmetric LGNB function can take on a wider range of shapes than a symmetric LGNB function and hence can fit features with a single submovement that would require multiple symmetric to fit.

Other parameter values in the sensitivity analysis can be predicted based on the lengths of “tails” of the various submovement shapes. The “tails” of a function can be mathematically defined as the fraction of the movement duration for which movement speed remains below some small fraction, say 2%, of peak speed. A long-tailed function and a short-tailed function fit to the same features would have similar peak speed values, submovement counts, and inter-peak intervals, however, long tails would greatly change both submovement duration and overlap.

The duration of Gaussian submovements is taken to be six standard deviations, giving it long tails. In some cases the asymmetric LGNB also has long tails, particularly when asymmetry is high. Minimum-jerk typically has the shortest tails. This can be seen in the behavior of the submovement duration and overlap measures; duration and overlap increase from minimum-jerk to symmetric LGNB to Gaussian to asymmetric LGNB (see Figure 6-4 b, bb, e, and ee). Contrast this with submovement count, peak speed, and inter-peak interval; the Gaussian, symmetric LGNB, and asymmetric LGNB compare directly with the minimum-jerk decomposition with 1.5 s maximum duration and 10% maximum error requirement.

### **6.3.2 Parameter *changes* are consistent between decomposition conditions**

The most notable result of the sensitivity analysis is that direction of parameter change is robust to decomposition conditions. In every case where the parameter change in at least one decomposition was appreciable, say greater than 15% of the range, the sign of the change was consistent for every decomposition.

Another strong result of the sensitivity analysis is that the statistical significance

of the parameter changes is robust to details of the extraction algorithm parameters. In every case where a strongly significant change ( $p < 0.001$ ) existed in at least one decomposition, a significant change was reported by every decomposition attempt.

## 6.4 Conclusion

The sensitivity analysis indicates that, although the scattershot algorithm cannot promise that the submovements resulting from extraction necessarily represent those originally used to construct the movement, it can provide a probable ranges for the submovement parameters. The key result of the analysis is that, despite uncertainties, the scattershot algorithm can reliably detect the direction and significance of submovement parameter changes. The following chapter presents the results of applying the scattershot algorithm to 31 patients' data.

# Chapter 7

## Submovements grow larger, fewer, and more blended during stroke recovery

### 7.1 Summary

The component submovements of stroke patients' point-to-point movements were estimated using a novel submovement extraction algorithm. Over the course of therapy, patients' submovements tended to increase in peak speed and duration. The number of submovements employed to produce a given movement decreased. The time between the peaks of adjacent submovements decreased for inpatients (those less than 1 month post-stroke), but not for outpatients (those greater than 12 months post-stroke) as a group. Submovements became more overlapped for all patients, but more markedly for inpatients. This pattern of changes in the extracted submovement parameters 1) provides an objective basis for evaluating patients' state of motor recovery and 2) provides some degree of support for the existence of submovements.

## 7.2 Methods

Subjects, Apparatus, and Procedure was described in Chapter 2. Thirty-one patients' movement data were decomposed as described by the Analysis and Statistical Tests sections in Chapter 6.

### 7.2.1 Neuromotor noise test

As an alternative hypothesis to the existence of submovements, it is instructive to consider whether velocity fluctuations are caused by noise in the neuromuscular system. To test whether observations of submovements in the data could be explained by the presence of neuromotor noise, a simulation was constructed. Twenty movements per day for forty simulated therapy days were generated. Each movement consisted of a 1.66 second long, smooth (minimum-jerk) speed profile superimposed with filtered Gaussian noise. Although the duration selected was somewhat lower than those typically observed in patient movements, a 1.66 second duration was selected to allow the entire movement to be described by a single submovement of reasonable duration. It should be noted that the overall movement duration tended to decrease for most patients, and this feature could be incorporated into future neuromotor noise simulation. However, the features of the submovements themselves (other than their number) are likely to be a strong function of the noise properties only, and to be only weakly affected, if at all, by the length of the movement.

The Gaussian noise was of low frequency content. (It was low pass filtered at 2 Hz; the vast bulk of its power was at frequencies less than 5 Hz, matching the frequency content of typical human arm movements.) The amplitude of the noise on the first therapy day (six standard deviations in the Gaussian distribution) was twice the peak amplitude of the underlying minimum-jerk profile. The amplitude of the noise decreased linearly each day until the fortieth therapy day, when it became zero (see Figure 7-1. This simulation approximates the observed smoothing of movement with a decreasing noise process.

The simulated data were decomposed as described in the Analysis section of Chap-

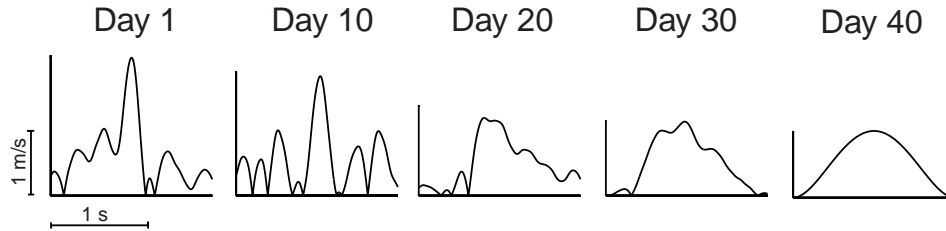


Figure 7-1: Typical simulated movements at various times during the progression of the simulation. Over the 40 simulated therapy days, the amplitude of the additive low-frequency Gaussian noise decreased, yielding speed profiles qualitatively resembling those observed in patients.

ter 6. The maximum permitted submovement duration was 1.66 seconds, set to match the length of the movement, and the allowable fitting error was set at six percent. Six percent was used instead of 10%, because

## 7.3 Results

### 7.3.1 Submovement Characteristics

Figure 7-2 shows the changes in the patients' submovement characteristics over the course of therapy. Figure 7-3 summarizes the trends in each metric for the patient population as a whole and for inpatient and outpatient groups. Despite wide variations between patients, several general observations can be made. The subjects' submovements tended to increase in duration and in peak speed. The number of submovements employed in making a given movement decreased. The extent to which submovements overlapped increased without exception in every patient, reaching statistical significance in 22 of 31 patients. The inter-peak interval decreased for

inpatients, but tended to increase slightly for outpatients.

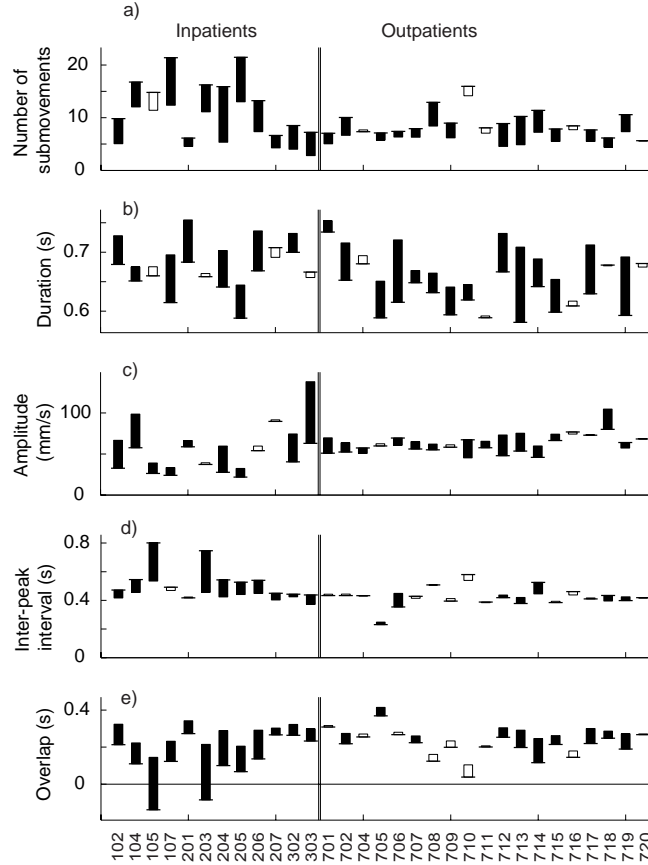


Figure 7-2: Changes in submovement characteristics by patient. Changes in submovement parameters from the first day to the last day of therapy are shown for all patients. The initial value is represented by the end of the bar with a horizontal bar. For statistically significant changes ( $p < 0.05$ ) the box is filled, otherwise it is left hollow. For an illustration of the construction of a “change bar”, see Figure 6-2

In every case except for submovement duration, the changes in inpatients’ submovement characteristics were greater than those of outpatients (significant at  $p < 0.05$ ). In the amplitude, the inter-peak interval, and the overlap, both the initial and final values in outpatients appear to be closely grouped around a common mean. Inpatients’ values appear to converge to these common means during therapy. For example, in Figure 7-2, panel d), outpatients’ initial and final values for inter-peak interval are all grouped tightly around 0.4 s. In patients’ initial values tend to be higher than 0.4 s, but (with two exceptions) decrease significantly. The final values are much more closely grouped around 0.4 s. Again, it should be noted that the



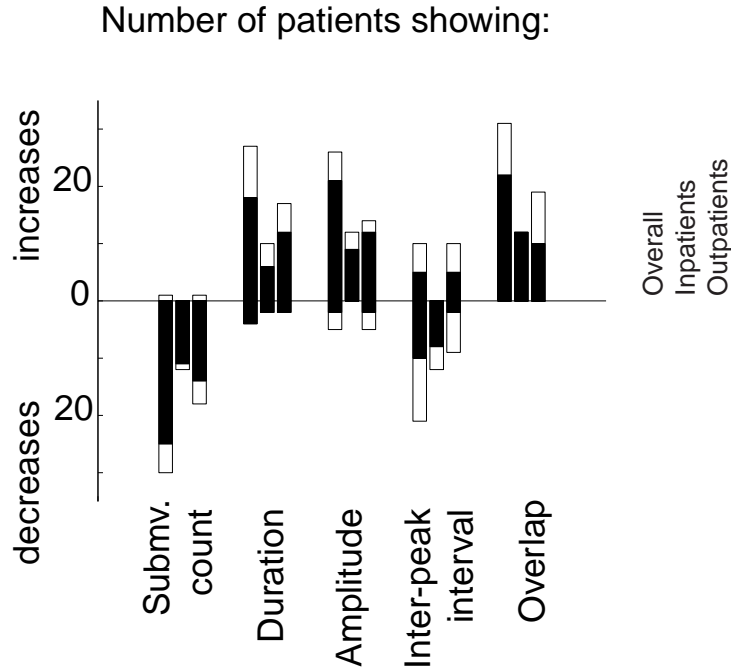


Figure 7-3: The number of patients who showed increases and decreases in each of five submovement characteristics, by inpatient group, outpatient group, and overall. White bars indicate the total number of subjects in each group showing a change, and black bars indicate how many of those were statistically significant at the  $p < 0.05$  level.

value of 0.4 s should be interpreted with care: the value itself may or may not be meaningful, but the fact that all subjects are grouped around a common value is.

### 7.3.2 Neuromotor noise test

The results of the decomposition of the simulated data corrupted with neuromotor noise are shown in Table 7.1. Extracted submovements grew fewer, increased in duration, decreased in peak speed, and grew both further apart and more overlapped as the amplitude of noise decreased. The decrease in the number of submovements is to be expected, since, as the noise amplitude decreases, the speed profile approaches a minimum-jerk form and can be more easily fit with fewer submovements. This also accounts for the increase in submovement duration and inter-peak interval.

Although patient data also shows submovements increasing in duration and decreasing in number, the patient data differs from the simulation in that it shows

Changes in submovement parameters in the neuromotor noise simulation					
	number of submovements	submovement duration (s)	peak speed (m/s)	inter-peak interval (s)	overlap (s)
initial	7.72	0.31	0.82	0.22	0.13
final	2.11	0.87	0.57	0.37	0.43
change	-5.60	0.56	-0.25	0.14	0.29

Table 7.1: Summarized changes in the submovement parameters of simulated data containing Gaussian noise. Noise amplitude decreased linearly with time. All changes shown are highly significant ( $p < 10^{-6}$ ). Number of submovements and peak speed decreased, all other quantities increased. These patterns are not consistent with those observed in patient data.

submovements growing closer together rather than growing further apart, and increasing in amplitude, rather than decreasing. This indicates that the data is not well modeled by a noise process like the one simulated, and that patients’ velocity fluctuations were not caused by neuromotor noise of this type.

The periods of nearly complete rest between portions of movement observed in more heavily impaired patients provide additional evidence that the velocity fluctuations were not caused by random noise; the probability of a random signal producing this pattern with any regularity is negligibly low. For example, if the data points 0.5 s apart are independent (a reasonable assumption, given the cutoff frequency of 2 Hz) and the noise process must maintain a constant amplitude of, say,  $1 \pm 0.05$  standard deviations in order to cancel out the underlying continuous movement process and produce a period of “no movement”, the probability of this happening for three seconds is approximately 2 in a billion. These patterns in the subject data are almost certainly not caused by random fluctuations made while executing an otherwise smooth movement trajectory. Neuromotor noise can be effectively ruled out as a source of the intermittency observed in subjects movements.

## 7.4 Discussion

This work presupposes that the movements analyzed are composed of submovements. Although the existence of submovements has not been proven, it is consistent with

all available observations (see section 3.3.3), unlike alternative explanations that have been proposed, such as neural noise, neuromuscular mechanics, and the effects of visual feedback (see section 3.3.2). The existence of submovements will be employed as a working hypothesis for the remainder of the discussion.

Alternatively, patients' submovements tend to increase in duration and peak speed over therapy. Could the increases in submovement amplitude and duration reflect peripheral factors, such as restoring the capability of the system to recruit a sufficiently large number of motor units? If impaired patients were only limited by the magnitude of their neural activation signals, and this quantity increased over the course of recovery, then this theory would predict an increase in peak speed of the overall movements as well. The data does not support this hypothesis, however. More subjects show peak speed decreases than show increases [75].

It can be hypothesized that these increases in duration and peak speed reflect an improving ability to predict the movement that will result from a given motor command. As this predictive ability or "motor confidence" increases, the expected error resulting from a given command decreases, and submovements can become faster and longer in duration while still maintaining acceptable levels of error; the motor control system can increase the magnitude of its "feedforward" commands. Both the increase in accuracy and the larger distance covered by each submovement makes it so that fewer submovements are required to reach the target.

It is possible that the neural mechanism responsible for providing a "map", some known one-to-one relationship, between high-level motor commands and motor output is in some way disturbed by stroke. As the now distorted map is slowly refined, the ability of the motor planning system to predict the results of a given command increases. This increase in "motor confidence" allows the motor planning system to project further into the future, executing longer and longer submovements.

Additionally, decreases in the inter-peak interval may reflect the refinement of a second map that may have been disrupted by the stroke: the map between motion and proprioceptive and kinesthetic feedback. As this map is refined, so is the ability of the motor planning system to monitor the state of a movement in progress, based

on visual, tactile, and other sensory feedback. Due to the similarity in shape of the submovements (all plausible submovement models are bell-shaped, smooth, and vary from each other by only a few percent [72]) accurate knowledge of the state of a submovement in progress allows approximate prediction of the rest of the time course of that submovement, including an estimate of the time to submovement termination, and an estimate of the endpoint error. As the map between motion and proprioceptive feedback improves, it becomes possible to predict the results of a movement in progress earlier, and hence allows subsequent submovements to be initiated earlier in the submovement. This would tend to decrease the inter-peak interval.

It is to be expected that the inter-peak interval would have a lower bound. Not only is it bounded below by zero (by definition), but evidence of a psychological refractory period [81] suggests that the lower bound may be significantly higher. The data shows evidence of inter-peak intervals descending to an asymptote. Although inpatients began with a wide range of inter-peak intervals (from 0.4 s to 0.8 s), at the completion of therapy they all fell within a narrow band centered approximately at 0.4 s (from approximately 0.38 s to 0.43 s). With one exception, outpatients all began and ended therapy within that same band, most of them showing no significant change. The sensitivity analysis revealed that, although the exact value of the asymptote cannot be determined (inter-peak intervals varied by a factor of two between different decomposition conditions), the observation of an asymptote that is approached by inpatients is reliable and would result from decomposition under any of the conditions tested.

Although outpatients' submovements did not generally show a decrease in inter-peak interval, they did show an increase in overlap. This is consistent with the observed increase in submovement duration, indicating that although outpatients' submovements still occurred at approximately the same intervals, they increased in duration and hence became increasingly overlapped, resulting in smoother movement.

### 7.4.1 Recovery as system identification

Taken together, the changes observed are consistent with a model of recovery in which two maps are being learned: 1) a map between a motion and its resulting sensory information (a forward model) and 2) a map between a desired motion and the motor command required to make it occur (an inverse model). A number of models of human movement production have been proposed, based on paired forward and inverse models [40, 77, 29, 7], although to date they have all employed continuous motor commands, rather than discrete, submovement-like commands. The Bhushan and Shadmehr model is notable for its ability to produce segmented movements in simulations of force-field reaching movements. However this ability is due to the time delays it incorporates, rather than to its continuous nature. A model of similar structure that incorporates discrete submovements is much more likely to reproduce the salient characteristics of movement during stroke recovery, including both segmentation and periods of rest.

It is interesting to note that the inter-peak interval, a quantity directly related to the quality of the forward model, reaches an asymptotic level in outpatients, while amplitude and duration, quantities related to the quality of the inverse model, continue to increase in outpatients. This suggests that the forward model may be learned more quickly than the inverse model. It is interesting to note that the Bhushan and Shadmehr model implies that, when computational resources are limited, performance is most quickly improved by learning the forward model first, then refining the inverse model [7].

Another way to describe the recovery process is as system identification. If portions of the CNS involved in producing forward and inverse models of movement are damaged in a stroke, then some compensatory behavior by the remaining CNS takes place, perhaps by recruiting other areas of the brain (adjacent or analogous contralateral regions), employing neosynaptogenesis, utilizing existing neural connections, or all of the above. Regardless of the underlying nature of the compensatory behavior, the remaining portion of the CNS is required to identify the motor system: to char-

acterize the motions that result from a given motor command (the actuation system) and the sensory feedback that results from a given motion (the feedback system).

### **Implications for therapy**

One conclusion that follows from a system identification model of recovery is that requiring patients to make self-initiated movements in therapy is more effective in promoting recovery than allowing the patient to simply be moved, although both should provide some benefit. Movement of the patient's arm with no voluntary involvement from the patient may allow the map from motion to sensory feedback (the feedback system) to be refined, but would not aid refinement of the map between descending motor command and motion (the actuation system), due to the lack of descending motor commands. This implies that therapy tools that gently aid movement, such as MIT-MANUS, are preferable to therapy tools which rigidly dictate movement, such as continuous passive motion devices. The former requires patient involvement, while the latter do not.

Thus, the system identification theory of motor recovery can be tested by comparing the relative effects of therapy in which the patient is a passive participant, such as therapy received on a Continuous Passive Motion (CPM) machine, with the effects of therapy in which the patient makes self-initiated moves, such as that described in the Procedure section of Chapter 2.

# Chapter 8

## Conclusion and future work

### 8.1 Conclusion

#### 8.1.1 Motor behavior during stroke recovery

The answer to the question posed in Chapter 1:

**Does the evolution of the nature of segmentation in stroke patients' upper-limb movements follow a stereotypical pattern during recovery?**

has been answered with a yes.

Stroke patients' movements grow smoother during therapy, a change that can be explained by the progressive blending of submovements. The changes in stroke patients' submovements suggest an increased ability to perceive the position of their hand and an increased ability to predict the result of their movement. Furthermore, the ability to perceive one's kinematic state appears to be developed first. It may be possible that some types of rehabilitation exercise are more effective at training both for position perception and action prediction, while some train primarily position perception. This remains as a hypothesis to be tested.

### 8.1.2 Submovements

This work has produced additional evidence for the existence of submovements. The fine details of observations of increased movement smoothness in recovering stroke patients is consistent with the theory. Submovement-based analysis of patients' data also shows clear patterns which are consistent with modern theories of motor learning. At the very least, submovements provide a useful theoretical window through which to monitor motor behavior.

Even if their existence were a given fact, extracting submovements from continuous data is a subtle and arduous chore. If the direct study of submovements is the goal of a research endeavor, then the experiment design may need to be carefully considered and directed toward that goal. See [85, 72, 49, 67, 27] for some examples of how this has been done in the past. However, if large amounts of data are available then changes in submovement characteristics over time can be found statistically, as in Chapter 6.

### 8.1.3 Applications of submovements

Just as measurements of jerk have allowed identification of pre-symptomatic individuals with Huntington's disease when clinical measurements have not [79], the high resolution and specificity of other kinematic measures may allow observation of other previously unobservable phenomena. Such measures would serve to complement time-tested clinical scales, such as the Fugl-Meyer. Several research groups have used kinematic and force measures to quantify movement deficits in stroke patients [91, 2, 83, 50, 53, 38]. Our results extend their work by showing clear increases in smoothness in both acute and chronic populations, even in subjects who did not show an increase on the Fugl-Meyer scale. Measurement of smoothness may provide a meaningful, objective quantification of motor performance that could be used to augment clinical evaluations. Alternatively, to the extent that smoothness is result of submovement blending, direct estimation of submovement blending characteristics may provide an even more intuitive and robust measure of recovery.



The existence of submovements might indicate a discrete internal representation of motor commands. Strong direct evidence for discrete movement primitives in frog wiping reflexes has been shown [28, 39] in both force profiles and EMG measurements. Physiological evidence for discrete submovements has been reported in healthy human subjects as well; in slow finger movements Vallbo and Wessberg [85] showed both discrete kinematic jumps in finger position, as well as synchronized pulses of EMG activity in the finger flexors and extensors. If it is shown to be feasible, locating and measuring this internal coding of motor commands could lead to insight into the nature of human motor behavior and motor system pathologies. A similar coding of movement may be employed in neural-machine interfaces [90]. A control system based on discrete submovements requires much less information to be transferred (i.e. lower average communication bandwidth) between the controller and the system being controlled. Initial experiments into brain-computer interfaces are promising, but have shown very limited bandwidth capabilities [48]. Using discrete feed-forward control commands may make practical applications of neural interfaces realizable.

It should be noted that other, non-discrete models may be capable of describing decreasingly segmented behavior. However, in order to be fully successful, a model of recovery must produce movements that have significant periods of rest, as is often observed in stroke patients. For example, a continuous forward and inverse adaptive model pair described by Bhushan and Shadmehr [7] incorporates time delays representative of those in the visual and spinal feedback loops and predicts segmented behavior when learning to move in a novel force field. It predicts that the segmentation will decrease as the models become trained, but is unlikely to predict periods of rest.

As an aside, the behavior of the Bhushan and Shadmehr model is due to its structure and the existence of time delays, rather than to its continuous nature. A similar model could be implemented in discrete terms equally plausibly. A discrete submovement model of this structure is much more likely to reproduce the salient characteristics of movement during stroke recovery, including both segmentation and periods of rest.

There are control system applications for submovements, as well. Transmission delays tend to have a destabilizing effect on closed-loop control systems and often exist in teleoperated systems. The discrete nature of motor commands may be a mechanism by which control of movement is stabilized despite 100 ms and greater delays in neural pathways and in the visual feedback loop; the central nervous system may be stably “teleoperating” the periphery using submovements. Telerobotic systems in space, medicine, and hazardous material handling that adopt control architectures based on discrete feed-forward commands may become more stable, increasing performance. In addition, where the delay in these systems is due to bandwidth limitations, the concise nature of discrete command representation would decrease average bandwidth requirements and further improve system performance. As an added benefit, control system resources previously dedicated to continuously monitoring input and output commands would be freed to execute other tasks.

## 8.2 Future Work

This work has focused on analysis of tangential velocity profiles, following along the lines of theory 1, listed in Chapter 3. There may be merit in investigating submovements at other levels, such as with vector-summed velocity data, or with force data. If clear data could be taken, EMG-based studies of submovements may be the most revealing. And, if feasible, higher-level studies in animals and humans may lead to proving the existence of submovements and pinning down their origin in the CNS.

Several lines of research could branch out from this point:

### 8.2.1 Brain-computer interfaces (BCI’s)

Submovements can be accurately described with few parameters. This provides a efficient basis for describing even complex movements, which may reduce the amount of information transfer required to control movement. The simple coding of submovements may make BCI’s practical. BCI’s have shown promise [12, 66], but are currently bandwidth limited [48]. If it proves feasible, directly accessing a compressed repre-

sentation of movement through brain activity measurement may yield much higher performance from BCI's than is currently observed.

In order to isolate and decode the neural representation of submovements for use in BCI's, it will be necessary to measure neural signals at various levels in the neuro-muscular system during movement. A first step in this direction is to measure EMG of flexors and extensors in a single degree-of-freedom slow movement task to answer the question "What form does flexor and extensor EMG activity take during submovements?" Subsequent studies could apply similar methods using a variety of sensing techniques, including electro-encephalograms (EEG's).

### **8.2.2 Biologically-motivated discrete control systems**

By utilizing submovements, the human motor control system may gain robustness to uncertainty and time variation in 1) the dynamic model of the arm, 2) the environment, and 3) feedback delay. This level of robustness is desirable in many automation applications, but is extremely difficult to implement stably for systems of any significant complexity. A discrete controller modeled after patterns in human submovement production may impart these characteristics to automated systems, as well as robustness to unmodeled higher-order dynamics and to sensor and actuator failure (where there is sufficient redundancy). At the cost of control bandwidth, this would allow unprecedented robustness of performance. Initial experiments might focus on quantifying this robustness in first single-, then multiple-degree-of-freedom mechanical systems.

In addition, my research has hinted at the nature of operation of a hypothesized forward and inverse model pair responsible for selecting and executing discrete commands. By implementing this supervisory learning layer, a discrete submovement-based controller gains the additional advantage of requiring no a priori assumptions about the system model. The learning process will cause the system performance to improve over time and eventually become optimal for stationary systems. A second round of experiments would seek to quantify the performance of learning models of this type.

A biologically-motivated discrete controller would have application wherever it is desirable to trade bandwidth for the robustness properties listed above. Some potential applications include flexible robots, robots that physically interact with humans, unmanned underwater vehicles, teleoperated nuclear waste cleanup devices, space robots, or robots teleoperated via the internet.

### **8.2.3 Manually-operated systems**

Manually-operated systems that can be easily controlled by submovement-like discrete commands may exhibit improved performance over continuously controlled systems in several ways:

#### **Degrees of freedom**

While it is theoretically possible to simultaneously control as many independent degrees of freedom as there are in human biomechanics, in practice it is often difficult to control more than two or three. This limitation is encountered in the control of arm prostheses, in which it is rare that more than two degrees of freedom are actively controlled at one time. However, well known discrete-command interfaces provide notable exceptions; for example, a pianist has 88 “degrees-of-freedom” at her disposal, simultaneously providing inputs to as many as 10. There is a potential for discrete commands to allow control of a large number of degrees of freedom.

#### **Bandwidth**

Voluntary human movements of the type that have been applied to machine operation (e.g. turning a steering wheel, manipulating a joystick) rarely exceed 4 Hz. Discrete commands can be made at a much higher rate. Taking the example of typing, 100 5-letter words per minute corresponds to 1800 keystrokes per minute (including spaces) or 30 keystrokes per second (30 Hz). It is possible that, using discrete commands, human operators may teleoperate robots with a higher bandwidth than they themselves are capable of achieving in continuous motion. This might be tested by constructing

a keyboard-like interface for human control of a robot and assigning a complete feed-forward command to each key. Using a setup such as this, it would be possible to have subjects attempt to execute a task similar to Fitts' tapping task, where the goal would be to rapidly move the robot arm back and forth between two target regions. Maximum bandwidth could easily be calculated from such a task and compared with known limits of humans' continuous movement bandwidth.

## **Stability**

The feed-forward nature of discrete commands helps avoid plant instability in the presence of significant transmission delays, common in space telerobotic and tele-medical applications. Delay-induced instability can be avoided by updating feedforward commands at intervals greater than the delay. In addition, instability due to unmodeled high-frequency dynamics is also avoided by a discrete controller when the interval between commands is greater than the time required for the high frequency transient to die off. High-frequency transients can also be avoided by employing smooth feedforward commands, such as is the case in human submovements. These commands contain relatively little high-frequency content and avoid exciting high-frequency dynamics at all.

Studying human motor control rarely yields clear pictures of the inner workings of the CNS and the neuromuscular system, and it never produces stories that are not challenged by others in the community. There is debate over whether motor control is continuous or discrete. Among those that consider motor control to be discrete, there is still no consensus about the nature of the discrete units and their origin. Although these observations of submovement patterns in stroke recovery do not begin to resolve these debates, it is hoped that this work adds some small piece to the grand puzzle of motor control and will motivate others in some way to answer the questions that remain.



# Appendix A

## Mathematical definitions of curvature

### A.1 Summary

Three different definitions of curvature are compared and found to be mathematically equivalent. An intuitive derivation of one of the definitions is outlined.

### A.2 Introduction

Multiple mathematical expressions of curvature can sow confusion and mask the fact that they are all consistent with each other. The purpose of this appendix is to establish that the various expressions of curvature are indeed mathematically synonymous and to show how to manipulate each to get the others.

## A.3 Comparison

### A.3.1 The “rate of change of the unit tangent vector” formula

Curvature can be defined as

$$\kappa = \left\| \frac{d\vec{T}}{ds} \right\| \quad (\text{A.1})$$

where  $T$  is the unit tangent vector to the curve, defined by

$$\vec{T} = \frac{\vec{v}}{\|\vec{v}\|} \quad (\text{A.2})$$

and  $s$  is path length along the curve. [47, pg 825]

In Krebs et al. [45], curvature is defined as

$$\kappa = \frac{d\theta}{ds} \quad (\text{A.3})$$

where  $\theta$  is the instantaneous velocity angle. However, this is equivalent to equation A.1, due to the fact that any change in  $\vec{T}$  must change its direction, rather than its magnitude (it is by definition a unit vector). For small  $\Delta T$ ,  $\Delta T = \Delta\theta$ , the angle of rotation of  $\vec{T}$ .

Equation A.1 is also consistent with the commonly used formula (employed by Abend et al. [1]):

$$\kappa = \frac{v_y a_x - v_x a_y}{(v_x^2 + v_y^2)^{\frac{3}{2}}} \quad (\text{A.4})$$

where the quantities  $v_x, v_y, a_x, a_y$  are the velocities and accelerations along a planar trajectory. This can be demonstrated as follows. If all quantities are parameterized in time (making  $s(t)$ ,  $T(t)$ , and  $\kappa(t)$ ), then equation A.1 can be expressed as:

$$\kappa = \left\| \frac{\frac{dT}{dt}}{\frac{ds}{dt}} \right\| \quad (\text{A.5})$$



Assuming a planar path,  $\vec{v}$  and  $\vec{a}$  can be expressed in terms of orthogonal axes:

$$\vec{v} = v_x \hat{i} + v_y \hat{j} \quad (\text{A.6})$$

$$\vec{a} = a_x \hat{i} + a_y \hat{j} \quad (\text{A.7})$$

The rate of change of  $s$  is simply equal to the tangential velocity along the path:

$$\frac{ds}{dt} = \|\vec{v}\| \quad (\text{A.8})$$

The rate of change of  $\vec{T}$  can be calculated by substituting A.6 into A.2, yielding the following:

$$\frac{d\vec{T}}{dt} = \frac{d}{dt} \left[ \frac{v_x \hat{i} + v_y \hat{j}}{\|v_x \hat{i} + v_y \hat{j}\|} \right] \quad (\text{A.9})$$

By the product rule this becomes:

$$\frac{d\vec{T}}{dt} = (v_x \hat{i} + v_y \hat{j}) \frac{d}{dt} \left[ \frac{1}{\sqrt{v_x^2 + v_y^2}} \right] + \quad (\text{A.10})$$

$$\left[ \frac{1}{\sqrt{v_x^2 + v_y^2}} \right] \frac{d}{dt} (v_x \hat{i} + v_y \hat{j}) \quad (\text{A.11})$$

Break the expression down into its parts:

$$\frac{d}{dt} [(v_x^2 + v_y^2)^{-\frac{1}{2}}] = \frac{-v_x a_x - v_y a_y}{(v_x^2 + v_y^2)^{\frac{3}{2}}} \quad (\text{A.12})$$

$$\frac{d}{dt} [v_x \hat{i} + v_y \hat{j}] = a_x \hat{i} + a_y \hat{j} \quad (\text{A.13})$$

Substitute A.12 and A.13 into A.11:

$$\frac{d\vec{T}}{dt} = \frac{(v_x\hat{i} + v_y\hat{j})(-v_xa_x - v_ya_y) + (v_x^2 + v_y^2)(a_x\hat{i} + a_y\hat{j})}{(v_x^2 + v_y^2)^{\frac{3}{2}}} \quad (\text{A.14})$$

Simplify:

$$= \frac{[v_y^2a_x - v_xv_ya_y]\hat{i} + [v_x^2a_y - v_xv_ya_x]\hat{j}}{(v_x^2 + v_y^2)^{\frac{3}{2}}} \quad (\text{A.15})$$

$$= \frac{Cv_y\hat{i} - Cv_x\hat{j}}{(v_x^2 + v_y^2)^{\frac{3}{2}}}, \text{ where } C = v_ya_x - v_xa_y \quad (\text{A.16})$$

Evaluate the absolute value:

$$\left\| \frac{d\vec{T}}{dt} \right\| = \frac{\sqrt{C^2(v_x^2 + v_y^2)}}{(v_x^2 + v_y^2)^{\frac{3}{2}}} \quad (\text{A.17})$$

$$= \frac{C}{(v_x^2 + v_y^2)} \quad (\text{A.18})$$

With equation A.8, substitute equation A.18 back into equation A.5:

$$\kappa = \frac{\left\| \frac{d\vec{T}}{dt} \right\|}{\left\| \frac{ds}{dt} \right\|} \quad (\text{A.19})$$

$$= \frac{C}{(v_x^2 + v_y^2)} \frac{1}{(v_x^2 + v_y^2)^{\frac{1}{2}}} \quad (\text{A.20})$$

Substitute in equation A.16:

$$\kappa = \frac{v_ya_x - v_xa_y}{(v_x^2 + v_y^2)^{\frac{3}{2}}} \quad (\text{A.21})$$

This is a restatement of equation A.4, verifying the assertion that it is mathematically equivalent to equation A.3.

### A.3.2 Frenet Formula

It is also stated in [45] that equation A.3 is equivalent to the Frenet Formula:

$$\kappa = \frac{[(\vec{v} \cdot \vec{v})(\vec{a} \cdot \vec{a}) - (\vec{v} \cdot \vec{a})^2]^{\frac{1}{2}}}{(\vec{v} \cdot \vec{v})^{\frac{3}{2}}} \quad (\text{A.22})$$

Substituting equations A.6 and A.7 into equation A.22 and evaluating the expression verifies that equation A.4 is simply a reformulation of the Frenet Formula in the plane.

$$\kappa = \frac{[(\vec{v} \cdot \vec{v})(\vec{a} \cdot \vec{a}) - (\vec{v} \cdot \vec{a})^2]^{\frac{1}{2}}}{(\vec{v} \cdot \vec{v})^{\frac{3}{2}}} \quad (\text{A.23})$$

$$= \frac{\left[(v_x^2 + v_y^2)(a_x^2 + a_y^2) - (v_x a_y + v_y a_x)^2\right]^{\frac{1}{2}}}{v_x^2 + v_y^2} \quad (\text{A.24})$$

$$= \frac{\left[v_x^2 a_x^2 + v_y^2 a_y^2 + v_x^2 a_y^2 + v_y^2 a_x^2 - v_x^2 a_x^2 - v_y^2 a_y^2 - 2v_x v_y a_x a_y\right]^{\frac{1}{2}}}{v_x^2 + v_y^2} \quad (\text{A.25})$$

$$= \frac{\left[v_x^2 a_y^2 - 2v_x v_y a_x a_y + v_y^2 a_x^2\right]^{\frac{1}{2}}}{v_x^2 + v_y^2} \quad (\text{A.26})$$

$$= \frac{\left[(v_x a_y - v_y a_x)^2\right]^{\frac{1}{2}}}{v_x^2 + v_y^2} \quad (\text{A.27})$$

$$= \frac{v_x a_y - v_y a_x}{v_x^2 + v_y^2} \quad (\text{A.28})$$

This shows that equations A.3 and A.22 are indeed equivalent. A similar method can be used to determine curvature formulas for 3- and higher-dimensional spaces. For example, the corresponding formula for 3D space (as employed in [22]) is:

$$\sqrt{\frac{(v_y a_z - v_z a_y)^2 + (v_z a_x - v_x a_z)^2 + (v_x a_y - v_y a_x)^2}{(v_x^2 + v_y^2 + v_z^2)^3}} \quad (\text{A.29})$$

### A.3.3 The “cross product” formula

Another equation for curvature is given by [47]:

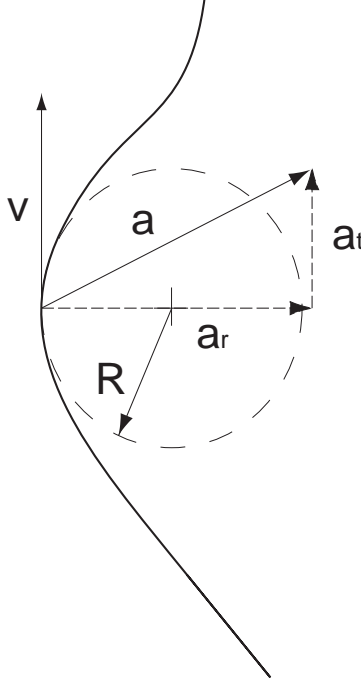


Figure A-1: Instantaneous velocity, acceleration, and radius of curvature in a movement trajectory.

$$\kappa = \frac{\|\vec{v} \times \vec{a}\|}{\|\vec{v}\|^3} \quad (\text{A.30})$$

Again, substituting in equations A.6 and A.7 permits derivation of equation A.4, showing mathematical equivalence.

$$\frac{\|\vec{v} \times \vec{a}\|}{\|\vec{v}\|^3} = \frac{v_x a_y - v_y a_x}{(v_x^2 + v_y^2)^{\frac{3}{2}}} \quad (\text{A.31})$$

This expression of curvature suggests an intuitive derivation. Consider the path, in figure A-1. The radius of curvature of any curve is given by:

$$r = \frac{1}{\kappa} \quad (\text{A.32})$$

For a particle traveling at tangential velocity,  $\vec{v}$ , the radial acceleration  $\vec{a}_r$  is given by:

$$\vec{a}_r = \frac{\|\vec{v}\|^2}{r} \quad (\text{A.33})$$

The cross product of the velocity and acceleration allows expression of the radial acceleration:

$$\|\vec{v} \times \vec{a}\| = \|\vec{v}\| \|\vec{a}\| \sin(\theta) \quad (\text{A.34})$$

$$= \|\vec{v}\| \|\vec{a}\| \cos\left(\frac{\pi}{2} - \theta\right) \quad (\text{A.35})$$

$$= \|\vec{v}\| \|\vec{a}_r\| \quad (\text{A.36})$$

where  $\theta$  is the angle between the velocity and acceleration vectors. Combining equations A.32, A.33, and A.36 returns A.30, completing the derivation.

## A.4 Conclusion

The three definitions of curvature, the “rate of change of the unit tangent vector” formula (equation A.1), the Frenet Formula (equation A.22), and the “cross product” formula (equation A.30) all can be reduced to equation A.4 for the 2D case, verifying their mathematical equivalence.



# Appendix B

## Derivations related to the Branch-and-Bound algorithm of Chapter 5

### B.1 Calculating $U\prime$

What follows is an outline of the calculation of the upper bound on  $\frac{\partial \mathcal{E}}{\partial p_i}$ , that is, the change in error,  $\mathcal{E}$ , with respect to each parameter,  $p_i$ , over each subspace. This is also identified as  $U\prime$ . These derivations are graphically motivated; the optimization criterion has been chosen to be the absolute error ( $\int |f(t) - g(t)| dt$ ), rather than the rms error ( $\int (f(t) - g(t))^2 dt$ ) in order to facilitate this. The change in error with a change in each parameter ( $\frac{\partial \mathcal{E}}{\partial p_i}$ ) can be visualized as the change in *area* between the candidate function the objective function. The change in error can be no more than the sum of the area newly occupied and the area vacated by the function during the parameter change.

### B.1.1 Minimum-jerk submovements

Minimum-jerk submovements can be uniquely described by three parameters, the amplitude of the peak  $A$ , the time at which the peak occurs  $t$ , and the duration of the movement  $w$ :

$$v(\tau) = \frac{A}{1.875} \left( 30 \left( \frac{\tau - t + \frac{w}{2}}{w} \right)^2 - 60 \left( \frac{\tau - t + \frac{w}{2}}{w} \right)^3 + 30 \left( \frac{\tau - t + \frac{w}{2}}{w} \right)^4 \right) \quad , t - \frac{w}{2} \leq \tau \leq t + \frac{w}{2} \quad (\text{B.1})$$

$$= 0 \quad , \text{ otherwise} \quad (\text{B.2})$$

The area under a minimum-jerk curve is equal to  $wA/1.875$ .

#### Bounding $\frac{\partial \mathcal{E}}{\partial t}$

For all unimodal (single-peaked) submovements, changes in  $t$  will both occupy and vacate no more than a rectangle of width  $\Delta t$  and height equal to the height of the function.

$$\Delta \mathcal{E} \leq 2 \Delta t A \quad (\text{B.3})$$

$$\frac{\Delta \mathcal{E}}{\Delta t} \leq 2A \quad (\text{B.4})$$

$$\frac{\partial \mathcal{E}}{\partial t} \leq 2A_{MAX} \quad (\text{B.5})$$

where  $A_{MAX}$  is the maximum amplitude of the submovement over the current subspace.

#### Bounding $\frac{\partial \mathcal{E}}{\partial w}$

Changes in  $w$  will either vacate area or occupy new area, but not both. The change in area occupied is given by:



$$\Delta\mathcal{E} = \frac{\Delta w}{w} \text{ (area under min-jerk curve)} \quad (\text{B.6})$$

$$\Delta\mathcal{E} = \frac{\Delta w}{w} \left( \frac{wA}{1.875} \right) \quad (\text{B.7})$$

$$\Delta\mathcal{E} = \frac{\Delta w A}{1.875} \quad (\text{B.8})$$

$$\Delta\mathcal{E}\Delta w = \frac{A}{1.875} \quad (\text{B.9})$$

$$\frac{\partial\mathcal{E}}{\partial w} \leq \frac{A_{MAX}}{1.875} \quad (\text{B.10})$$

**Bounding  $\frac{\partial\mathcal{E}}{\partial A}$**

As with  $w$ , changes in  $A$  will either vacate area or occupy new area, but not both. The area scales linearly with amplitude.

$$\Delta\mathcal{E} = \frac{\Delta A}{A} \text{ (area under min-jerk curve)} \quad (\text{B.11})$$

$$\Delta\mathcal{E} = \frac{\Delta A}{A} \left( \frac{wA}{1.875} \right) \quad (\text{B.12})$$

$$\mathcal{E} = \frac{\Delta A w}{1.875} \quad (\text{B.13})$$

$$\frac{\Delta\mathcal{E}}{\Delta A} = \frac{w}{1.875} \quad (\text{B.14})$$

$$\frac{\partial\mathcal{E}}{\partial A} \leq \frac{w_{MAX}}{1.875} \quad (\text{B.15})$$

### B.1.2 Gaussian submovements

Gaussian speed curves can also be uniquely described by three parameters, the amplitude of the peak  $A$ , the time at which the peak occurs  $t$ , and the standard deviation of the curve  $\sigma$ :  $v(\tau) = Ae^{\frac{(\tau-t)^2}{2\sigma^2}}$ . The area under such a Gaussian curve is equal to  $\sqrt{2\pi}\sigma A$ .

### Bounding $\frac{\partial \mathcal{E}}{\partial t}$

Because Gaussian curves are unimodal, changes in  $t$  will both occupy and vacate no more than a rectangle of with  $\Delta t$  and height equal to the height of the function.

$$\Delta \mathcal{E} \leq 2\Delta t A \quad (\text{B.16})$$

$$\frac{\Delta \mathcal{E}}{\Delta t} \leq 2A \quad (\text{B.17})$$

$$\frac{\partial \mathcal{E}}{\partial t} \leq 2A_{MAX} \quad (\text{B.18})$$

where  $A_{MAX}$  is the maximum amplitude of the submovement over the current subspace.

### Bounding $\frac{\partial \mathcal{E}}{\partial \sigma}$

Changes in  $\sigma$  will either vacate area or occupy new area, but not both. The change in area occupied is given by:

$$\Delta \mathcal{E} = \frac{\Delta \sigma}{\sigma} (\text{area under a Gaussian curve}) \quad (\text{B.19})$$

$$\Delta \mathcal{E} = \frac{\Delta \sigma}{\sigma} (\sqrt{2\pi} \sigma A) \quad (\text{B.20})$$

$$\frac{\Delta \mathcal{E}}{\Delta \sigma} = \sqrt{2\pi} A \quad (\text{B.21})$$

$$\frac{\partial \mathcal{E}}{\partial \sigma} \leq \sqrt{2\pi} A_{MAX} \quad (\text{B.22})$$

### Bounding $\frac{\partial \mathcal{E}}{\partial A}$

As with  $\sigma$ , changes in  $A$  will either vacate area or occupy new area, but not both. The area scales linearly with amplitude.

$$\Delta\mathcal{E} = \frac{\Delta A}{A} \text{ (area under a Gaussian curve)} \quad (\text{B.23})$$

$$\Delta\mathcal{E} = \frac{\Delta A}{A} (\sqrt{2\pi}\sigma A) \quad (\text{B.24})$$

$$\mathcal{E} = \sqrt{2\pi}\sigma \Delta A \quad (\text{B.25})$$

$$\frac{\Delta\mathcal{E}}{\Delta A} = \sqrt{2\pi}\sigma \quad (\text{B.26})$$

$$\frac{\partial\mathcal{E}}{\partial A} \leq \sqrt{2\pi}\sigma_{MAX} \quad (\text{B.27})$$



# Appendix C

## Empirical submovement descriptions

Several sets of experimental results suggest typical parameters for submovements, particularly in timing, and highlight considerations in choosing a candidate submovement shape.

### C.1 Submovements in tangential velocity data

#### C.1.1 Symmetric vs. asymmetric submovement velocity profiles

Although submovement velocity profiles have often been described using symmetric functions (e.g. minimum-jerk curves, Gaussian curves, cubic B-splines), several researchers have reported significant asymmetry in the profiles when examined more closely [95, 68, 62]. Plamondon et al [72] show that asymmetric profiles fit significantly better than their symmetric counterparts. Vallbo and Wessberg [85] also note asymmetry in finger flexion velocity profiles. The direction and magnitude of asymmetry has been shown to be dependent on movement speed [65], with moderate-speed arm movements happening to possess near symmetry.

### C.1.2 Straightness of submovements

Morasso and Mussa Ivaldi [63], two of the first to propose an overlapping-submovement model for movement, used curved submovements with cubic polynomial velocity profiles. Curvilinear submovements were chosen because they provided a better fit to the trajectories and velocity and curvature profiles of their data. In addition, their model required that two submovements be active at all times (double-overlapping), a constraint that they justified based on their choice of velocity profile. They did not report considering other velocity profiles or how other profiles might affect the double-overlap constraint or the choice of curved vs. straight submovements.

Although human point-to-point arm movements are very nearly straight, they contain subtle, apparently repeatable deviations from straightness. Harris and Wolpert [33] were able to reproduce these deviations with a surprisingly simple model: a controller that minimizes endpoint variance, given neural noise that is proportional to the size of the control signal. This suggests that the observation of straightness in human movements may be a side-effect of some type of variance optimization, rather than a product of kinematic optimization.

Studying point-to-point movements may allow the assumption of (very-roughly) straight line movement. This may be feasible, despite the fact that the movement is not actually very well described by a straight line. As observed by Morasso and Mussa Ivaldi [63], changing the direction of submovements caused significant differences in plots of movement path, but very little difference in plots of tangential velocity. If submovements are inferred from tangential velocity, straightness and direction of submovements may be less relevant.

### C.1.3 Inter- and intra-subject consistency

Milner and Ijaz [61] and Vallbo and Wessberg [85] both observe that velocity profiles for single submovements are quite consistent for individual subjects, but vary somewhat more between subjects. Novak et al. [67] note that even within single subjects, submovement shape varies considerably from movement to movement.

### **C.1.4 Frequency of submovements**

The work of several authors involving reaching movements show submovements that occur at 4-5 Hz [87, 22]. However, Vallbo and Wessberg [85] found that the submovements in finger movements occurred at about 8-10 Hz.

### **C.1.5 Duration of submovements**

Fetters and Todd showed a tight clustering of infants' submovement durations around 200 ms [22].

Frend and Büdingen showed that the fastest voluntary contractions in human arm muscle reached peak force in about 83 ms. They observed that this time was fairly invariant with force level, force production capability of the muscle being measured, and level of muscle tension before the contraction. They also showed in preliminary measurements that human calf muscle reaches peak force between 80-90 ms. [25]

Smith et al. discovered that the movements of patients with Huntington's disease become irregular 200-300 ms after movement initiation [79]. This is suggestive of the onset of a second submovement. Smith et al. conclude that Huntington's Disease manifests itself as a deficiency in the error correction process that occurs during movement.

### **C.1.6 Shape of submovements**

Krylow and Rymer suggest that the bell-like shape of movements may be due primarily to the intrinsic properties of muscle [46]. The similarity they show, however, is on the leading edge of the bell. They do not address the trailing edge and models of single muscle activation do not indicate a symmetric or nearly-symmetric trailing edge.

Several researchers, however, have demonstrated highly correlated agonist/antagonist bursts of EMG [16, 27, 85]. It may be that such coordinated activity is necessary to produce the observed symmetry. It may also be that coordination of this type allows the motor control system to work around the limited bandwidth of the neuromuscular

system to a certain extent [16].

## C.2 Submovements in force data

Gordon and Ghez conducted a series of experiments in which subjects' arms were immobilized, and subjects were asked to follow certain "force trajectories", that is, recreate certain time histories of forces [27]. The authors speculate that the first peak of the second derivative of force is used by internal motor control processes to estimate what the peak in force is likely to be. (It should be noted that this can only be done if the shape of the force curve is well known.) This estimate is then used to initiate a corrective action, bringing the actual peak force nearer to the desired value [30, 31].

The rise time in the experiments of Gordon and Ghez was in some cases less than 150 ms. In order for corrective actions to have effect, they must have been initiated earlier than 150 ms into the movement.

As an aside, it is interesting to consider how closely the second derivative of force mimicked the sum of the agonist and antagonist EMG signals (see figure 3A, p 230, [27]). It may be profitable to compare the second derivative of force to acceleration or jerk or a combination thereof. They may be related by a model of the mechanical impedance of the arm. If jerk also appeared to be related to EMG magnitude, theories which postulate the minimization of jerk as an optimization criterion for movement may be shown to be similar to Harris and Wolpert's theory [33] postulating minimization of endpoint variance in the presence of signal-dependent noise as an optimization criterion.

## C.3 Submovements in EMG data

Vallbo and Wessberg's observations of regular, coordinated, pulsatile EMG signals accompanying slow finger movements shows perhaps the clearest picture of submovements any where in the literature.



Cooke and Brown [16] demonstrated in arm movements a tight coupling of agonist/antagonist burst pairs. This could conceivably be used as a foundation for describing submovements. In order to do this, however, it would be necessary to address the observations of Ghez and Gordon [27] that the antagonist burst can be suppressed if the subject is given appropriate feedback and asked to do so.



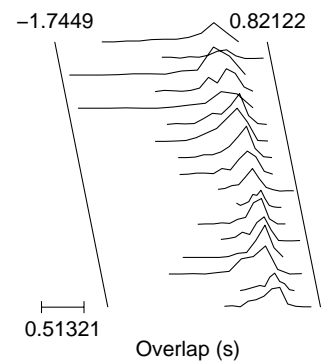
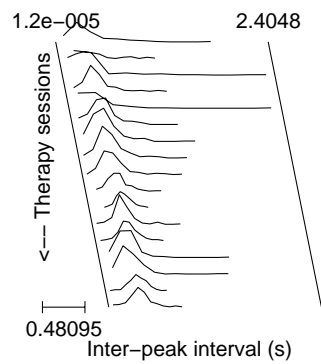
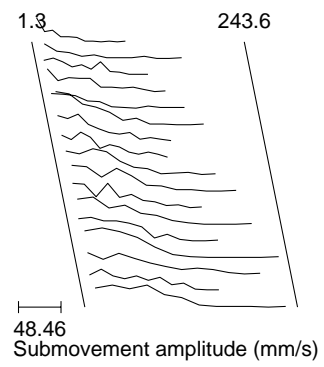
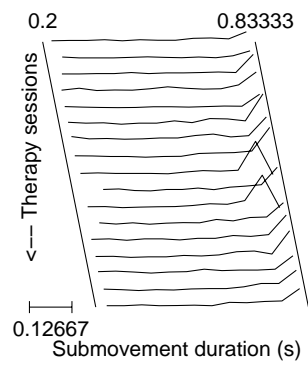
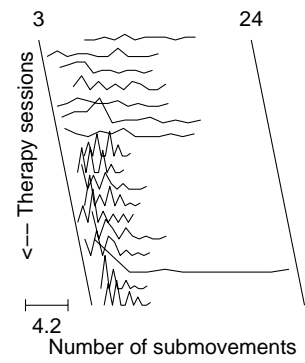
# Appendix D

## Raster plots of submovement characteristics

This Appendix contains raster plots of the submovement characteristics for the subjects' data reported in this thesis. The plots show the relative frequency of occurrences for particular values of each submovement characteristic.

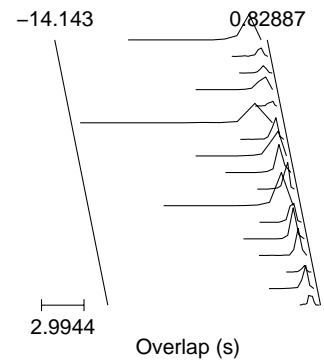
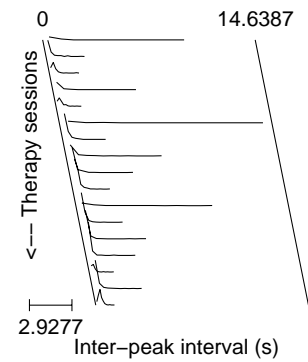
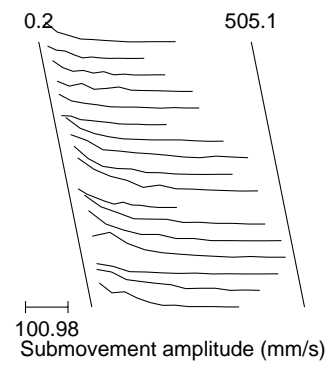
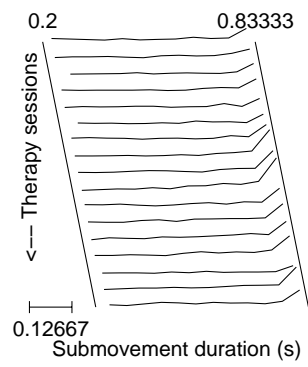
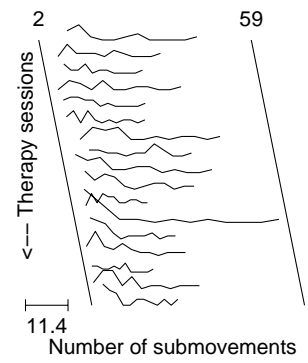
# Submovement characteristics

raster plots for D:\db\spaulding\motor\102



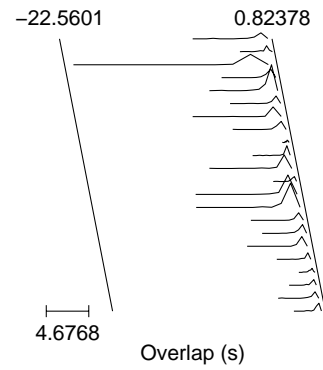
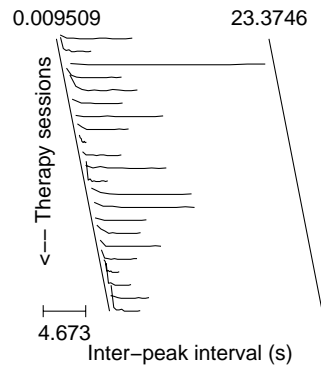
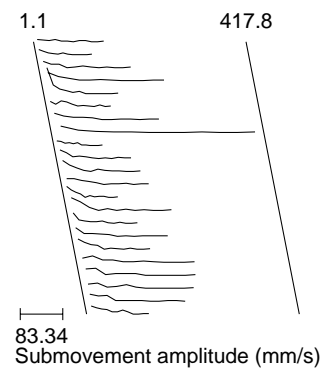
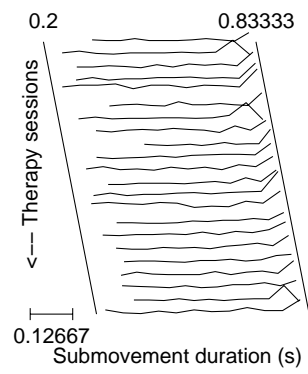
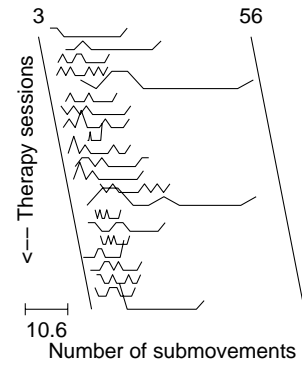
# Submovement characteristics

raster plots for D:\db\spaulding\motor\104



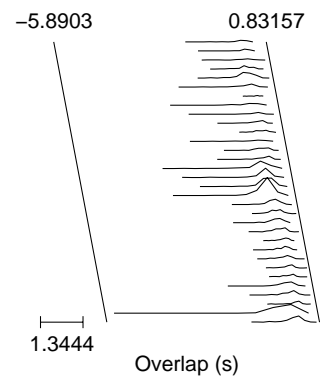
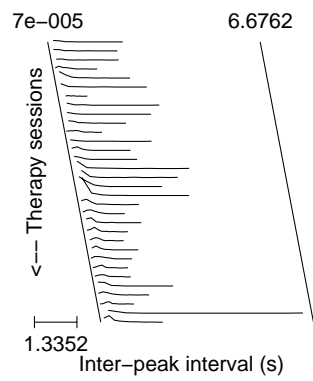
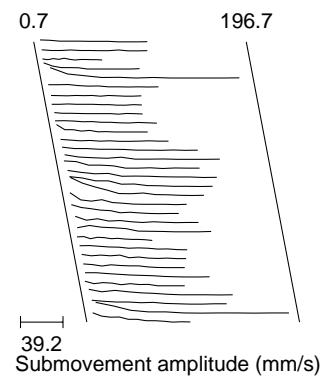
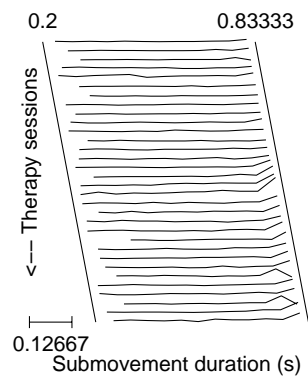
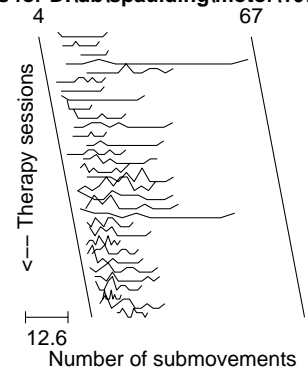
# Submovement characteristics

raster plots for D:\db\spaulding\sensory\105



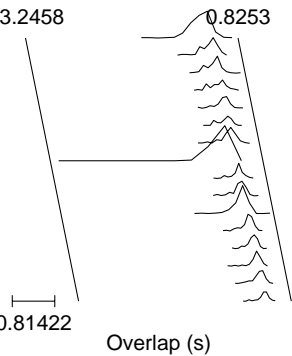
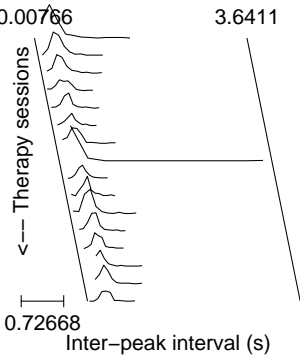
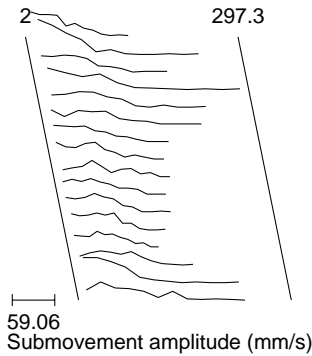
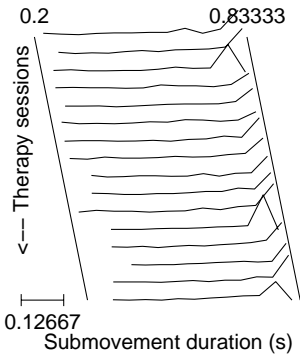
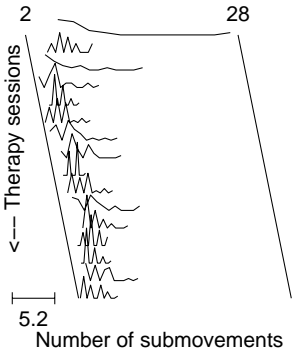
# Submovement characteristics

raster plots for D:\db\spaulding\motor\107



Submovement characteristics

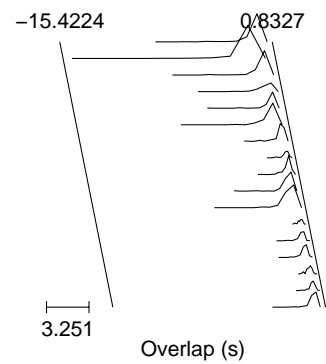
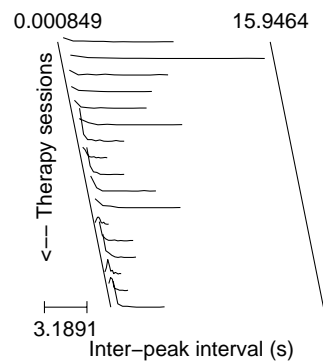
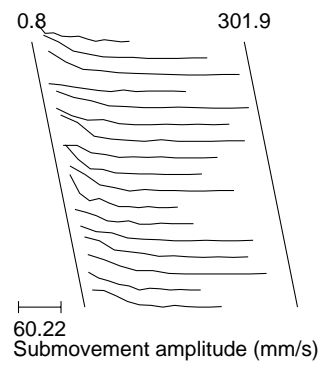
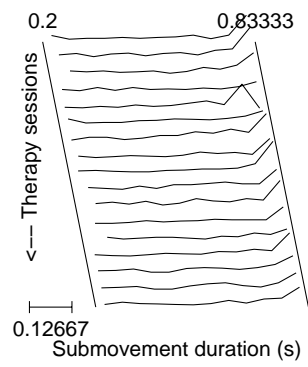
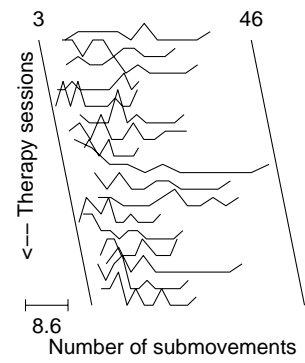
raster plots for D:\db\spaulding\sensory\201





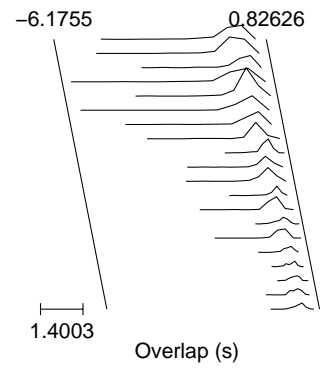
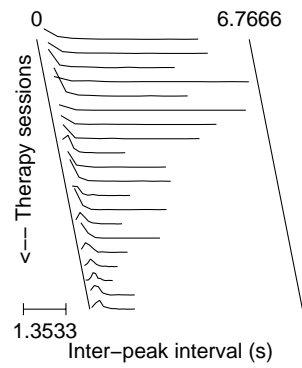
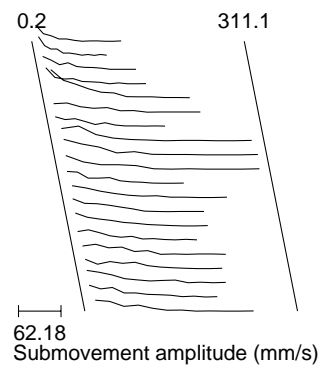
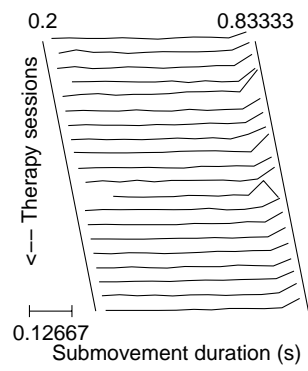
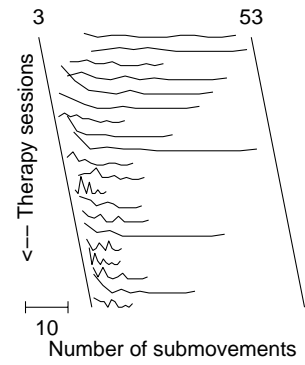
# Submovement characteristics

raster plots for D:\db\spaulding\motor\203



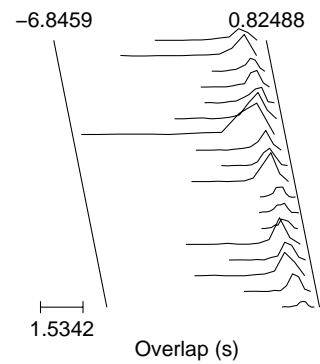
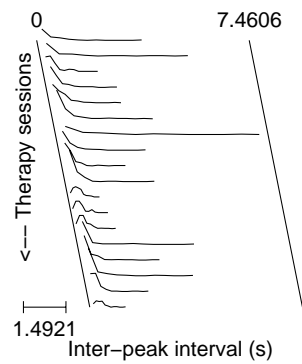
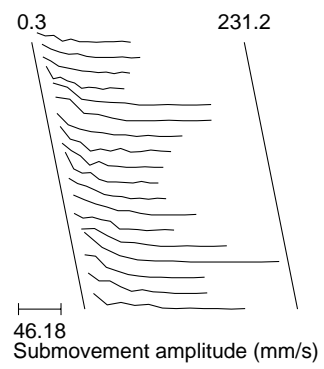
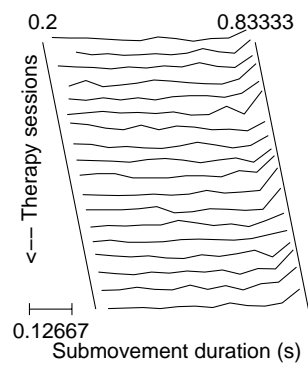
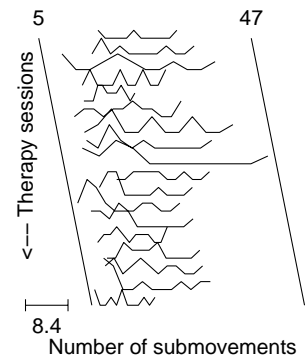
# Submovement characteristics

raster plots for D:\db\spaulding\motor\204



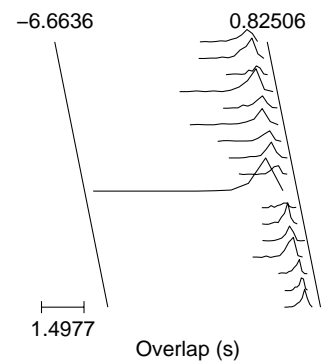
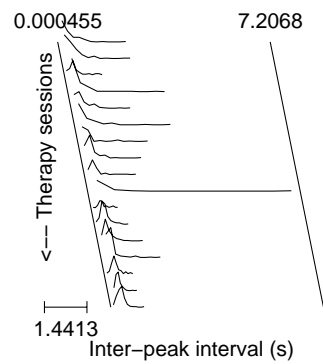
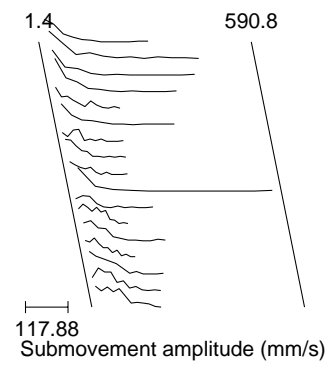
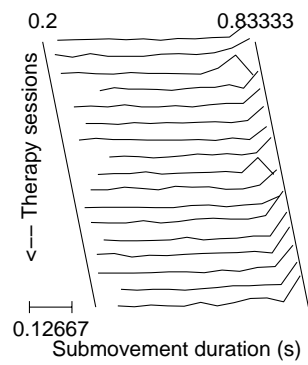
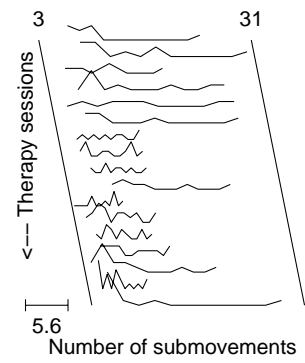
# Submovement characteristics

raster plots for D:\db\spaulding\motor\205



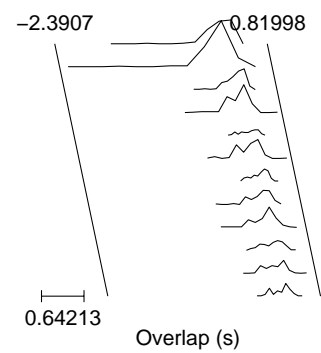
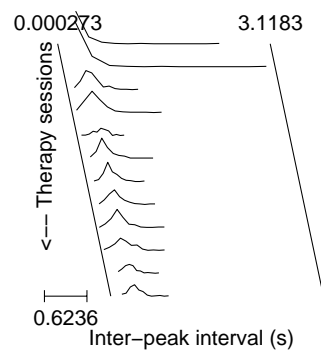
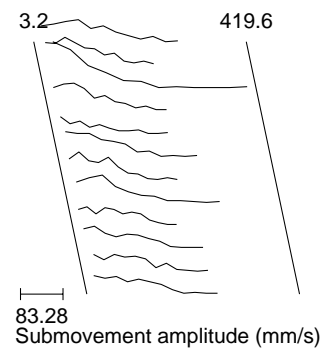
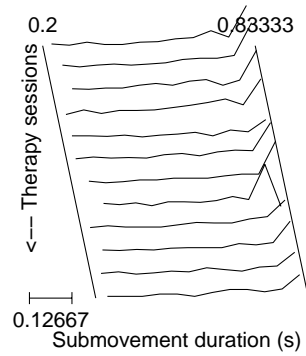
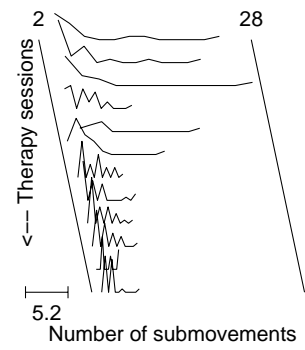
# Submovement characteristics

raster plots for D:\db\spaulding\motor\206



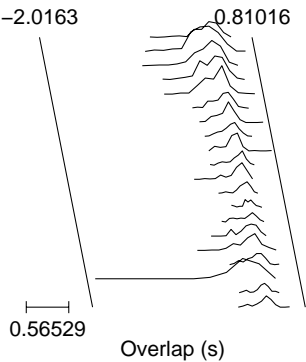
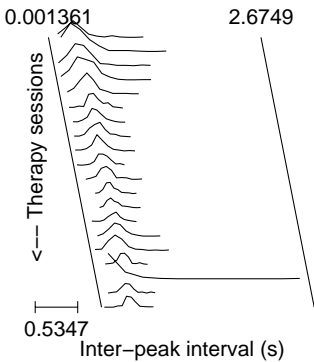
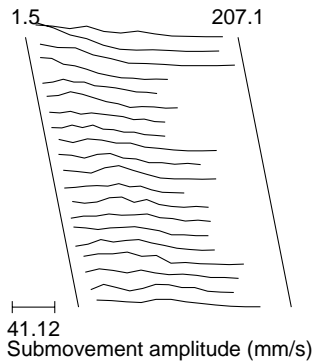
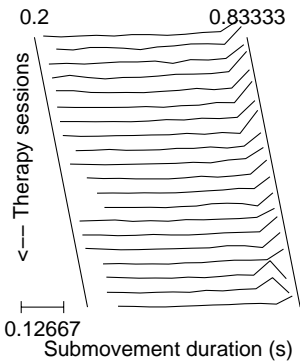
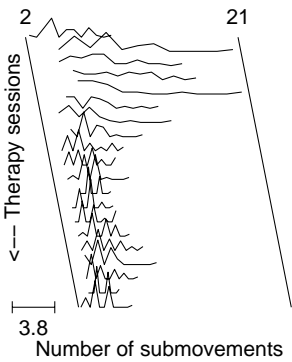
# Submovement characteristics

raster plots for D:\db\spaulding\motor\207



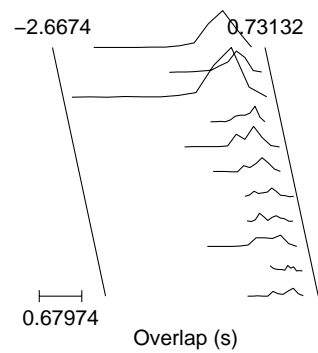
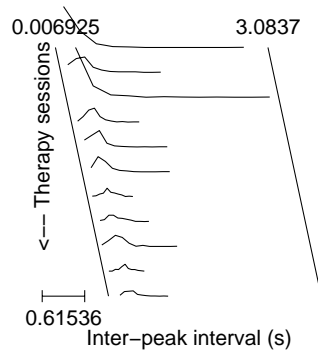
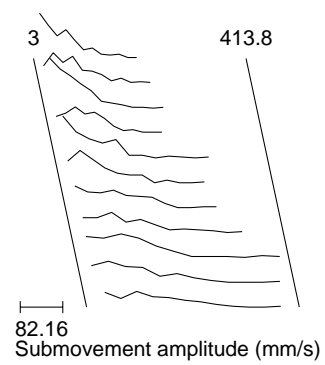
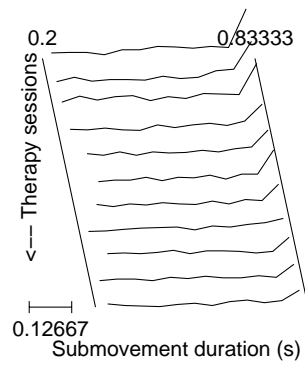
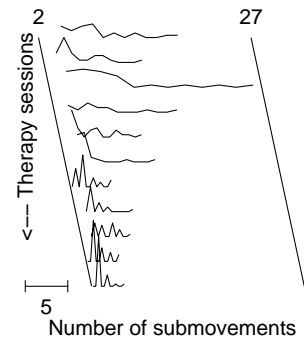
Submovement characteristics

raster plots for D:\db\spaulding\strength\302



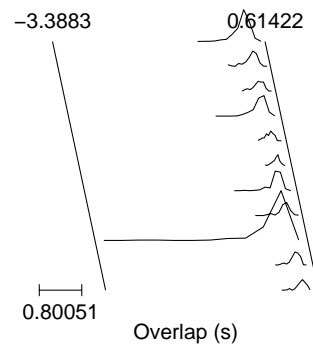
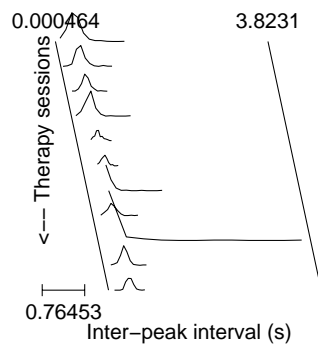
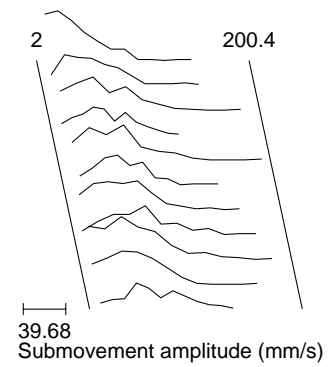
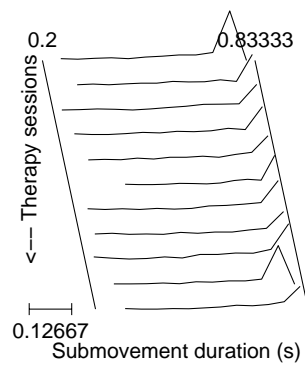
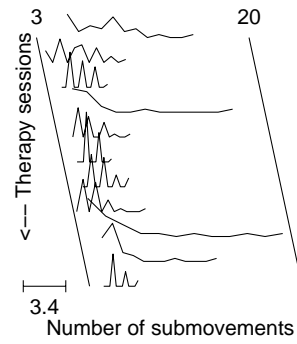
# Submovement characteristics

raster plots for D:\db\spaulding\sensory\303



## Submovement characteristics

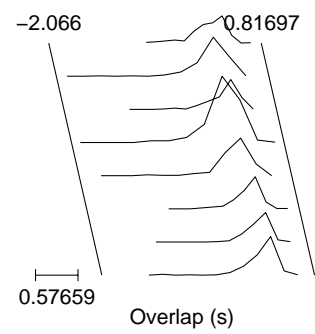
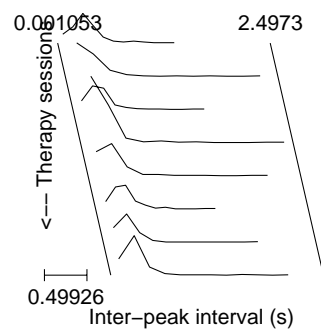
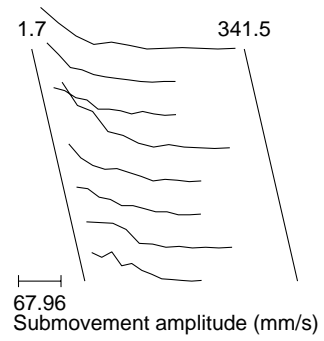
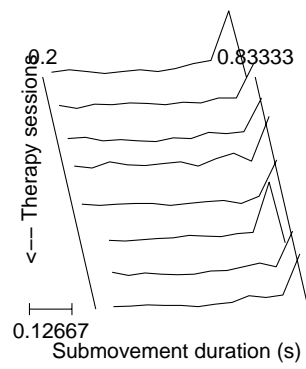
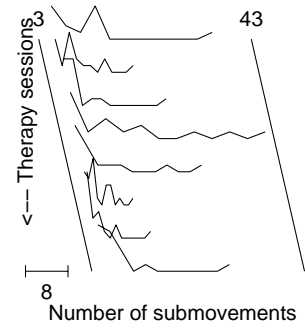
raster plots for D:\db\spaulding\strength\701





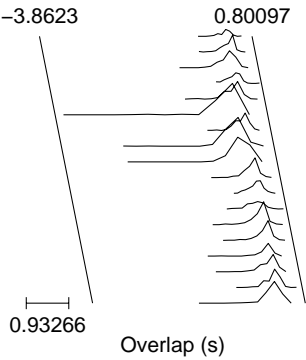
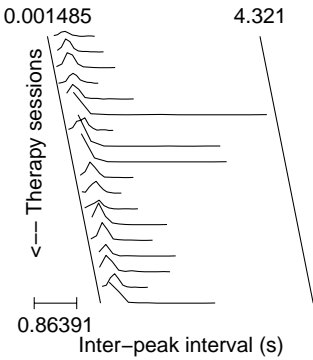
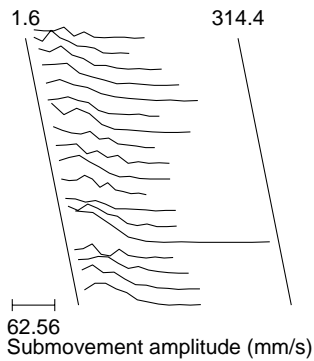
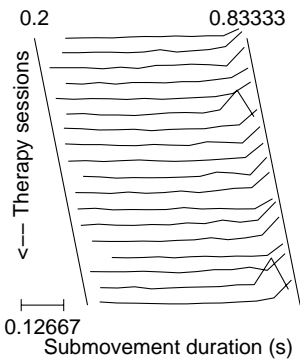
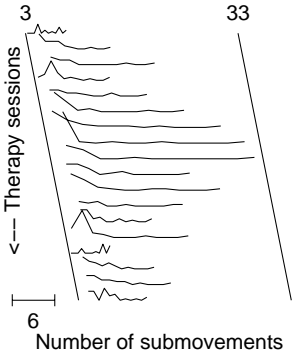
# Submovement characteristics

raster plots for D:\db\spaulding\motor\702



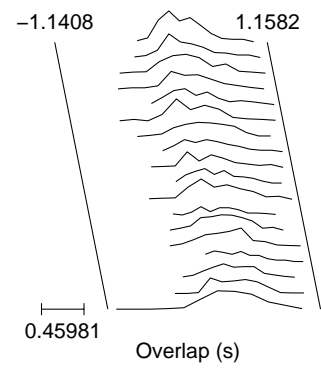
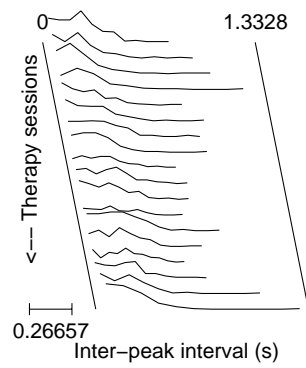
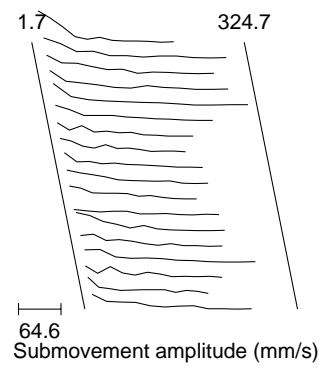
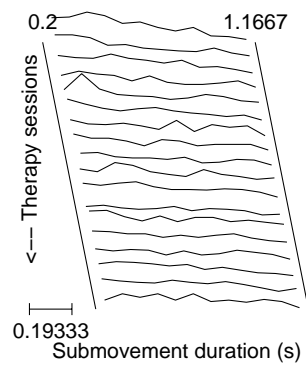
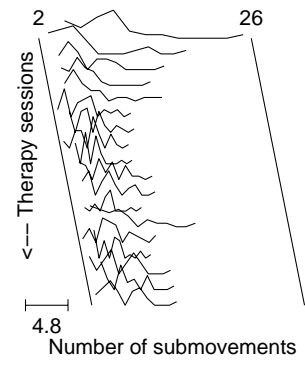
Submovement characteristics

raster plots for D:\db\spaulding\strength\704



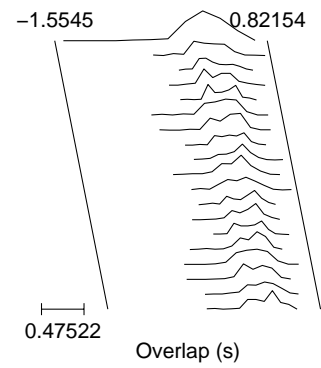
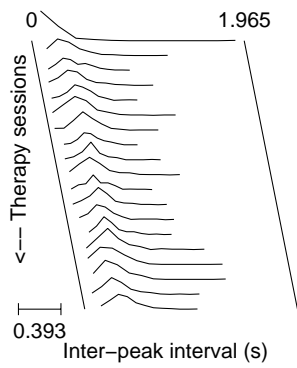
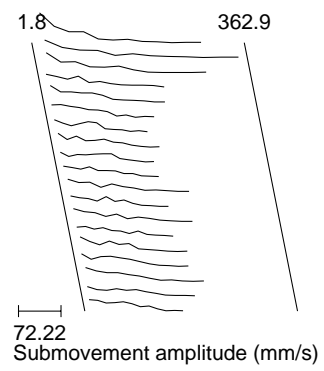
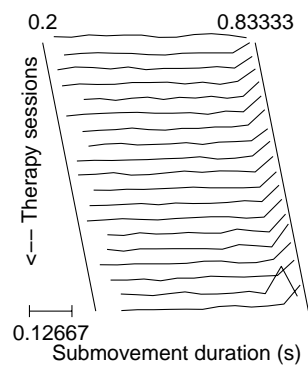
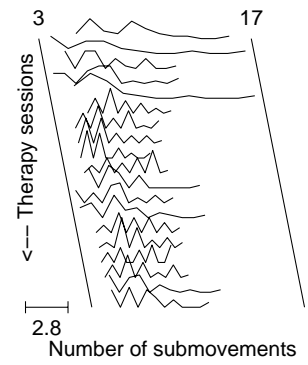
# Submovement characteristics

raster plots for D:\db\spaulding\motor\705



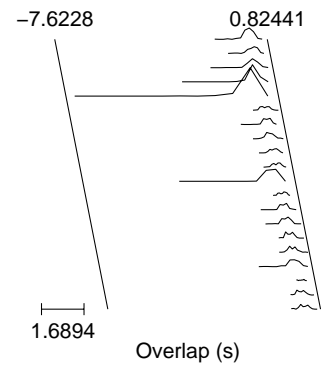
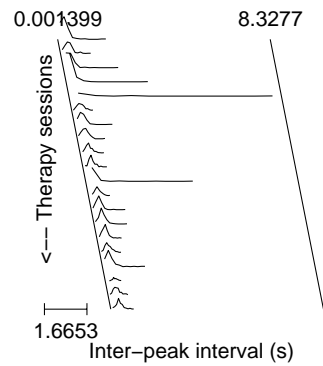
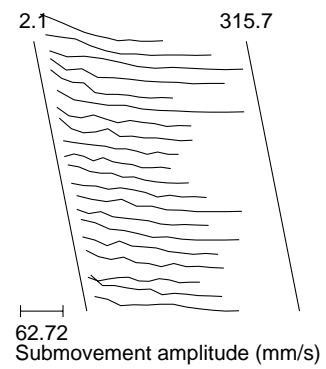
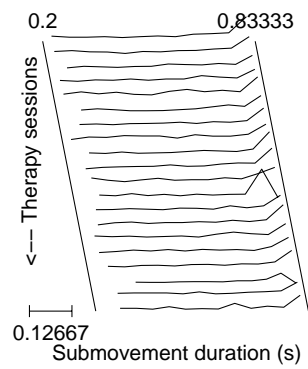
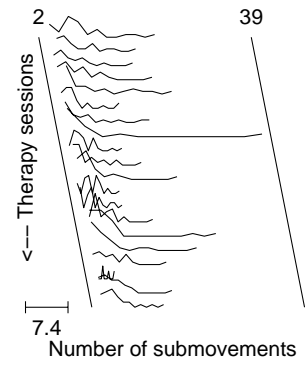
# Submovement characteristics

raster plots for D:\db\spaulding\motor\706



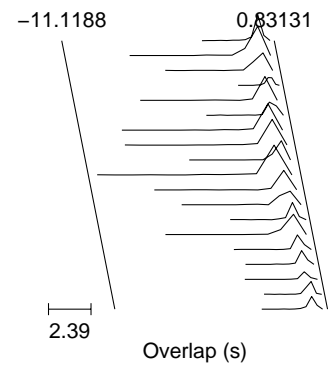
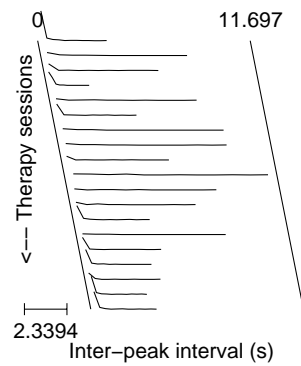
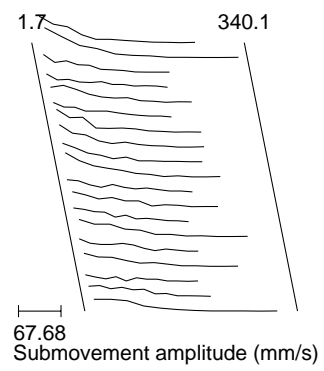
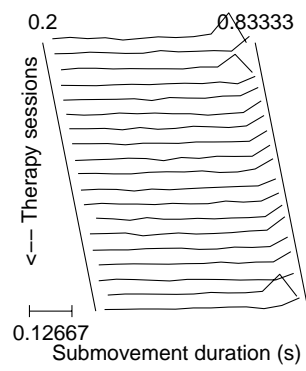
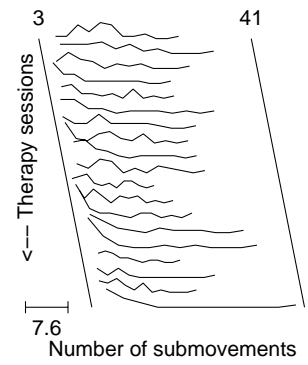
# Submovement characteristics

raster plots for D:\db\spaulding\motor\707



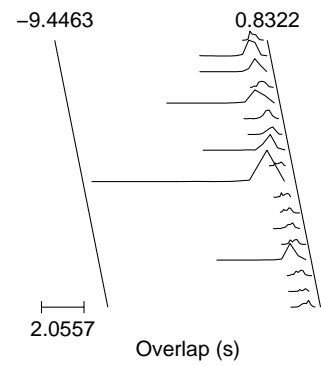
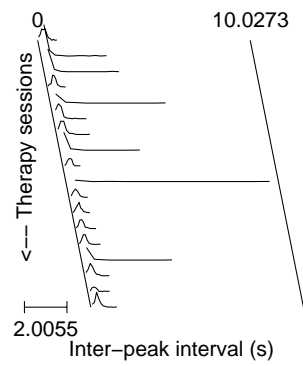
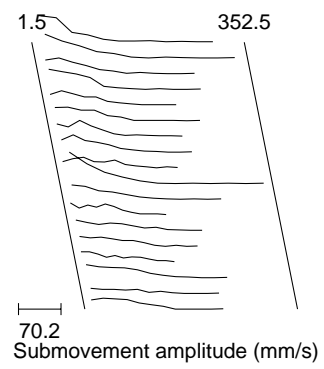
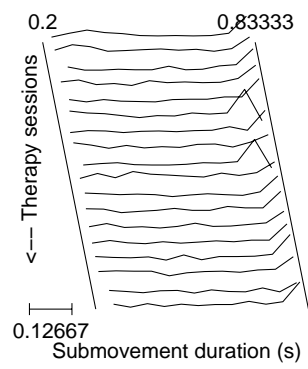
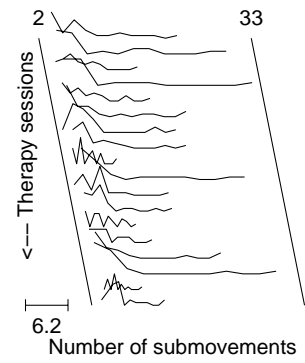
# Submovement characteristics

raster plots for D:\db\spaulding\motor\708



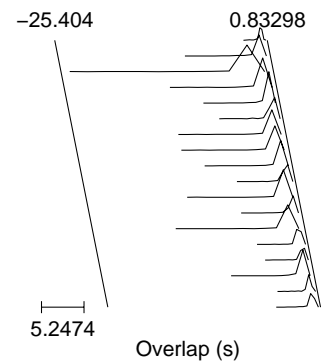
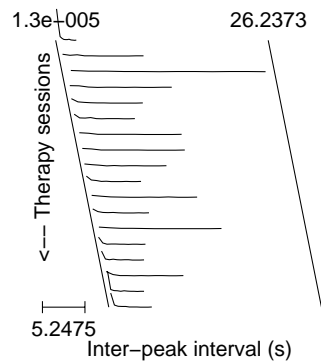
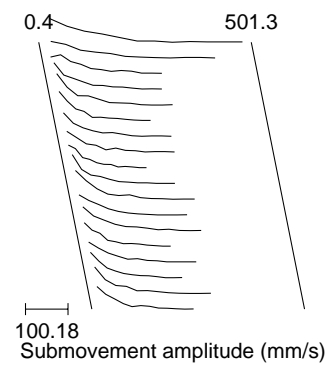
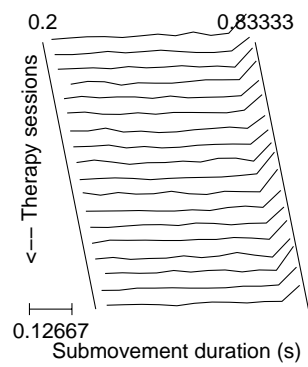
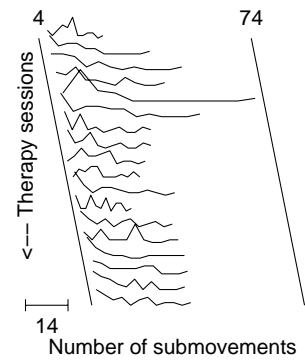
# Submovement characteristics

raster plots for D:\db\spaulding\motor\709



# Submovement characteristics

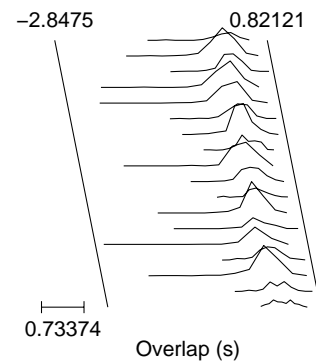
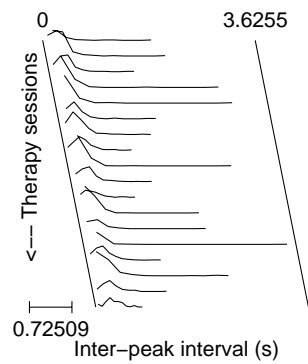
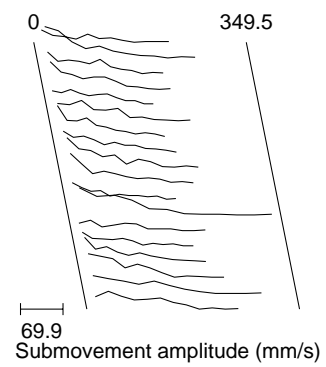
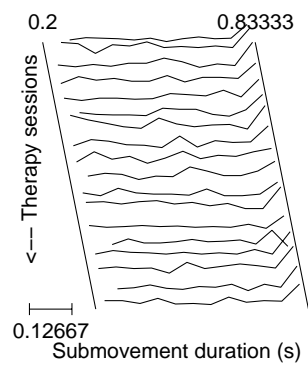
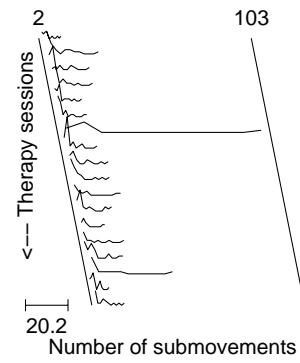
raster plots for D:\db\spaulding\motor\710





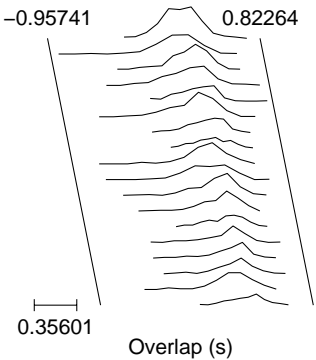
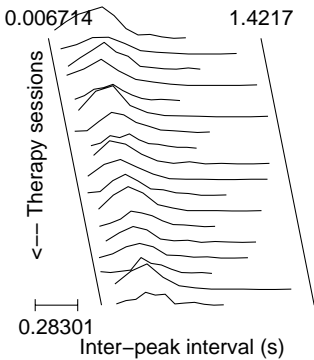
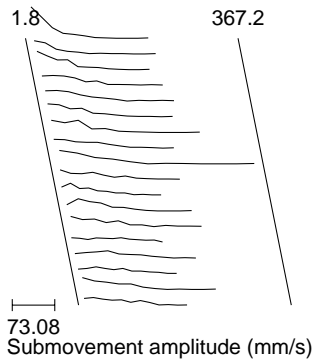
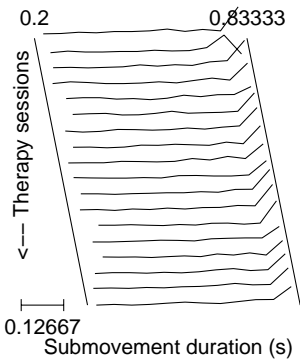
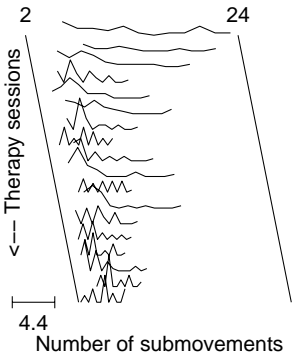
# Submovement characteristics

raster plots for D:\db\spaulding\motor\711



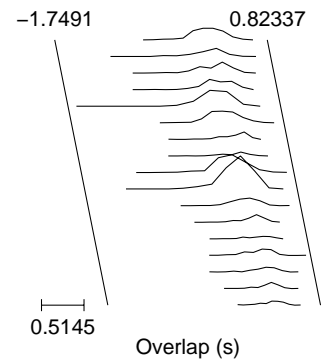
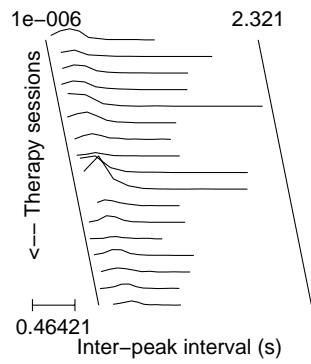
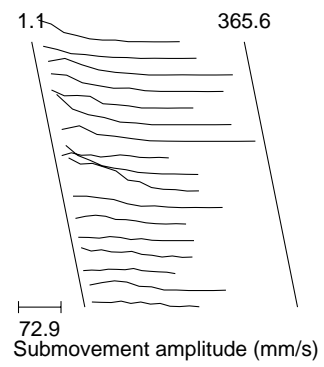
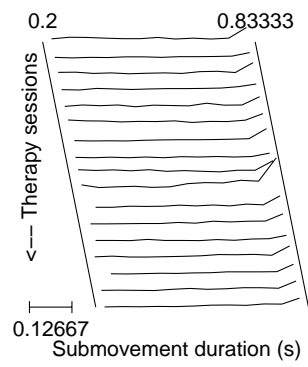
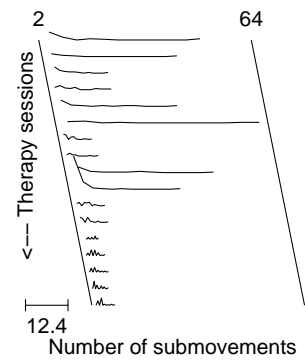
Submovement characteristics

raster plots for D:\db\spaulding\strength\712



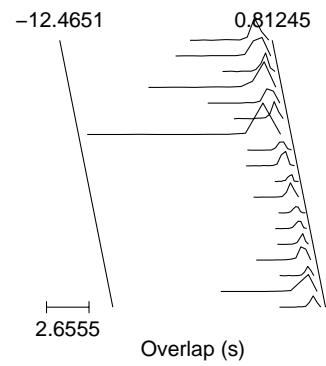
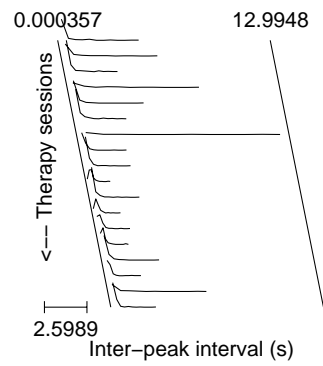
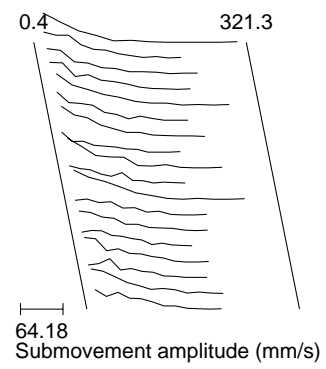
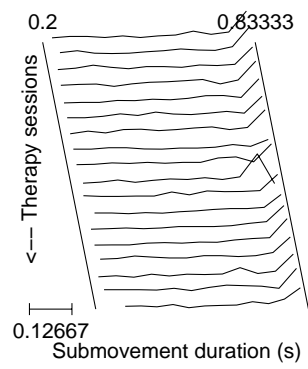
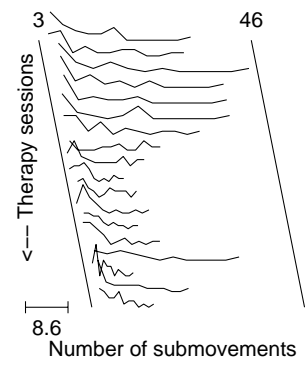
# Submovement characteristics

raster plots for D:\db\spaulding\motor\713



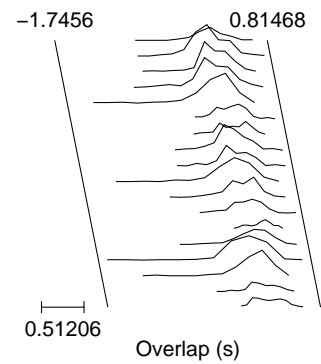
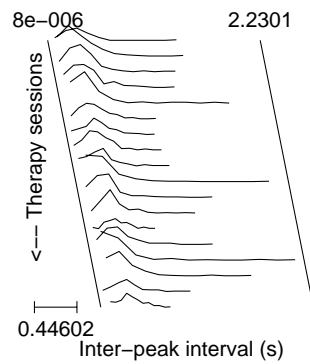
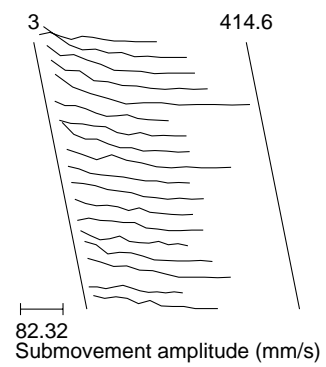
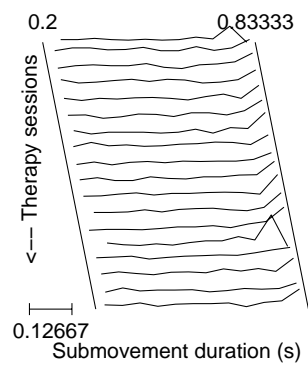
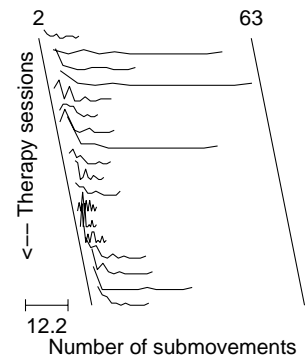
# Submovement characteristics

raster plots for D:\db\spaulding\motor\714



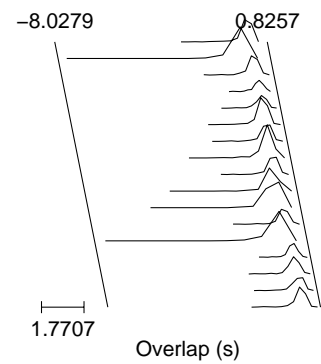
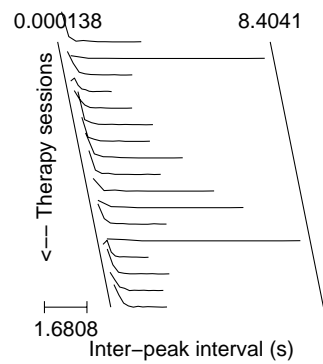
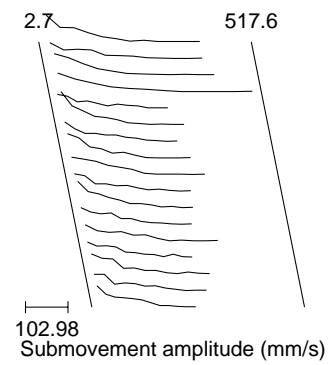
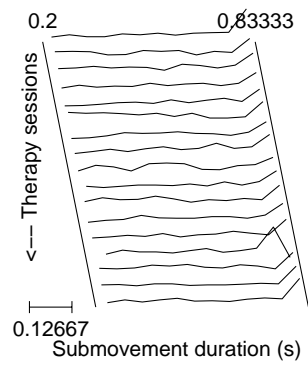
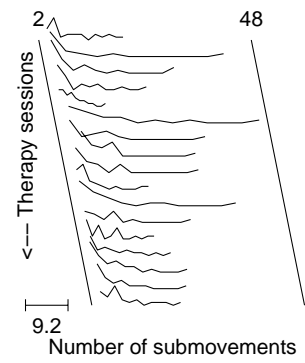
# Submovement characteristics

raster plots for D:\db\spaulding\motor\715



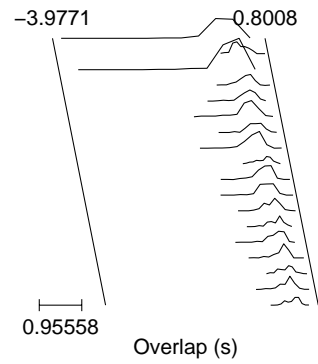
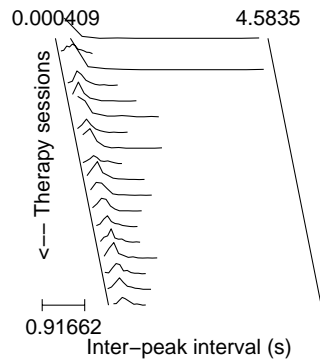
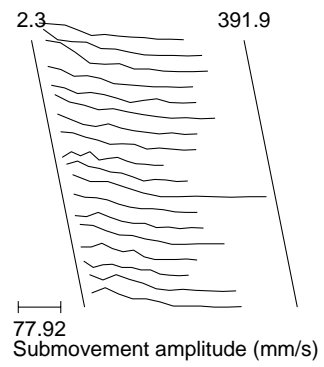
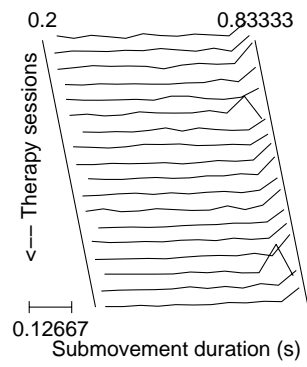
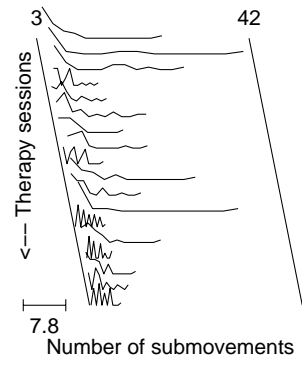
# Submovement characteristics

raster plots for D:\db\spaulding\motor\716



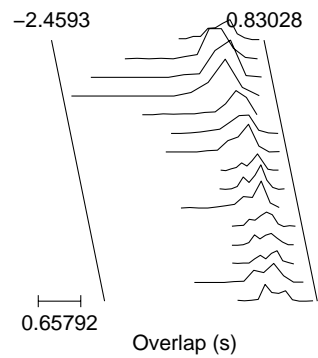
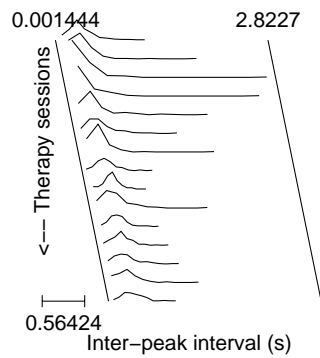
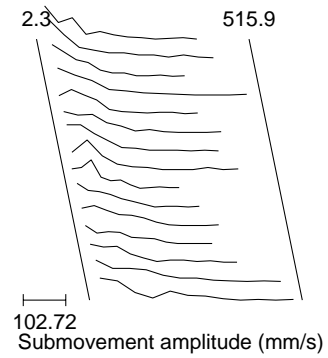
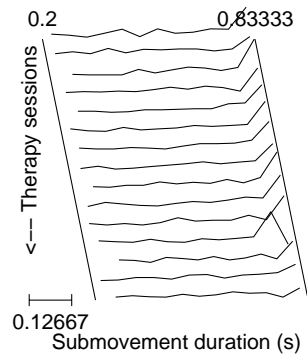
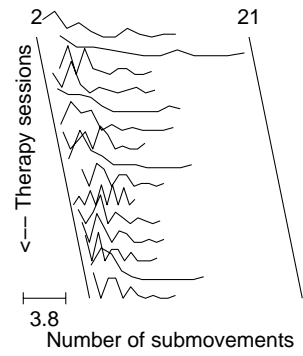
# Submovement characteristics

raster plots for D:\db\spaulding\strength\717



# Submovement characteristics

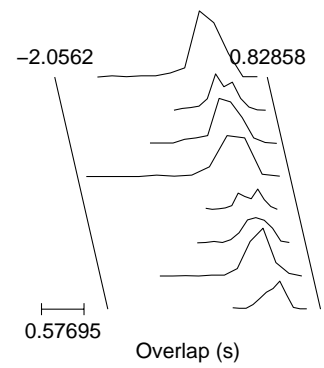
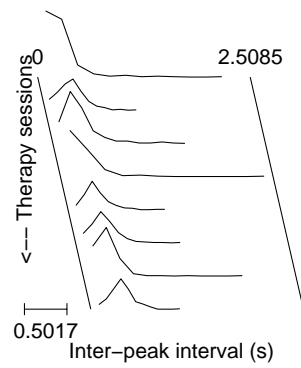
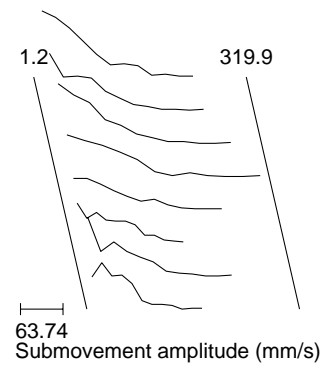
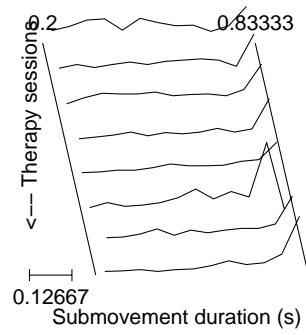
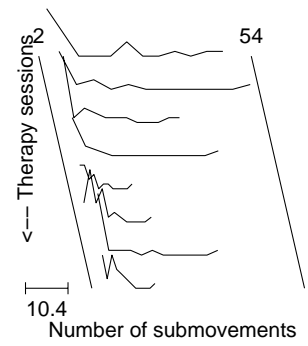
raster plots for D:\db\spaulding\strength\718





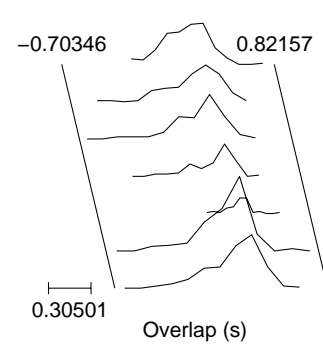
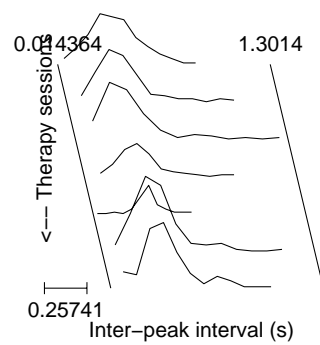
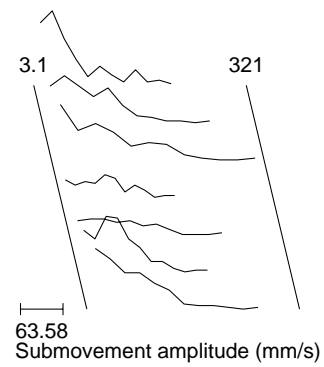
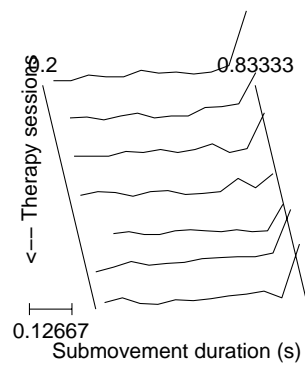
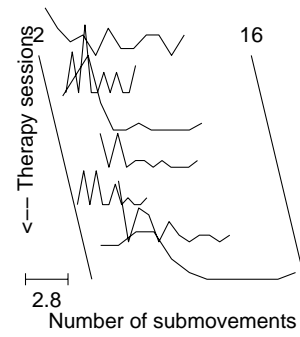
# Submovement characteristics

raster plots for D:\db\spaulding\motor\719



# Submovement characteristics

raster plots for D:\db\spaulding\motor\720



# Bibliography

- [1] W. Abend, E. Bizzi, and P. Morasso. Human arm trajectory formation. *Brain*, 105:331–348, 1982.
- [2] Louise Ada, Nicholas J. O’Dwyer, and Peter D. Neilson. Improvement in kinematic and coordination following stroke quantified by linear systems analysis. *Human Movement Science*, 12:137–153, 1993.
- [3] American Heart Association. 2001 Heart and stroke statistical update. [Online] Available: <http://www.americanheart.org/statistics/stroke.html>, Copyright 2001, Accessed: June 25, 2001.
- [4] National Stroke Association. Brain attack statistics. [Online], Copyright 1999, Accessed: June 25, 2001.
- [5] H Beppu, M Suda, and R Tanaka. Analysis of cerebellar motor disorders by visually guided elbow tracking movement. *Brain*, 107:787–809, 1984.
- [6] Neil E. Berthier. Learning to reach: A mathematical model. *Developmental Psychology*, 32(5):811–823, 1996.
- [7] N. Bhushan and R. Shadmehr. Computational nature of human adaptive control during learning of reaching movements in force fields. *Biological Cybernetics*, 81:39–60, 1999.
- [8] V.B. Brooks. *Control of Posture and Locomotion*, chapter The continuity of movements. Plenum Press, New York, 1973.

- [9] E. Burdet and T. E. Milner. Quantization of human motions and learning of accurate movements. *Biological Cybernetics*, 78:307–318, 1998.
- [10] United States Census Bureau. IDB Summary Demographic Data for United States [Online] Available: <http://www.census.gov/cgi-bin/ipc/idbsum?cty=US>, May 10, 2000, Accessed: June 25, 2001.
- [11] William H. Calvin. The emergence of intelligence. *Scientific American*, pages 101–107, October 1994.
- [12] J.K. Chapin, K.A. Moxon, R.S. Markowitz, and M.A.L. Nicolelis. Real-time control of a robot arm using simultaneously recorded neurons in the motor cortex. *Nature Neuroscience*, 2(7):664–670, 1999.
- [13] Scott Shaobing Chen, David L. Donoho, and Michael A. Saunders. Atomic decomposition by basis pursuit. *SIAM Journal of Scientific Computing*, 20(1):33–61, 1998.
- [14] F. Chollet, V. DiPiero, R. J. S. Wise, D. J. Brooks, R. J. Dolan, and R. S. J. Frackowiak. The functional anatomy of motor recovery after stroke in humans: A study with positron emission tomography. *Annals of Neurology*, 29(1):63–71, January 1991.
- [15] M. C. Cirstea and M. F. Levin. Compensatory strategies for reaching in stroke. *Brain*, 123:940–953, 2000.
- [16] J. D. Cooke and S. H. Brown. Movement-related phasic muscle activation. *Journal of Neurophysiology*, 63(3):465–472, 1990.
- [17] E. R. F. W. Crossman and P. J. Goodeve. Feedback control of hand-movements and fitt’s law. *Quarterly Journal of Experimental Psychology*, 35A:251–278, 1983. Paper presented at the meeting of the Experimental Psychology Society, Oxford, July 1963.

- [18] M. Dam, P. Tonin, S. Casson, M. Ermani, G. Pizzolato, V. Iaia, and L. Battistin. The effects of long-term rehabilitation therapy on post stroke hemiplegic patients. *Stroke*, 24:1186–91, 1993.
- [19] Joseph A. Doeringer. *An Investigation into the Discrete Nature of Human Arm Movements*. PhD thesis, Massachusetts Institute of Technology, 1999.
- [20] Joseph A. Doeringer and Neville Hogan. Serial processing in human movement production. *Neural Networks*, 11:1345–1356, 1998.
- [21] S Edelman and T Flash. A model of handwriting. *Biological Cybernetics*, 57:25–36, 1987.
- [22] Linda Fetters and James Todd. Quantitative assessment of infant reaching movements. *Journal of Motor Behavior*, 19(2):147–166, 1987.
- [23] T Flash and N Hogan. The coordination of arm movements: An experimentally confirmed mathematical model. *Journal of Neuroscience*, 5:1688–1703, 1985.
- [24] Tamar Flash and Ealan Henis. Arm trajetory modifications during reaching towards visual targets. *Journal of Cognitive Neuroscience*, 3(3):220–230, 1991.
- [25] H.-J. Freund and H.J. Büdingen. The relationship between speed and amplitude of the fastest voluntary contractions of human arm muscles. *Experimental Brain Research*, 31:1–12, 1978.
- [26] AR Fugl-Meyer, L Jaasko, I Leyman, S Olsson, and S Seglind. The post-stroke hemiplegic patient. I. a method for evaluation of physical performance. *Scandinavian Journal of Rehabilitation Medicine*, 7:13–31, 1975.
- [27] C. Ghez and J. Gordon. Trajectory control on targeted force impulses: I. Role of opposing muscles. *Experimental Brain Research*, 67:225–240, 1987.
- [28] Simon Giszter and William Kargo. Conserved temporal dynamics and vector superposition of primitives in frog wiping reflexes during spontaneous extensor deletions. *Neurocomputing*, 32-33:775–783, 2000.

- [29] H. Gomi and M. Kawato. The cerebellum and VOR/OKR learning models. *Trends in Neuroscience*, 15:445–453, 1992.
- [30] J. Gordon and C. Ghez. Trajectory control on targeted force impulses: II. Pulse height control. *Experimental Brain Research*, 67:241–252, 1987.
- [31] J. Gordon and C. Ghez. Trajectory control on targeted force impulses: III. Compensatory adjustments for initial errors. *Experimental Brain Research*, 67:253–269, 1987.
- [32] Paul L. Gribble and David J. Ostry. Origins of the power law relation between movement velocity and curvature: Modeling the effect of muscle mechanics and limb dynamics. *Journal of Neurophysiology*, 76(5):2853–2860, 1996.
- [33] Christopher M. Harris and Daniel M. Wolpert. Signal-dependent noise determines motor planning. *Nature*, 394:780–784, 20 August 1998.
- [34] N. Hogan, H. I. Krebs, A. Sharon, and J. Charnnarong. U.S. Patent 5,466,213, 1995.
- [35] Neville Hogan. An organizing principle for a class of voluntary movements. *The Journal of Neuroscience*, 4(11):2745–54, November 1984.
- [36] Neville Hogan, Joseph A. Doeringer, and Hermano Igo Krebs. Arm movement control is both continuous and discrete. *Cognitive Studies*, 6(3):254–273, September 1999.
- [37] Seema Jaggi, William C. Karl, Stephane Mallat, and Alan S. Willsky. High resolution pursuit for feature extraction. Technical Report LIDS-P-2371, Laboratory for Information and Decision Systems, Massachusetts Institute of Technology, November 1996.
- [38] L E Kahn, M L Zygmans, W Z Rymer, and D J Reinkensmeyer. Effect of robot-assisted and unassisted exercise on functional reaching in chronic hemiparesis.

In *Proceedings of the 23th Annual International Conference of the IEEE/EMB Society*, Istanbul, Turkey, October 2001.

- [39] William Kargo and Simon Giszter. Rapid correction of aimed movements by summation of force-field primitives. *Journal of Neuroscience*, 20:409–426, 2000.
- [40] M. Kawato. Adaptation and learning in control of voluntary movement by the central nervous system. *Advanced Robotics*, 3:229–249, 1989.
- [41] M. Kawato. *Attention and Performance XIV*, chapter Optimization and learning in neural networks for formation and control of coordinated movement. Erlbaum, Hillsdale, NJ, 1991.
- [42] H. I. Krebs, M. L. Aisen, B. T. Volpe, and N. Hogan. Quantization of continuous arm movements in humans with brain injury. *Proceedings of the National Academy of Science*, 96:4645–9, April 1999. Neurobiology.
- [43] H. I. Krebs, T. Brashers-Krug, S. L. Rauch, C. R. Savage, N. Hogan, R. H. Rubin, A. J. Fischman, and N. M. Alpert. Robot-aided functional imaging: application to a motor learning study. *Human Brain Mapping*, 6:59–72, 1998.
- [44] Hermano Igo Krebs. *Robot-Aided Neurorehabilitation and Functional Imaging*. PhD thesis, Massachusetts Institute of Technology, 1997.
- [45] Hermano Igo Krebs, Neville Hogan, Mindy L. Aisen, and Bruce T. Volpe. Robot-aided neurorehabilitation. *IEEE Transactions on Rehabilitation Engineering*, 6(1):75–87, March 1998.
- [46] Andrew M. Krylow and W. Zev Rymer. Role of intrinsic muscle properties in producing smooth movements. *IEEE Trans on Biomedical Engineering*, 44(2):165–175, February 1997.
- [47] Roland E. Larson, Robert P. Hostetler, and Bruce H. Edwards. *Calculus with Analytic Geometry*. D. C. Heath and Company, 125 Spring St., Lexington, MA, 1994.

- [48] Richard T. Lauer, P. Hunter Peckham, Kevin L. Kilgore, and William J. Heetderks. Applications of cortical signals to neuroprosthetic control: A critical review. *IEEE Transactions on Rehabilitation Engineering*, 8(2):205–208, June 2000.
- [49] D Lee, N L Port, and A P Georgopoulos. Manual interception of moving targets II. On-line control of overlapping submovements. *Experimental Brain Research*, 116:421–422, 1997.
- [50] Mindy F. Levin. Interjoint coordination during pointing movements is disrupted in spastic hemiparesis. *Brain*, 119:281–293, 1996.
- [51] JDC Little, KG Murty, DW Sweeney, and C Karel. An algorithm for the traveling salesman problem. *Operations Research*, 11:972–989, November 1963.
- [52] John D. C. Little. Branch and bound methods for combinatorial problems. Technical Report 178–66, Working paper (Sloan school of Management, M.I.T.), Cambridge, Massachusetts, 1966.
- [53] Peter S. Lum, Charles G. Burgar, Deborah E. Kenney, and H. F. Machiel Van der Loos. Quantification of force abnormalities during passive and active-assisted upper-limb reaching movements in post-stroke hemiparesis. *IEEE Transactions on Biomedical Engineering*, 46(6):652–62, June 1999.
- [54] S Mallat and Z Zhang. Matching pursuit with time-frequency dictionaries. *IEEE Transactions on Signal Processing*, 1993.
- [55] Joe T. Massey, Joseph T. Lurito, Giuseppe Pellizzer, and Apostolos P. Georgopolous. Three-dimensional drawings in isometric conditions: relation between geometry and kinematics. *Experimental Brain Research*, 88:685–690, 1992.
- [56] David E. Meyer, J. E. Keith Smith, Sylvan Kornblum, Richard A. Abrams, and Charles E. Wright. *Attention and Performance XIII*, chapter 6: Speed-accuracy tradeoffs in aimed movements: Toward a theory of rapid voluntary action, pages 173–226. Lawrence Erlbaum Associates, 1990.



- [57] R. C. Miall. Task-dependent changes in visual feedback control: A frequency analysis of human manual tracking. *Journal of Motor Behavior*, pages 125–135, 1996.
- [58] RC Miall, DJ Weir, and JF Stein. Visuomotor tracking with delayed visual feedback. *Neuroscience*, 16(3):511–520, 1985.
- [59] RC Miall, DJ Weir, and JF Stein. Intermittency in human manual tracking tasks. *Journal of Motor Behavior*, 25(1):53–63, March 1993.
- [60] T. E. Milner. A model for the generation of movements requiring endpoint precision. *Neuroscience*, 49:365–374, 1992.
- [61] T. E. Milner and M. M. Ijaz. The effect of accuracy constraints on three-dimensional movement kinematics. *Neuroscience*, 35:487–496, 1990.
- [62] S. P. Moore and R. G. Marteniuk. Kinematic and electromyographic changes that occur as a function of learning a time-constrained aiming task. *Journal of Motor Behavior*, 18:397–426, 1986.
- [63] P. Morasso and F. A. Mussa-Ivaldi. Trajectory formation and handwriting: A computational model. *Biological Cybernetics*, 45:131–142, 1982.
- [64] Thomas L. Morin. Branch-and-bound strategies for dynamic programming. Technical Report 750–74, Working paper (Sloan school of Management, M.I.T.), Cambridge, Massachusetts, 1974.
- [65] H. Nagasaki. Asymmetric velocity and acceleration profiles of human arm movements. *Experimental Brain Research*, 74:319–326, 1989.
- [66] M.A.L. Nicolelis. Actions from thoughts. *Nature*, 409(6818):403–407, 2001.
- [67] K E Novak, L E Miller, and J C Houk. Kinematic properties of rapid hand movements in a knob turning task. *Experimental Brain Research*, 132:419–433, 2000.

- [68] D. J. Ostry, J. D. Cooke, and K. G. Munhall. Velocity curves of human arm and speech movements. *Experimental Brain Research*, 68:37–46, 1987.
- [69] Richard W. Pew, John C. Duffendack, and Linda K. Fensch. Sine-wave tracking revisited. *IEEE Transactions on Human Factors in Electronics*, HFE-8(2):130–134, June 1967.
- [70] R. Plamondon. *Tutorials in Motor Behavior II*, chapter A theory of rapid movements, pages 55–69. Elsevier Science Publishers, 1992.
- [71] R. Plamondon and A. Alimi. Speed/accuracy trade-offs in target-directed movements. *Behavioral and Brain Sciences*, 20:279–349, 1997.
- [72] Rejean Plamondon, Adel M. Alimi, Pierre Yergeau, and Franck Leclerc. Modeling velocity profiles of rapid movements: a comparative study. *Biological Cybernetics*, 69:119–128, 1993.
- [73] T. Platz, P. Denzler, B. Kaden, and K.-H. Mauritz. Motor learning after recovery from hemiparesis. *Neuropsychologia*, 32(10):1209–1223, 1994.
- [74] William H. Press, Saul A. Teukolsky, William T. Vetterling, and Brian P. Flannery. *Numerical Recipes in C*, chapter 15, pages 661–665. Cambridge University Press, New York, second edition, 1992.
- [75] B. Rohrer, S. Fasoli, H. I. Krebs, R. Hughes, B. Volpe, W. R. Frontera, J. Stein, and N. Hogan. Movement smoothness changes during stroke recovery. in review, 2002.
- [76] Stefan Schaal and Dagmar Sternad. Origins and violations of the 2/3 power law in rhythmic three-dimensional arm movements. *Experimental Brain Research*, 136:60–72, 2001.
- [77] R. Shadmehr. Learning virtual equilibrium trajectories for control of a robot arm. *Neural Computation*, 2:436–446, 1990.

- [78] Reza Shadmehr and Fernando A. Mussa-Ivaldi. Adaptive representation of dynamics during learning of a motor task. *The Journal of Neuroscience*, 14(5):3208–24, May 1994.
- [79] Maurice A. Smith, Jason Brandt, and Reza Shadmehr. Motor disorder in Huntington’s disease begins as a dysfunction in error feedback control. *Nature*, 403:544–549, February 3 2000.
- [80] Dagmar Sternad and Stefan Schaal. Segmentation of endpoint trajectories does not imply segmented control. *Experimental Brain Research*, 124:118–136, 1999.
- [81] C. W. Telford. The refractory phase of voluntary and associated responses. *Journal of Experimental Psychology*, 14:1–36, 1931.
- [82] Emanuel Todorov and Michael I. Jordan. Smoothness maximization along a predefined path accurately predicts the speed profiles of complex arm movements. *Journal of Neurophysiology*, 80:696–714, 1998.
- [83] Catherine A. Trombly. Observations of improvement of reaching in five subjects with left hemiparesis. *Journal of Neurology, Neurosurgery, and Psychiatry*, 56:40–45, 1993.
- [84] West Virginia University. West virginia health page: Stroke: Statistics of stroke. [Online] Available: <http://www.wvhealth.wvu.edu/clinical/stroke/strkstat.htm>, Copyright 2000, Accessed: June 25, 2001.
- [85] Å. B. Vallbo and J. Wessberg. Organization of motor output in slow finger movements in man. *Journal of Physiology*, 469:673–691, 1993.
- [86] Paolo Viviani and Marco Cenzato. Segmentation and coupling in complex movements. *Journal of Experimental Psychology: Human Perception and Performance*, 11(6):828–845, 1985.
- [87] Claes von Hofsten. Structuring of early reaching movements: A longitudinal study. *Journal of Motor Behavior*, 23(4):280–292, 1991.

- [88] John Wann, Ian Nimmo-Smith, and Alan M. Wing. Relation between velocity and curvature in movement: Equivalence and divergence between a power law and a minimum-jerk model. *Journal of Experimental Psychology: Human Perception and Performance*, 14(4):622–637, 1988.
- [89] D. J. Weir, J. F. Stein, and R. C. Miall. Cues and control signals in visually guided tracking. *Journal of Motor Behavior*, 21(3):185–204, 1989.
- [90] Norbert Wiener. *Cybernetics*. MIT Press, Cambridge, 1961.
- [91] A. M. Wing, S. Lough, A. Turton, C. Fraser, and J. R. Jenner. Recovery of elbow function in voluntary positionin of the hand following hemiplegia due to stroke. *J Neurol Neurosurg Psych*, 53(2):126–134, 1990.
- [92] Alan M. Wing and Ed Miller. Research note: Peak velocity timing invariance. *Psychological Research*, 46:121–127, 1984.
- [93] D. M. Wolpert, Z. Gharamani, and M. I. Jordan. Perceptual distortion contributes to the curvature of human arm movements. *Experimental Brain Research*, 98:153–156, 1994.
- [94] R. S. Woodworth. The accuracy of voluntary movement. *Psychology Review Monogr Suppl*, 1899.
- [95] H. N. Zelaznik, R. A. Schmidt, and S. C. A. M. Gielen. Kinematic properties of rapid-aimed head movements. *Journal of Motor Behavior*, 18:353–372, 1986.